Characterisation of multifunctional composites exhibiting mechanical and thermal management capabilities

A thesis submitted in fulfilment of the requirements for the degree of Master by research

Sanghyun Yoo

B. Eng (Aerospace) (Hon I)

School of Engineering

College of Science Engineering and Health

RMIT University

June 2016

Declaration

I certify that except where due acknowledgement has been made, the work is that of the author alone; the work has not been submitted previously, in whole or in part, to qualify for any other academic award; the content of the thesis is the result of work which has been carried out since the official commencement date of the approved research program; any editorial work, paid or unpaid, carried out by a third party is acknowledged; and, ethics procedures and guidelines have been followed.

Sanghyun Yoo

June 2016

Abstract

Thermal storage systems based on latent heat are among the efficient energy saving solutions. Unlike the sensible heat, much higher storage densities and narrow operating temperatures can be achieved using latent heat. To utilise these advantages, Phase Change Materials (PCMs) have been integrated into load- and non-load-bearing components to enhance their thermal storage capacity. PCMs are capable of absorbing, storing and releasing a large amount of thermal energy so-called latent heat. Thermal energy is absorbed and released during the phase change without changing the temperature itself. In this regard, multifunctional composite exhibiting both structural properties and thermal storage capability can be a viable solution to reduce energy consumption in engineering applications.

In order to develop PCM-incorporated multifunctional composites, it is necessary to characterise the inclusion effect of PCMs on the host composite laminates. In particular, micro-PCMs are integrated into traditional Fibre Reinforced Polymer (FRP) composite and its influence was investigated. Furthermore, thermal management capabilities are strongly influenced by not only the filler but also thermo-mechanical properties of the matrix. The characterisation of viscoelastic properties is important due to the viscoelastic nature of the polymer matrix. As a result, the micro-PCMs inclusion effect on mechanical, thermophysical and viscoelastic properties of composites was experimentally investigated.

It was found that the tensile, compressive, and flexural properties of multifunctional composites were reduced by increasing the weight fraction of micro-PCMs. The failure mechanism changed from matrix to interfacial failure after incorporating 12 wt.% of microencapsulated PCMs. Using short-beam-strength (SBS) tests and SEM analysis, it was identified that a significant reduction in the interfacial shear strength is contributing towards

the degradation of mechanical properties. The interfacial adhesion between micro-PCMs and matrix was deteriorated due to the poor wetting of the fillers during manufacturing. On the other hand, the embedded micro-PCMs improved Mode I interlaminar fracture toughness due to the particle toughening mechanisms (i.e. crack pinning and debonding). The effect of solid ↔ liquid phase transition of micro-PCMs on the mechanical properties of composites was also studied through SBS tests, at temperatures below and above the melting temperature of PCM.

The influence of micro-PCMs on the thermophysical properties of multifunctional laminates was also examined. While the thermal storage capacity (heat of fusion) of the composites was directly proportional to the weight fraction of micro-PCMs, the thermal and dimensional stability of the multifunctional composites were significantly affected by increasing microencapsulated PCMs concentration. The thermal decomposition temperature was reduced and the coefficient of thermal expansion (CTE) was increased due to the inclusion of micro-PCMs. These observations indicate that the interfacial properties between micro-PCMs and matrix play a crucial role in determining the thermal and dimensional stability of the composites.

Finally, by investigating the viscoelastic properties, it was revealed that the glass transition temperature of the composites was also affected since incorporating micro-PCMs promotes segmental motions of epoxy. The viscoelasticity of micro-PCMs-enhanced FRP composites was investigated using multi-frequency scans through the concept of activation energy and free volume. In addition, an unusual transition in the storage and loss moduli of composites was observed at lower temperature ranges which was attributed to phase transition of micro-PCMs (solid → liquid phase) and confirmed by the correlation between DMA and DSC analysis of micro-PCMs capsules.

Acknowledgements

I sincerely thank my supervisors; A./Prof. Akbar Afaghi Khatibi and Dr. Kandare from RMIT University where I received brilliant guidance through my Master by research program. I would like to express my gratitude towards my external supervisor, Prof. Mariam Ali S A Al-Maadeed from Qatar University. Her expertise and guidance has been critical to the success of this project. In particular, Qatar University's support during my research travel to Doha is highly appreciated.

I would like to thank all those have contributed to the work in this project including Mr. Robert Ryan for assistance in manufacturing specimens and Mr. Peter Tkatchyk for mechanical testing. Furthermore, I would like to express my sincere thanks and appreciation to E./Prof. Robert Shanks for valuable inputs and support in conducting thermal analysis and to Mrs. Nadia Zakhartchouk for technical assistance from the School of Science, RMIT University.

Foremost, to my wife Kyoung A Ha, who always supports and encourages me, I am indebted to her beyond measure.

List of Publication

The work has resulted in a number of publications including three peer-reviewed journal papers and one peer-reviewed conference paper.

[Journal paper]

[1] Yoo S, Kandare E, Shanks RA, Mariam A-AAa, Khatibi AA. Thermophysical Properties of Multifunctional Glass Fibre Reinforced Polymer Composites Incorporating Phase Change Materials. J Therm Anal Calorim. 2015 (Submitted).

[2] Yoo S, Kandare E, Shanks RA, Mariam A-AAa, Khatibi AA. Effect of Microencapsulated Phase Change Materials on Viscoelastic Properties of Glass/Epoxy Composites. J Mater Sci. 2016 (In progress).

[3] Yoo S, Kandare E, Mahendrarajah G, Mariam A-AAa, Khatibi AA. Mechanical and thermal charactrisation of multifunctional composites incorporating phase change materials. Materials & Design. 2016 (Submitted).

[Conference paper]

[1] Yoo S, Khatibi AA, Kandare E. Multifunctional composites exhibiting structural and thermal management capabilities. AIAC16: 16th Australian International Aerospace Congress, Melrobune, Victoria: Engineers Australia; 2015.

Table of contents

List of figure

List of tables

List of Abbreviation

PCMs	Phase Change Materials
Micro-PCMs	Microencapsulated Phase Change Materials
DCB	Double Cantilever Beam
DSC	Differential scanning calorimetry
TPS	Transient Plane Source
TGA	Thermogravimetric Analysis
TMA	Thermomechanical Analysis
mT-TMA	Modulated-temperature Thermomechanical Analysis
DMA	Dynamic Mechanical Analysis
SEM	Scanning Electron Microscopy
CTE	Coefficient of Thermal Expansion
HDPE	High-Density Polyethylene
HGM	Hollow Glass Microsphere
MMCs	Metal Matrix Composites
CMCs	Ceramic Matrix Composites
PMCs	Polymer Matrix Composites

Nomenclature

E	Young's modulus
σ	Stress
ε	Strain
ρ	Density
G_{Ii}	Crack initiation mode I fracture toughness
G_{Ic}	Steady-state mode I fracture toughness
T	Temperature
t	Time
T_g	Glass transition
T_m	Melting temperature
ΔH_m	Calculated melting enthalpy (Heat of fusion)
ΔH_c	Calculated crystallisation enthalpy (Heat of crystallisation)
C_p	Specific heat
φ	Heat flux
k	Thermal conductivity
α	Coefficient of thermal expansion
E*	Complex modulus
E´	Storage modulus
E´´	Loss modulus
tan δ	Loss factor
ΔE_a	Activation energy
ΔF_g	Fractional free volume
wt.%	Weight fraction

1. INTRODUCTION

1.1. Motivation

Multifunctional composite materials/structures are capable of simultaneously performing structural and non-structural functions. Concurrent consideration of the load-carrying capability and other functional requirements in multifunctional design results in optimised structures that have integral non-load-bearing functions without compromising usable structural volume [1, 2]. The most desirable non-load-carrying functionalities are the tuneable thermo-physical properties of an engineering structure. Currently, there are great interests in the development of new materials that could lead to the reduction in energy consumption associated with heating and cooling of buildings, electrical packages and other engineering applications. Multifunctional composites exhibiting thermal storage properties can be considered as a viable solution in this regard to reduce the energy consumption and associated carbon footprint while addressing energy constraints.

Due to an inherent thermal storage capacity of PCMs, the design of multifunctional composites incorporating PCMs is one of the promising solutions to offer an excellent thermal management system. PCMs have been adopted in engineering applications such as buildings and textile industry. In order to develop PCM-incorporated multifunctional composites, it is necessary to characterise the inclusion effect of PCMs on the structural and thermal management properties of the host composite laminates. This study reports on the thermophysical, mechanical and viscoelastic properties of novel multifuctional FRP composites incorporating micro-PCMs.

1.2. The aim and objectives

The aim of this project was to design, fabricate and characterise multifunctional structural composites incorporating phase change materials for thermal management applications. The specific research objectives to achieve this goal were formulated as follows:

- Investigate effective methods to integrate microencapsulated PCMs into glass fibre-reinforced epoxy composites.
- Evaluate the mechanical properties of micro-PCMs enhanced FRP composites and investigate associated failure mechanisms.
- Study the thermal management effectiveness of micro-PCMs enhanced FRP composites.

1.3. Research question

Based on a comprehensive literature review, research gaps in achieving above mentioned objectives were identified and the following research questions have been formulated.

Question 1: How can the thermal storage properties of FRP composites be enhanced without adversely influencing the baseline mechanical properties?

- What are the effects of incorporating micro-PCMs on the mechanical properties of FRP composites?
- What are the effects of micro-PCMs on the failure mechanisms of the FRP composite?

Question 2: How can the thermal properties be effectively controlled in micro-PCMs-reinforced FRP composites?

- What effects do fibre reinforcements have on the thermophysical properties of micro-PCMs?
- How does the solid↔liquid phase transition influence the mechanical and thermophysical properties of the micro-PCMs-enhanced composites?

1.4. Thesis outline

The body of this thesis consists of five chapters. A comprehensive literature review is presented in Chapter 2. In addition to the types of PCM, the inclusion effects of micro-sized particulates on mechanical and thermophysical properties of polymer-matrix composites are reviewed. Chapter 3 starts by presenting the manufacturing method adopted in this study and report the effect of micro-PCM inclusion on the **mechanical properties** of host composite laminates. Tension, compression, and flexural properties of multifunctional composites are presented. The interfacial characteristics of micro-PCMs and matrix as well as Mode I interlaminar fracture toughness of these newly developed composites are discussed in this chapter. In addition, the failure mechanisms deduced from high definition digital camera and Scanning Electron Microscopy (SEM) images of the fractured specimens are reported. Chapter 4 is dedicated to discussing the influence of micro-PCMs on **the thermophysical properties** of the host composite. Thermal properties including enthalpy (heat of fusion), specific heat capacity as well as thermal stability and thermal decomposition temperatures are discussed. In addition, analysis of dimensional stability using mT-TMA to evaluate the coefficient of thermal expansion (CTE) is presented in this chapter. The heat flux apparatus, constructed in this project and used to characterise the bulk thermal storage capacity of the multifunctional composites is also illustrated in this chapter. The **viscoelastic properties** of micro-PCM incorporated composite laminates were studied using DMA and are discussed in Chapter 5. Furthermore, the glass transition (T_g) of the composite laminates and the effects of PCM phase transition (solid ↔ liquid) on the thermo-mechanical properties of multifunctional composites are reported. Finally, Chapter 6 concludes with the overview and the research findings. Also, recommendations for the future research considering thermal management capabilities, sandwiched multifunctional composite structures and nano-modified composites with improved thermal properties are discussed.

1.5. Significance

Current composite design methodologies consider structural and thermophysical properties independently. The interdependent consideration of micro-PCMs-enhanced FRP composites will be a significant step towards the development of new bifunctional materials exhibiting structural and thermal management capabilities. It is, therefore, important to understand the influence of the embedded micro-PCMs on the resultant multifunctional FRP composite. This project contributes to the development of innovative versatile composite with potential scientific benefits to the composite industry. Therefore, the outcome of this project contributes towards the design and development of multifunctional composites that can provide mechanical and thermal superiority over conventional materials.

2. LITERATURE REVIEW

2.1. Introduction

The usage of Fibre Reinforced Polymer (FRP) composites has increased due to demand for more structurally efficient materials over conventional metallic alloys. The main advantages of FRP composites are high strength/stiffness-to-weight ratios and low density as well as excellent fatigue and corrosion resistance. Owing to these desirable properties, composite materials have been used in many applications, such as aerospace and automotive structures [3-5]. Multifunctional structural composites can simultaneously carry structural loads and exhibit functionalities working in synergy to provide the advantages beyond the sum of the individual capabilities [6]. In particular, there are increased interests in the development of multifunctional composites that combine structural and non-structural properties. The traditional approach to designing multifunctional structures involves independent considerations of the load bearing capacity and functionality (e.g., electrical and thermal properties). Recently, multifunctional design requirements including light-weightiness have driven the development of new composite materials that can perform multiple functions without compromising usable structural volume [1, 2]. The integration of functionality without a penalty on the structural weight directly translates to cost-effectiveness. The reduction in fuel consumption for automobiles [7] and aircraft [8] may increase the operational performance, the range as well as the payload.

From non-structural properties, tuneable thermo-physical properties are among the most desirable [1]. Effective methods to manage heat have increasingly been the focus of numerous material scientists and engineers. For example, there are increasing demands on new design approaches towards the development of lightweight electronic packaging systems. According to Moore's law [9], the number of transistors on integrated circuits is projected to

double every couple of years. Thus, with increased transistor compactness and high performance demands, the heat density in electronic circuits will increase drastically [10]. Problems such as the development of hot-spots during the operation as well as operating temperatures beyond the operational envelope may result in performance degradation [11]. Also, there are tremendous interests in the development of new materials that could lead to the reduction in energy consumption associated with heating and cooling systems for buildings. Therefore, multifunctional composite materials exhibiting thermal storage properties may reduce the carbon footprint while addressing world energy constraints by reducing energy consumption [12].

2.2. Polymer-Matrix Composites with potential thermal management

In general, composites can be classified under three categories namely, metal matrix composites (MMCs), ceramic matrix composites (CMCs), and polymer matrix composites (PMCs) according to the type of matrix. PMCs have traditionally been used for structural loading bearing engineering applications. In particular, fibre-reinforced polymer composites have demonstrated tremendous advantages, high strength and stiffness to weight ratios. FRP composites have been considered a commodity in many applications where structural weight is critical, such as aerospace and automotive structures due to a high performance with low density [3-5]. Composite properties are strongly dependent on the properties of reinforcements. This provides a tailorability on desirable properties such as matching coefficients of thermal expansion with other part of the structure as well as lower density and cost effectiveness. Furthermore, composite materials are ideally suitable to acquire multi-functionality since they combine different materials to achieve targeted performance [13].

The architecture for thermal management system with latent heat storage capacity can be one of the most efficient ways of managing thermal energy. Unlike the sensible heat storage, the

latent heat storage method provides much higher storage density with smaller temperature differences between heat storage and heat release. A large amount of thermal energy in latent heat is absorbed and released during the phase change without changing the temperature itself. Therefore, thermal management systems incorporating PCMs can provide heat absorption and releasing characterises. In order to achieve multiphase composites with desired structural and thermal storage capacity, micro-PCMs will be integrated into FRP composites. Such materials can be utilised for thermal protection and thermal stabilisation of thermo-sensitive applications.

2.3. Phase Change Materials (PCMs)

2.3.1. Introduction

The design of multifunctional composites incorporating PCMs is one of the promising solutions to offer a good thermal management system.. Due to their inherent thermal storage capacity properties, PCMs have been incorporated into wearable textiles [14-16], spacecraft protective gear [17], building materials such as wallboard [18], gypsum [19], concrete [20] and mortar [21], thermal storage structures [22-26] and electronic packaging [10, 27, 28].

In the early 80s, space suits were developed with the innovative textile technology using fibres incorporating microencapsulated PCMs under the National Aeronautics and Space Administration (NASA) research programme. The aim of that project was to stabilise temperature fluctuations encountered by astronauts in outer space. Since their inception thermal insulating clothing materials have been successfully developed and commercialised [16]. PCMs have also been integrated into building materials, such as mortar, wallboard and concrete with the objective to stabilise room temperature levels thereby reducing the amount of energy required for heating and cooling purposes [29, 30]. In this chapter, the

classification/types of PCMs is comprehensively reviewed, and the selected material systems for this project is then described.

2.3.2. Classification of PCMs

Abhat [22] has classified the PCMs for thermal energy storage application based on the chemical composition as shown in Fig. 2-1.

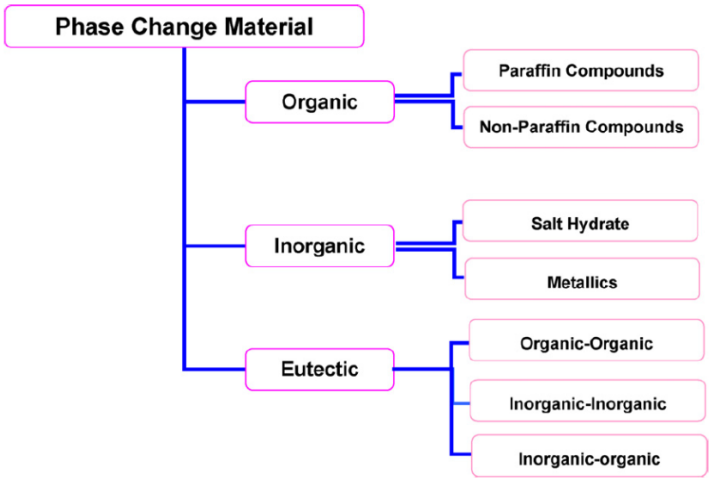

Figure 2-1 Classification of PCMs according to chemical composition [22]

2.3.2.1. Organic PCMs

2.3.2.1.1. Paraffin wax

Paraffin wax is one of the important organic PCMs, which consist of the straight chain *n*-alkanes, which are defined by a chemical composition of C_nH_{2n+2} as listed in Table 2-1. As the number of carbon atom (molecular weight) increases, the melting temperature and latent heat of fusion increase. Due to its availability over a wide range of temperature for commercial application, moderate latent heat, chemical compatibility, low toxicity and relatively low cost, paraffin wax has been studied for decades. However, paraffin expands by about 10-15% during melting process, which can lead to the complexity of the container

design. Also, higher PCM volumes per given heat storage are required due to its low specific gravity [31, 32].

Table 2-1 Thermal properties of paraffin waxes with the number of C atoms ranging between 12 and 28 [32]

Paraffin wax	Molecular formula	Molar mass /g mol^{-1}	Melting temperature /◦C	Crystallization temperature /◦C	ΔH_{fus} /kJ·kg^{-1}
n-Dodecane	$CH_3(CH_2)_{10}CH_3$	170.3	−10	−16	216
n-Tridecane	$CH_3(CH_2)_{11}CH_3$	184.4	−5	−9	160
n-Tetradecane	$CH_3(CH_2)_{12}CH_3$	198	5–6	0	227
n-Pentadecane	$CH_3(CH_2)_{13}CH_3$	212	10	5	205
n-Hexadecane	$CH_3(CH_2)_{14}CH_3$	226	18–19	17	237
n-Heptadecane	$CH_3(CH_2)_{15}CH_3$	240	22	22	171
n-Octadecane	$CH_3(CH_2)_{16}CH_3$	254	28	25	242
n-Nonadecane	$CH_3(CH_2)_{17}CH_3$	268	32–33	27	222
n-Eicosane	$CH_3(CH_2)_{18}CH_3$	282	36–37	31	247
n-Heneicosane	$CH_3(CH_2)_{19}CH_3$	296	39–41	32	201
n-Docosane	$CH_3(CH_2)_{20}CH_3$	310	42–45	43	157
n-Tricosane	$CH_3(CH_2)_{21}CH_3$	324	48.9	51	142
n-Tetracosane	$CH_3(CH_2)_{22}CH_3$	338	50–51	48–49	160
n-Pentacosane	$CH_3(CH_2)_{23}CH_3$	352	54	47	164
n-Hexacosane	$CH_3(CH_2)_{24}CH_3$	366	56	53–54	255
n-Heptacosane	$CH_3(CH_2)_{25}CH_3$	380	59	53	159
n-Octacosane	$CH_3(CH_2)_{26}CH_3$	394	61	54	202

Despite desirable properties, the heat dissipation rate is generally slow due to the low thermal conductivity. This is a major disadvantage limiting the implementation of paraffin wax in engineering applications. In order to overcome this drawback, several techniques were investigated such as integration with high thermally conductive fillers (carbon-based filler [33] or ceramic-based filler [34]) and immersing on porous graphite matrix [35].

2.3.2.1.2. Fatty acids

Fatty acids, naturally occurring vegetable and animal oils are purified and subsequently separated in the form of $CH_3(CH_2)_{(n-2)}COOH$, and are listed in Table 2-2. Fatty acids have been introduced due to the interests in renewable resources.

Table 2-2 Solid-liquid phase change thermal properties of the fatty acids with the number of C atoms ranging from 4 to 23 [32]

Chemical formula	IUPAC name	Common name	Melting temperature /◦C	ΔH_{fus} /kJ·kg^{-1}
$CH_3(CH_2)_2COOH$	n-Butanoic acid	Butyric acid	−5.6	126
$CH_3(CH_2)_4COOH$	n-Hexanoic acid	Caproic acid	−3	131
$CH_3(CH_2)_6COOH$	n-Octanoic acid	Caprylic acid	16–17	148–149
$CH_3(CH_2)_8COOH$	n-Decanoic acid	Capric acid	30–32	153–163
$CH_3(CH_2)_{10}COOH$	n-Dodecanoic acid	Lauric acid	41–44	178–183
$CH_3(CH_2)_{11}COOH$	n-Tridecanoic acid	Tridecylic acid	41.4	154
$CH_3(CH_2)_{12}COOH$	n-Tetradecanoic acid	Myristic acid	49–58	167–205
$CH_3(CH_2)_{13}COOH$	n-Pentadecanoic acid	Pentadecanoic acid	52–53	178
$CH_3(CH_2)_{14}COOH$	n-Hexadecanoic acid	Palmitic acid	61–64	186–212
$CH_3(CH_2)_{15}COOH$	n-Heptadecanoic acid	Margaric acid	60	172.2
$CH_3(CH_2)_{16}COOH$	n-Octadecanoic acid	Stearic acid	65–70	196–253
$CH_3(CH_2)_{17}COOH$	n-Nonadecanoic acid	Nonadecylic acid	67	192
$CH_3(CH_2)_{18}COOH$	n-Eicosanoic acid	Arachidic acid	n.a.	n.a.
$CH_3(CH_2)_{19}COOH$	n-Heneicosanoic acid	Heneicosylic acid	73–74	193
$CH_3(CH_2)_{21}COOH$	n-Tricosanoic acid	Tricosylic acid	79	212

n.a., non-available.

The long-term availability of natural-based rather than petroleum-based paraffin wax has been of interest to the scientific community. Fatty acids share many phase change characteristics with organic paraffin wax including low thermal conductivity and high volumetric expansion on melting. However, they have lower latent heats of fusion when compared to paraffin wax with similar melting temperature ranges [31, 32].

2.3.2.2. Inorganic PCMs

Hydrated salts are solid solution of salts and water, and are defined as a chemical form of $M{\cdot}nH_2O$, where M is the salt molecule and n represents the number of water molecules in solid solution [31]. The phase change process of hydrated salts involves the dehydration and rehydration processes. Hydrated salts are one of the common phase change materials that have been studied due to their high volumetric storage density (~350 MJ m^{-3}), relatively higher thermal conductivity in comparison to organic PCMs and lower cost [23]. On the other hand, they exhibit semi congruent melting or incongruent melting due to the nature of multi-constituent materials. During the dehydration process, the phase separation of salt and water solution or a similar salt hydrate with a lower order of water molecules can be formed. In addition, phase segregation can be developed during repeated thermal cycling, which will reduce the thermal performance (reduction of latent heat). In general, the phase segregation and subcooling effects have limited the implementation of hydrated salts as phase change materials [31]. In order to overcome these problems, excessive water is often added to prevent phase segregation [22] or the thickening agents are used to improve long-term phase change stability [36].

2.3.2.3. Eutectic

Combination of organic-organic/ inorganic-inorganic/ organic-inorganic PCMs can be compounded to create the eutectic PCMs. Mixtures of fatty acids are less attractive since commercially manufactured fatty acids can generate strong odours. Some examples of eutectic PCMs can be found in Ref. [37].

2.3.3. Integration methods

2.3.3.1. Direct incorporation

Direct impregnation is the simplest technique to integrate PCMs into composite matrices. PCMs have been directly mixed with several construction materials such as gypsum, cement paste, mortar and concrete [38, 39]. However, the leakage of the PCM may affect the durability of the system, and the mechanical properties [40].

2.3.3.2. Shape-stabilised PCMs

The adoption of PCMs has been limited by the associated leakage problem during the solid ↔ liquid phase change. One solution to prevent the leakage of PCMs on melting is to blend them with compatible polymers such as high-density polyethylene (HDPE), styrene and butadiene. The supporting material and PCMs are melted and mixed at high temperature followed by the cooling till their glass transition temperature where the support material becomes solid [41].

Feldman *et al.* [42] investigated the form-stable materials based upon polymers and fatty acids. HDPE was used as the structure polymer material. Those materials were mixed in a blender and then moulded into a tile shape, which was the size of 200 mm × 200 mm× 20 mm. In general, the samples maintained their dimensional stability at temperatures as high as 37 - 43°C dependent on the composition of the fatty acids.

Inaba and Tu [43] investigated the density, specific heat, latent heat and effective thermal conductivity of the shape-stabilised PCMs constituting the latent heat storage material, pentacosane ($C_{25}H_{52}$) and HDPE. Pentacosane and HDPE were melted and mixed at above their melting temperature. When the temperature of the shape-stabilized paraffin was below the crystallisation temperature of HDPE and over the melting temperature of the paraffin, the liquid state of paraffin can be held by solidifying HDPE. At this state, the shape-stabilised paraffin can be kept in a solid without leakage with the aid of HDPE in solid. In order to reduce the leakage rate of the paraffin from the shape-stabilized composition, thermal cycling (melting and solidification process) was repeated and also low crystallinity and high viscosity resin such as ethylene-α olein was added to the paraffin as surfactant for enhancing compatibility. The composition of the samples were paraffin 74 wt.% and HDPE 26 wt.%. Experimental data from differential scanning calorimeter (DSC) showed that the measured latent heat of the samples was linearly proportional to the wt.% of dispersed paraffin.

2.3.3.3. Macroencapuslation

Plenty of PCMs can be contained in tubes, spheres, and panels for structural applications. The advantages of this technique are the container can be acting as an environmental barrier, and easy of handling.

Lazaro *et al.* [44] investigated the latent heat storage for free-cooling application in building incorporating PCMs. They prepared the real scale experimental set up with two types of heat exchangers based on encapsulated PCMs as shown in Fig. 2-2. They found that using aluminium panels resulted in no leakage while the leakage was observed in the aluminium pouches due to the thermal expansion of PCMs on melting. The cooling power, which was estimated from air inlet and outlet temperature, was higher in the case of aluminium panels compared to the heat exchange system involving aluminium pouches.

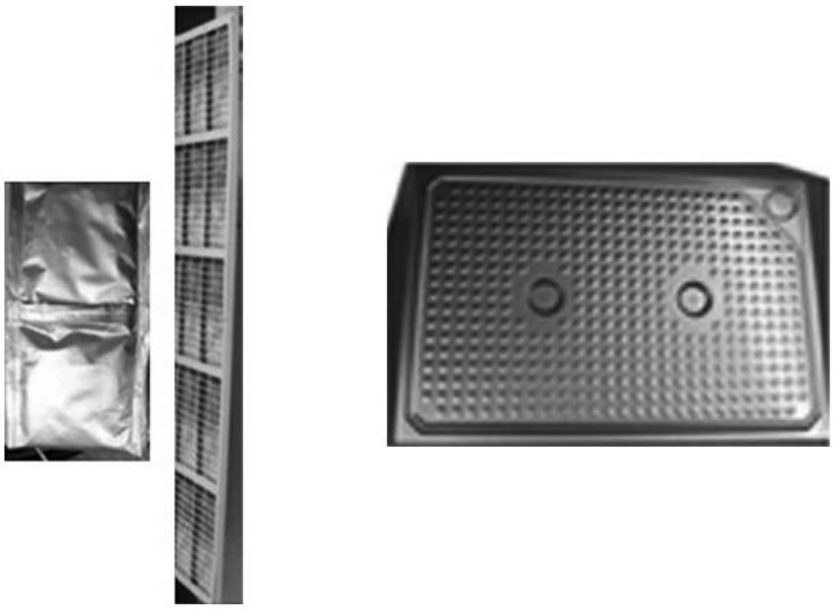

Figure 2-2 Prototype heat exchanger for free cooling application (a) aluminium pouches filler with organic PCMs and (b) aluminium panels filled with inorganic PCMs [44]

2.3.3.4. Microencapsulation

The microencapsulation is the process that solid particles, liquid droplets or gas bubble are coated in the thin solid shell material, of particle sizes between 1μm to 1,000 μm. The shell material of microcapsules can be manufactured through a variety techniques mainly classified under physical and chemical methods [41]. Further information can be found from open literature [45]. The main purpose of microencapsulation is to prevent the leakage of PCMs from the composite structure during the solid ↔ liquid phase transition [46]. In addition, microencapsulation is capable of resisting volume change during phase transition, and the thermal conductivity can be improved due to the increase in surface area per unit volume.

Hawlader *et al.* [47] assessed the performance of microencapsulated PCMs. The microcapsules were prepared by the coacervation technique. Thermal cyclic tests were conducted with a cyclic variation of temperature in a dryer from 500 - 1000 cycles. They found that the original geometrical profile could be maintained after 1000 thermal cycles as

shown in Fig. 2-3. These results indicated that the thermal energy storage capacity could be sustained in the microcapsule.

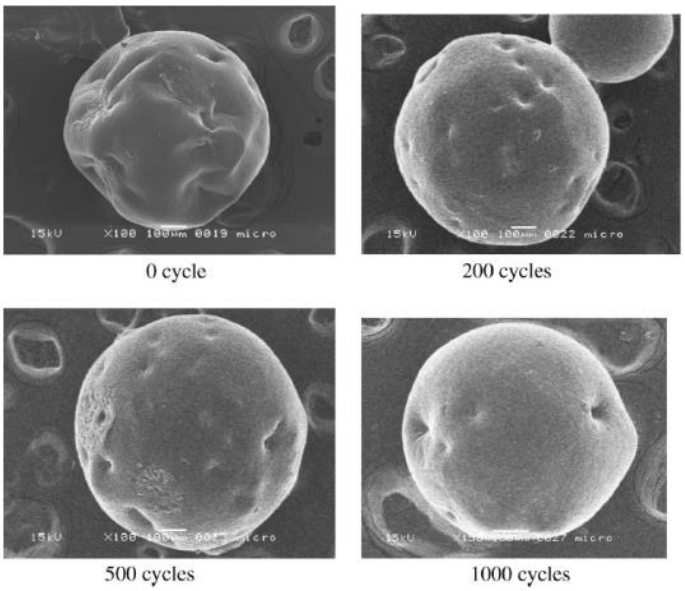

Figure 2-3 Microencapsulated paraffin profile evaluated by SEM at different thermal cycles [47]

2.4. Effect of spherical inclusions on mechanical properties

2.4.1. Introduction

In this section, the influences of inclusion on mechanical properties of polymer matrix composite have been reviewed. The inclusion effect due to the presence of the micro-sized fillers has been explored especially in the area such as toughening of polymer, and self-healing polymer. The elastic modulus of a composite is generally determined by the elastic properties of its individual components (the particle and matrix), concentration and particle size. On the other hand, strength shows a high dependence on the stress transfer between the particle and the matrix. Thus, in the case of well-bonded particles, the applied stress can be effectively transferred to the particles from the matrix. The interfacial strength and particle loading/size also affect the strength of the composite [48].

2.4.2. Tensile properties

Several studies on the influence of rubber [49, 50], thermoplastic [51-53] glass microsphere [54-57] fillers on polymer properties have been reported. It is known that the volume fraction and the size of the particle are the major factors influencing the tensile properties. For example, the effect of hollow glass microspheres on the tensile properties of particulate composite is abundant. Spanoudakis and Young [58] reported the dependence of the modulus of the epoxy resin reinforced with spherical glass particles upon the particle loading and size. The Young's modulus was almost identical for lower volume fraction (10-18 %) of glass particles while there was a slight decrease observed in higher particle loading (30-46 %). Also, the smallest particle size showed the highest modulus for a given volume fraction.

In another study by Cho *et al.* [59], the effect of inclusion size on particle-reinforced composites with micro- and nanoparticles was investigated; spherical glass beads and alumina particles, respectively. In the case of glass beads, it was found that the Young's modulus was insensitive to the particle size at lower volume fractions. However, as the volume fraction increased, slight reductions in the modulus of elasticity were observed. They concluded that the particle loading was a significant factor in determining the composite's modulus of elasticity. There was a threshold loading level where the Young's modulus became particle-size independent.

Wouterson *et al.* [60] reported the specific tensile properties of the epoxy incorporating two glass microspheres (different size) and hollow phenolic microspheres by varying the volume fraction. The tensile strength decreased with increasing microsphere concentration regardless of the type of microsphere due to the reduction of the volume fraction of epoxy, and the increasing inhomogeneity. Consequently, the tensile strength decreased as a result of poor interfacial strength between the matrix and the filler. On the other hand, the Young's modulus changed with the type of inclusion. The Young's modulus decreased when the smaller glass

and phenolic microsphere were used whereas that of the larger glass microspheres was increased. They assumed that the difference between the results of glass microspheres could be attributed to their size and thickness-to-radius ratio.

The effect of particle/matrix interfacial adhesion on the tensile behaviour was investigated by Dekkers and Heikens [61]. They experimentally investigated the tensile behaviour of polystyrene (PS)/glass beads. In order to study the effect of interfacial adhesion between glass-beads and polystyrene, the glass beads were surface treated with two different silane coupling agents. It was observed that the Young's modulus was hardly affected by the degree of interfacial adhesion. In contrast, the composite strength decreased with increasing glass content and was lower than that of the PS. This observation was due to the fact that, for the samples with larger beads concentration, more crazes readily formed than in the case of lower beads concentration. This indicated that as the craze density becomes extensively large, glass beads lose the controllability of craze growth. They concluded that interfacial adhesion has a little effect on the Young's modulus of particulate-filled composites. Moreover, craze formation at the glass beads due to the applied tensile stress is determined by the degree of interfacial adhesion. In the case of poor interfacial adhesion, de-wetting along the phase boundary causes extra stress concentration. Thus, crazes can form at lower stress levels.

The effect of a polymeric core-shell microsphere on tensile properties was studied by White *et al.* [62]. They studied the autonomic healing concept by incorporating a microencapsulated healing agent and a catalytic chemical trigger within an epoxy matrix. They found that the relative stiffness of the microcapsule on the propagation path was a key parameter on the mechanical triggering process. Fig. 2-4 represents the stress state of vicinity of crack tip and sphere itself is strongly affected by relative stiffness of sphere to matrix. In the case of stiffer inclusions, the crack is deflected away from the inclusion while the opposite is true in the case of compliant spherical inclusion.

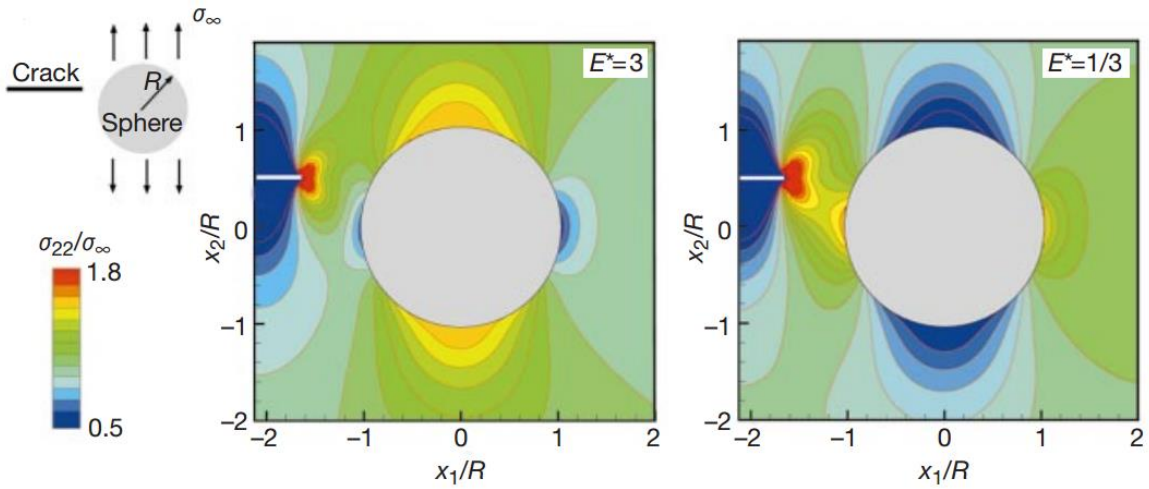

Figure 2-4 Stress state in the vicinity of a planar crack as it approaches a spherical inclusion embedded in a linearly elastic matrix and subjected to a remote tensile loading perpendicular to the fracture plane. The left and right figures correspond to an inclusion three times stiffer $E^* = E_{sphere}/E_{matrix} = 3$) and three times more compliant ($E^* = 1/3$) than the surrounding matrix, respectively. The Poisson's ratios of the sphere and matrix are equal (0.30) [62]

In addition, a similar experiment on self-healing microcapsule was conducted by Tao *et al.* [63]. They reported the study of self-healing woven glass/epoxy composite. The result of tensile stress-strain curves of the composites incorporating the microcapsules showed the earlier appearance of the knee point for higher microcapsule content laminates. This may suggest that the microcapsules could behave like stress concentration raisers when the cracking initiated at the interface. In their study, they reported a dependence of the Young's modulus and the tensile strength on the microcapsule content. The stiffness of the samples decreased with increasing the weight fraction of microcapsule due to the lower stiffness of the microcapsules. Moreover, it was found that a significant drop in the strength of the composites occurred at 20 wt. % of microcapsules. They claimed that this might relate to the change of the matrix viscosity. Further addition of the microcapsules significantly increased the viscosity, and this deteriorated the impregnation and interfacial coupling as increased porosity was observed in the laminate with 30 wt.% of microcapsules.

Mochane and Luyt [64] studied the influence of polystyrene (PS):wax microcapsule on tensile properties of the polypropylene (PP) composite. The tensile strength decreased with

increasing PS:wax content due to the weak interfacial interactions between the filler (PS:wax microcapsule) and matrix. In addition, the Young's modulus of modified composite was lower than that of neat resin.

2.4.3. Compressive properties

It is clear that the mechanical properties of the microsphere embedded composite are affected by particle size, particle concentration and the interfacial adhesion. It is interesting to note that the influence of the particle size on compressive properties was different to tensile properties Wouterson *et al.* [60] reported the specific compressive properties of syntactic foam. The microstructures of syntactic foams, manufactured with two glass microspheres (different size) and hollow phenolic microspheres with varying volume fraction was investigated. They investigated the effect of the wall thickness of microsphere and filler concentration on compressive properties. The large size glass microsphere (average wall thickness is 1.37 μm) was superior to that of small size glass microsphere (average wall thickness is 0.70 μm) regarding compressive properties. The compressive yield strength and moduli of large glass microspheres increased with increasing filler content whereas that of the small sized glass and phenolic microspheres decreased.

The influence of the type of particle was studied by Bagheri and Pearson [49] where they investigated on the role of particle cavitation in toughening. The comparative examination of epoxies modified by conventional rubber modifiers and hollow plastic particles was performed. They found that the conventional rubber modifiers and small hollow plastics particles (≤ 15μm) toughened epoxies with shear yielding at the crack tip. In the case of a larger hollow particle (40μm), the mechanism of microcracking was observed as well as shear yielding. The compressive yield stress in toughened epoxies decreases linearly with increasing volume fraction of the modifier. They claimed that the pre-cavitated, hollow,

plastic particles and the non-cavitated, rubber particles had a similar influence on the yield stress of the blend due to their stress concentration effect. Furthermore, Bunn and Mottram [63] reported the effect of phenolic microspheres on compressive properties. Phenolic microspheres filled epoxy composite was manufactured by varying the volume fractions. The compressive strength decreased from 71 to 28 MPa with the maximum microballon concentration (~53%). The compressive modulus changed from 2.7 to 0.8 GPa. The compressive properties revealed a fairly linear relation with the volume fraction of microballon.

2.4.4. Flexural properties

The behaviour of flexural properties of particulate composite incorporating microsphere is a mixture of tensile and compressive properties. In the related experimental work by Wouterson *et al.* [60], they reported the specific flexural properties of syntactic foam. The syntactic foams were manufactured with two glass microspheres, which had different wall thicknesses and hollow phenolic microspheres by varying the volume fraction. The flexural properties (yield strength and moduli) decreased with increasing filler concentration. This result shows a similar behaviour under tensile properties as discussed in section 2.3.1 because they showed a similar failure mode. In particular, the flexural strain was reduced with increasing filler contents. The syntactic foams incorporating hollow phenolic microspheres showed larger plastic deformation compared to glass microspheres due to the ductile deformation from the polymeric microsphere.

Tagliavia *et al.* [65] studied the flexural properties of hollow glass microsphere filled vinyl ester composite. The effect of wall thickness and volume fraction of hollow inclusion was investigated. The wall thickness strongly influenced the flexural modulus. The modulus of the composite contains thin-walled particle decreased with the increase in the volume fraction.

The trend was opposite in thicker-walled particle composite. In addition, it was found that the flexural strength decreases as the inclusion volume fraction increases and is independent of the inclusion wall thickness. These observations are similar to the results from the aforementioned literature regarding a flexural testing of the composite incorporating hollow glass microsphere.

2.4.5. Fracture toughness

There are several investigations of the fracture behaviour of microcapsules such as hollow glass microsphere [55-57, 66] and polymer microcapsule [67, 68] filled polymers. The increase in toughness by inorganic particles (e.g. glass microsphere) can be explained by the crack front bowing mechanism. Although the particle toughening mechanism is still arguable, the results from these investigations agree with toughening of polymer by 'crack pinning' and 'debonding', which triggers matrix plastic deformation.

Lee and Yee [66] studied the fracture behaviour of inorganic particle filled polymers. Glass bead filled epoxies having different glass bead contents and sizes were prepared to understand the fracture behaviour. They reported that three general trend of the effects of volume fraction and size of glass beads on fracture behaviour. Firstly, the fracture toughness of composites increases with the increasing the volume fraction of glass beads. Secondly, the incremental toughening effect diminishes with increasing volume fraction. Thirdly, the larger particle filled epoxy showed a higher toughness than smaller particle filled epoxy since the size of filler was found to have secondary effects on the fracture toughness. They found that the increase of debonding zone size, micro-shear band zone size, and the number of steps per unit length were noticed as glass bead content increase. The tensile moduli and fracture toughness increased with the increasing glass bead content.

Brown *et al.* [68] reported the toughening mechanism by embedded silica and polymer microcapsules. They found that the polymer microcapsules increased toughness by 127% at a concentration of 11 vol. % while the maximum toughness of 87 % was obtained from silica microspheres. The inclusion of silica microcapsule arrested the crack growth, then the crack propagates along the interface when sufficient energy is applied. On the other hand, the fracture behaviour of polymer microcapsule was somewhat similar to that of rubber toughened epoxy such as debonding and cavitation.

2.5. Effect of spherical inclusions on thermophysical properties

2.5.1. Introduction

Microstructural parameters such as different particle sizes, volume fractions, shapes and topologies are to determine the properties of the composite material. In this section, the thermophysical properties such as thermal conductivity and coefficient of thermal expansion of micro-size spherical filler embedded in the polymer were reviewed.

2.5.2. Phase change transition

When the phase change material melts or solidifies at a constant temperature, large amounts of thermal energy is stored or released as shown in Fig. 2-5. Thus, the effectiveness of the thermal management system using latent heat storage is strongly dependent on the phase transition properties. Microencapsulation prevents the leakage of PCMs during the phase transition from solid to liquid. In particular, organic PCMs have received greater attention amongst PCMs due to inherent problems with the inorganic PCMs such as supercooling and phase segregation during the phase transition [69]. The phase transition of paraffin wax (*n*-alkane) is depending on the molecular length. Even number *n*-alkane show only one solid-liquid transition when the number of carbon atoms is less than 20, whereas other *n*-alkane

(odd number larger than 15 or even number bigger than 20) show several stable and partially ordered phases. The partially ordered phase known as rotator phase is the intermediate phase between isotropic liquid and fully ordered crystalline phases [70]. Thus, the phase behaviour of microencapsulated organic PCMs is determined by the intrinsic features of a core material. The information on solid-solid transition in crystallisation through the metastable rotator is significantly important as it is associated with the phase change efficiency [71].

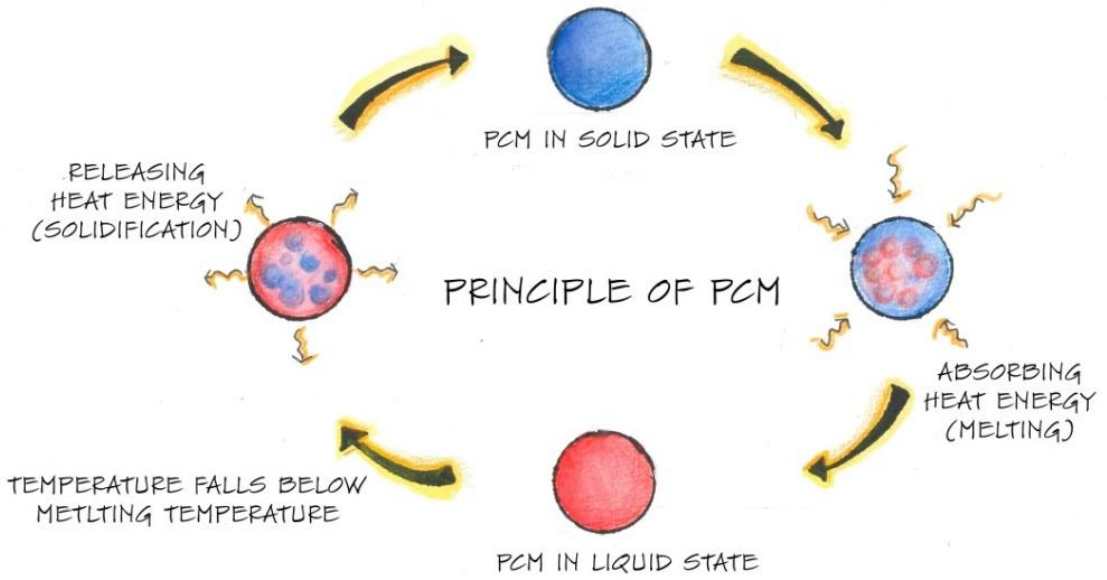

Figure 2-5 The principle of phase change materials (PCMs)

Zhang *et al.* [72] investigated the effect of micro-PCMs in gypsum for thermal regulation capabilities as a building material. The phase change behaviour was examined using Differential scanning calorimetry (DSC), and it was found that the integrity of micro-PCMs was not affected by the mixed gypsum and glass fibre.

Sari-Bey *et al.* [70] investigated the thermophysical properties of polycaprolactone (PCL) composite containing microencapsulated PCMs (Micronal® DS 5001 X). The phase change properties of the composite incorporating microencapsulated PCMs were investigated using DSC. It was found that the onset temperature remained the same, and the enthalpy of the composite was proportional to the weight fraction of microencapsulated PCMs used in the

composite. Furthermore, similar observations were reported by Krupa *et al.* [73]. They found that the phase change properties of microencapsulated PCMs remained after embedding in the polymer matrix as shown in Fig. 2-6.

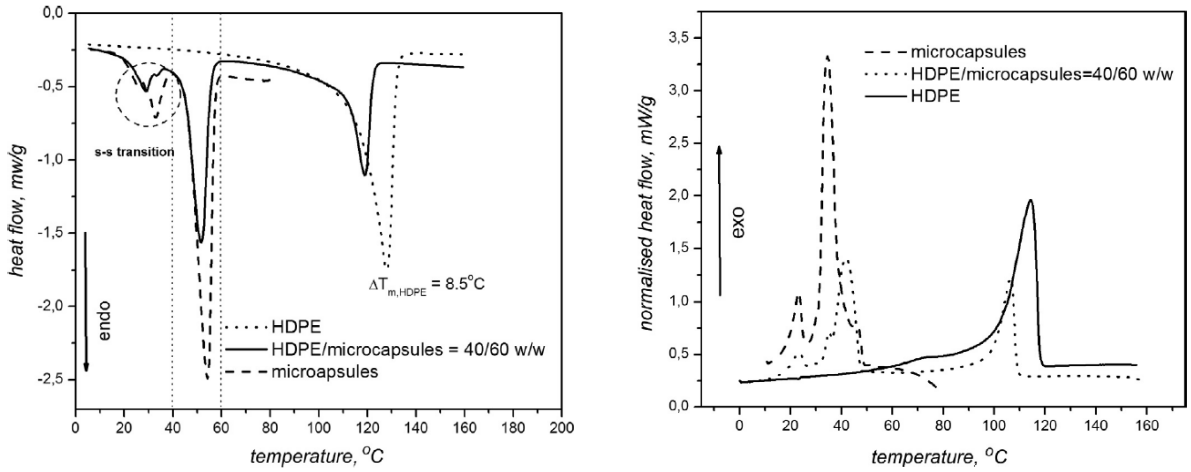

Figure 2-6 DSC (a) heating and (b) cooling curves for neat HDPE, neat microcapsules and HDPE/microcapsules = 40/60 w/w mixtures; blended [73]

DSC is the most commonly used instrument to study thermal analysis of phase change materials. However, there is a concern that the measured data is not representative of the bulk material given the minimal specimen sizes applicable to this technique. The determination of the heat storage capacity through DSC is intrinsically difficult due to inhomogeneity at the test sample size. Therefore, new methods have been developed to provide useful thermal storage data representative of dimensionally larger scale samples [74]. For example, the sample is sandwiched with heat exchange plates, tangential gradient flux meters and thermocouples. Then, experimental set-up is insulated to be a 1-D heat transfer problem. The apparent heat capacity and thermal conductivity can be evaluated by measuring the heat flux and the temperature on each side of the specimen [75, 76].

2.5.3. Thermal stability

Thermal stability of microencapsulated phase change material has been studied [77-79]. For example, Mochane and Luyt [64] prepared the microencapsulated paraffin wax with polystyrene (PS) as a shell material, and embedded in the polypropylene (PP) composite. Thermal stability was investigated using Thermogravimetric Analysis (TGA) as a function of weight fraction of microcapsule. The two-step degradation was observed in PS:wax microcapsules due to different decomposition behaviour of wax and PP. These weight loss processes were attributed to the initial decomposition of *n*-alkane and latter weight loss of the shell material [80, 81]. The first weight loss could be the evaporation or decomposition of core material, which diffuse out of shell rather than caused by the fracture of the microcapsule [82].

Furthermore, the thermal stability of microcapsule filled PP composites deteriorated with an increase in PS:wax microcapsule as a result of free radicals introduced due to the inclusion of microcapsule [64]. Tong *et al*. [83] worked on the surface modification of poly(melamine-urea-formaldehyde) microcapsules. The interfacial performance between the matrix and microcapsules of the composite (unsaturated polyester) were studied. They found that the surface modification on the microcapsule improved the thermal stability as a result of the improvement on the intermolecular forces and compatibility between the matrix and microcapsule.

2.5.4. Thermal conductivity

The effective thermal conductivity of the composite is affected by several parameters including geometry, thermal conductivity of the different constitutes, distribution within the medium and contact between fillers [84]. The heat transfer in non-metals occurs by phonons or lattice vibrations. The scattering of phonons in the composite material should be

minimised to maximise thermal conductivity. The phonon scattering is mainly due to the interfacial thermal barriers resulting from acoustic mismatch and interfacial flaws from different constituent phases [85]. When the spherical filler is embedded in the polymer, the thermal conductivity of the composite is function of the thermal conductivity of the filler and the matrix.

Kumlutaş *et al.* [84] reported the effective thermal conductivity of spherical aluminium filler high density polyethylene (HDPE) composite was investigated numerically and compared with experimental results and theoretical models. It was observed that the thermal conductivity of the composite increased with increasing volume fraction of aluminium filler due to the much higher thermal conductivity of aluminium (204 W m^{-1} K^{-1}) compared to that of HDPE (0.543 W m^{-1} K^{-1}). The study on thermally conductive polymer composite incorporating spherical metal fillers can be also found [86-88]. On the other hand, the effective thermal conductivity of the composite reduced with hollow glass microsphere (HGM) owing to its low thermal conductivity. Furthermore, Liang and Li [89] studied the effect thermal conductivity of HGM filled polypropylene (PP) composite. It was observed that the thermal conductivity decreased almost linearly with increase the volume fraction of HGM. The opposite trend was observed in the particle diameter. The similar observations on ceramic microsphere (glass microsphere) can be found [90, 91].

Karkri *et al.* [92] reported on the thermal properties of microencapsulated paraffin wax filled high-density polyethylene (HDPE) using an in-house experimental set-up (transient guarded hot plate). The microcapsule was prepared with paraffin wax, and melamine-formaldehyde as a shell material. The thermal conductivity of the composite was measured as function of particle concentration at room temperature. It was found that the thermal conductivity of the composite reduced when the concentration of the microencapsulated wax increased. Similar observations were reported in Ref. [70]. Furthermore, Salaün and Vroman [93] worked on the

influence of core material in thermal properties of microcapsules. They found that the chemical structure of the polymeric shell material on the microcapsule determined the thermal conductivity.

2.5.5. Coefficient of thermal expansion (CTE)

Holliday and Robinson [94] reported that the thermal expansion behaviour of the composite involves the stress transfer across an interface and elastic properties (i.e. Young's modulus) of the constituents. Consider a two phases composite, in which each phase is isotropic and homogeneous. The CTE for the matrix is defined as α_m and that for the dispersed inclusions as α_f. In the case where $\alpha_m > \alpha_f$, the matrix will expand more than the inclusions under heating, creating residual the thermal stress. The overall CTE of the composite can therefore be reduced if the matrix/inclusion interfaces are adequately capable of transmitting the stress. In addition, individual constituents with different CTE can give rise to elastic strains with changing temperature. The overall composite CTE is somewhat different from a simple calculation based on the rule of mixture. This suggests that the overall composite CTE reflect the relationship between the elastic moduli and thermal expansion of the composite constituents [95].

The inclusion effect of hollow glass microsphere filled epoxy composite was studied by Yung *et al.* [96]. They investigated the influence of HGM on thermal expansion behaviour of the composite. The coefficient of thermal expansion (CTE) decreased by more than 50% when the volume fraction of HGM was 0.51. In addition, the glass transition temperature (T_g) increased with the increase of volume fraction of HGM from 98°C to 136°C. The authors attributed the increasing in the glass transition temperature to the strong interaction between the filler and the matrix. Furthermore, Shunmugasamy *et al.* [97] reported on the CTE of a vinyl ester composite containing hollow glass particles. The variation in the composite CTE

with the wall thickness and volume fraction of the filler particles was investigated. It was found that of the variation in the volume fraction had a greater influence on the composite CTE than the wall thickness of the filler. The CTE of the composite reduced up to 60% at the highest glass content level in comparison to of the neat resin. It was clear that the inclusion of glass microsphere reduced the overall CTE due to the inherently lower CTE values for ceramic-based materials.

On the other hand, Yusriah *et al.* [98] investigated the effect of hollow phenolic microspheres and woven fabric on vinyl ester composite. The CTE for composite systems reinforced by varying woven fabrics and also containing 5 wt.% of microsphere was measured between 25°C to 165°C. It was found that the CTE decreased with addition of woven fabric due to the low CTE values of fabric compared to that of vinyl ester. The further decrease on the CTE was observed with inclusion of microspheres. The authors attributed this observation to the restricted molecular chain movement of matrix as the microspheres occupied the free volume in the composite.

2.5.6. Viscoelasticity

When the material is subjected to sinusoidal oscillating stresses, the strain is neither in phase with the stress (perfectly elastic solid) nor 90° out of phase (perfectly viscous liquid). The strain is out of phase with the applied stress by the phase angle, δ. Some of the applied stress is stored as potential energy in each cycle, and some is dissipated as heat upon deformation and this phenomenon is called viscoelastic. The structure of metals shows a small deviation from perfect elasticity whereas the mechanical behaviour of polymer is dominated by the viscoelastic phenomena [99, 100]. The viscoelastic behaviour of polymeric materials provides the information on the nature and the rates of the configurational rearrangements, and interaction of macromolecules. Dynamic Mechanical Analysis (DMA) has been widely

employed for investigating the viscoelastic behaviour of polymeric materials due to its accuracy. Owing to the viscoelastic nature of polymeric material, the modulus is significantly reduced at temperatures higher than the T_g. Segmental molecular chains gain enough mobility to slide past each other hence the transition from glassy to rubbery state above the T_g,. The T_g represent a major transition for the polymer as physical properties change drastically. It defines the maximum operating temperature of a given polymer as the upper limit for use. As a result, the investigation on the polymer based on viscoelastic properties provides the information to determine the operating rage of a polymer as shown in Fig. 2-7 [100].

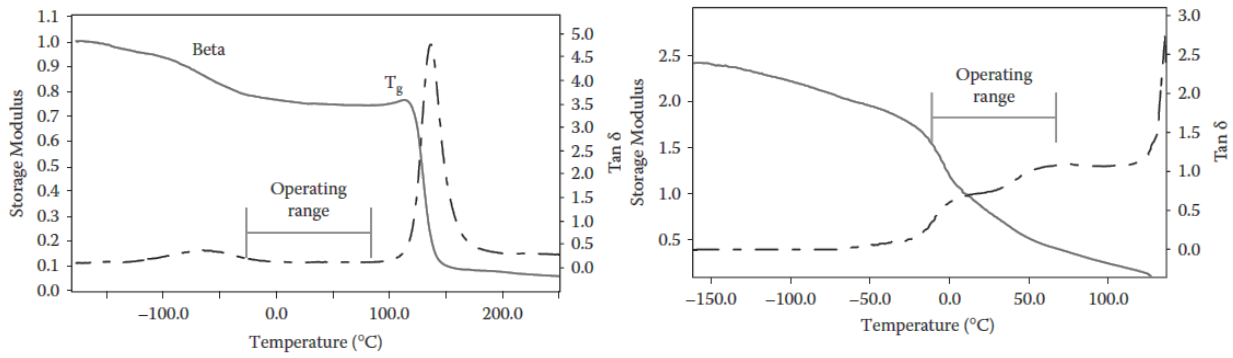

Figure 2-7 Definition of an operating range based on the position of T_g in (a) epoxy and (b) polypropylene [100].

The viscoelastic properties of the composite with different types of microsphere embedded in polymer have been reported [101-104]. For example, Liang *et al.* [105] investigated the dynamic mechanical properties of hollow glass microsphere filled thermoplastic composite. The HGM filled polypropylene (PP) composite was examined using the DMA. The results showed that the storage modulus (E') and loss modulus (E'') were increased with the increasing volume fraction of HGM. On the other hand, the mechanical damping (tan δ) did not reveal significant changes. Also, the glass transition temperature slightly increased with filler concentration. In regards to the filler size, the larger filler showed higher dynamic moduli than the smaller filler.

Mochane and Luyt [64] prepared the microencapsulated paraffin wax with polystyrene (PS) as a shell material and embedded in the polypropylene (PP) composite. The influence of PS:wax microcapsule on thermal and mechanical properties of the composite was investigated. The results of DMA scans revealed that storage modulus (E´) decreased with increasing the contents of PS:wax microcapsule. The melting of the wax was observed as well as other relaxations. The T_g was moved to the lower temperature when compared to that of PP.

2.6. Summary

As evident from the limited studies available in the literature, the integration of the micro-PCMs into FRP composite laminates to achieve both thermal management and structural functionalities has not been addressed comprehensively. Although several studies have reported on the inclusion effect of different microcapsules in polymer matrices, the failure mechanisms associated with the presence of micro-PCMs in FRP composites have not been adequately addressed in the open literature. It was clear that adhesion between the polymer matrix and filler is critical to determine the strength of the composite. The volume of PCMs can be affected by temperature changes causing the degradation of the interface during the solid ↔ liquid phase transition. However, the influence of the volume change on micro-PCMs has not been addressed in the determination of mechanical and thermophysical properties since the adhesion is crucial.

In regards to the thermophysical property, a majority of open literature has dealt with phase change properties/thermal stability of the composite incorporating micro-PCMs. The volume fraction is a principle parameter to determine the thermophysical properties. Thermophysical properties of the composite are strongly determined from the thermal conductivity of individual phase (the matrix and the filler). The interface between the filler and the matrix is

a key issue regarding thermophysical properties. However, there is still a gap in the influence of the continuous fibre on micro-PCMs into FRP composite. Given the amount of open literature, the information on other factors including the CTE and viscoelasticity are still lack.

2.6.1. Material selection

Based on the literature review, the woven fabric and microencapsulated PCMs (organic PCMs) were chosen to be implemented in this project. The main reasons to select the woven fabric can be summarised as: (1) the balanced in-plane properties, and (2) micro-PCMs can occupy available spaces between individual tows to minimise the inclusion effect (see Figure 2-8). The advantages of using organic-based micro-PCMs are twofold. With the microencapsulation technology, PCMs are protected from the surrounding environment. In addition, the shell material prevents the leakage during phase transition. These characteristics of micro-PCMs along with their availability as a commercial product, promotes the integration capability of microencapsulated PCMs into another material systems

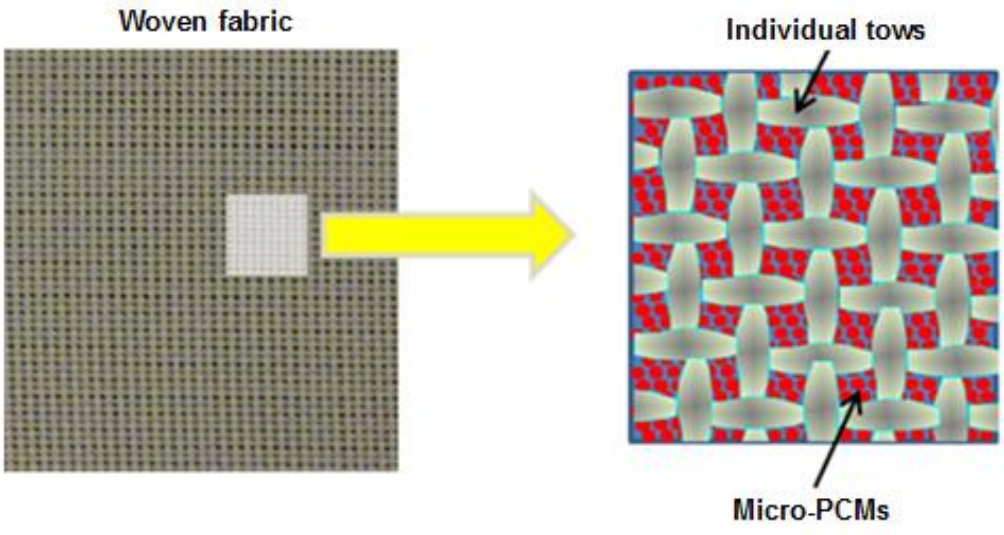

Figure 2-8 Micro-PCMs dispersion in available spaces between individual tows

3. EFFECT OF MICRO-PCMS ON MECHANICAL PROPERTIES OF MULTIFUNCTIONAL COMPOSITE

3.1. Introduction

As evident from the limited studies available in the literature, the integration of micro-PCMs into FRP composite laminates to achieve both thermal management and structural functionalities has not been addressed comprehensively. In order to develop FRP-incorporated multifunctional composites, it is necessary to fully understand the inclusion effect of micro-PCMs with respect to the mechanical properties of such composite laminates. Although several studies have been reported on the inclusion effect of different microcapsules in polymer matrices [67, 106-110], the failure mechanisms associated with the presence of micro-PCMs in FRP composites have not been adequately addressed in the open literature. This chapter reports an experimental study on the influences of incorporating micro-PCMs on the mechanical properties of glassfibre/epoxy composites.

3.2. Materials & Methods

3.2.1. Materials

A plain woven E-glass fabric (195 g m^{-2}) obtained from Colan Australia, Australia. Bisphenol F epoxy resin, RenLam® LY113, together with the corresponding amine-based hardener, RenLam® HY97-1, was purchased from Huntsman, Australia. Vinyl ester SPV 1265 and methyl ethyl ketone peroxide (MEKP) catalyst were supplied by Nuplex composite, Australia. Micro-PCMs (MPCM 37) were obtained from Microtek Laboratories Inc. The capsule composition was 85-90 wt.% Paraffin-based PCMs (*n*-Eicosane) and 10-15 wt.% polymer shell (melamine-formaldehyde) [111, 112]. The mean size of microcapsules was 18.5 ± 1.5 μm with melting temperature of 37°C and the heat of fusion of 190-200 J s^{-1}.

3.2.2. Fabrication of Epoxy/micro-PCMs composites

In order to study the effect of incorporating micro-PCMs on the mechanical properties of epoxy (LY113), specimens with 10, 20, 30, 40 and 50wt.% of PCMs microcapsules were manufactured. After adding pre-determined micro-PCMs to the epoxy resin, a mechanical mixer was used at 900 rpm for 30 min to achieve a uniform dispersion. The epoxy/ micro-PCMs slurry was then degassed for 30 min to eliminate any entrapped air before adding the hardener (HY113) at a weight ratio of 10:3. The epoxy/micro-PCMs/hardener mixture was briefly degassed for 3 min and then poured into a mould to be cured at room temperature for 24 hr. The panels were consequently post-cured according to the recommended thermal cycle provided by the supplier: 12 h at 40°C → 2 h at 60°C → 2 h at 80°C → 2 h at 100°C→ 12 h at 120°C. Tension samples of 250 mm length × 25 mm width according to ASTM D3039 and NASA short block compression coupons (52 mm length × 25 mm width) were then prepared.

3.2.3. Fabrication of Glass/Epoxy composite incorporating micro-PCMs

Plain woven E-glass fabric was used to fabricate composite specimens incorporated with micro-PCMs. Following the procedure mentioned above, the epoxy/micro-PCMs/hardener slurry was prepared and used to impregnate 16 layers of glass fabrics using wet hand lay-up method to achieve a fibre weight fraction of 60%. To study the effect of laminate configuration on mechanical properties of multifunctional composites, cross-ply $[0^o/90^o]_{8s}$ and quasi-isotropic $[0^o/90^o/\pm45^o]_{4s}$ specimens were manufactured. The laminates were vacuum-bagged and left to cure at room temperature for 24 hr followed by the post-curing cycle described in Section 3.2.2. Test coupons for tensile (250 mm length × 25 mm width), flexural (150 mm length × 25 mm width), short beam shear (18 mm length × 6 mm width) and NASA short block compression (52 mm length × 25 mm width) experiments were then cut using a diamond saw.

3.2.4. Fabrication of Double Cantilever Beam (DCB) specimen

To fabricate DCB specimens, micro-PCMs were added to the vinyl ester resin, and mixed for 1 hr followed by 1 wt.% application of MEKP as hardener. Test specimens were then manufactured using wet hand layup consisting of four layers of glass/vinyl ester incorporated with micro-PCM in the middle and 8 plies of conventional glass/vinyl ester plies on either side. A PTFE film (Teflon™) was inserted in the mid-plane of the laminate to provide an initial delamination length (a_o) of 50 mm. The laminates were then vacuum-bagged and left to cure at room temperature for 24 hr followed by post-curing at 120 °C for 2 hr. The test coupons were then cut into 170 mm long and 25 mm wide specimens using a diamond saw.

3.2.5. Characterisation techniques

Tensile testing was performed under displacement control at 2 mm/min using an Instron 5569 universal testing machine following the ASTM D3039-08 standard. In addition to load and displacement data, the tensile strain was recorded using an extensometer (Epsilon 3542) with a gauge length of 25 mm. Four-point flexural tests were also conducted on the same testing machine with a crosshead displacement rate of 1 mm/min, following ASTM D7264-07. The span-to-thickness ratio of 32:1 is suggested in the ASTM standard for a 4-mm thickness specimen. Since in this study, the average thickness of test coupons was 3 mm, therefore the support and loading spans were reduced to achieve a span-to-thickness ratio of 26:1. A linear variable displacement transducer (LVDT) was used to capture the out-of-plane flexural displacement at the mid-point of the specimen. Compression tests were conducted according to the NASA short block test standard [113] using the Instron 5569 universal test machine at a cross-head displacement of 0.5 mm/min. Compressive strains were also collected through an extensometer (Epsilon 3542) with a gauge length of 10 mm. Short beam shear (SBS) tests were performed according to the ASTM D2344-13 standard at a loading rate of 1.0 mm/min.

Since the specimen thickness varied with different micro-PCMs concentrations, an average thickness of 3 mm was used to determine the loading span length of 12 mm. This was based on the loading-span to thickness ratio of 4. It should be noted that the compressive strength was reported as the maximum stress instead of fracture strength. All tests were repeated at least three times and the average values are reported.

Mode I fracture toughness tests were conducted in accordance with ASTM D5528-13. A constant crosshead rate of 2 mm/min was used to open the crack until the crack length reached to 100 mm. Mode I interlaminar fracture toughness (G_I) was calculated using the Modified Beam Theory (MBT) method:

$$G_I = \frac{3P\delta}{2b(a+|\Delta|)} \qquad (3\text{-}1)$$

where P = load, δ = load point displacement, a = delamination length, b = specimen width, and $|\Delta|$ = a correction factor from cube root of compliance, $C^{1/3}$ as a function of delamination length. Surface morphologies of the fractured specimens were examined using a Scanning Electron Microscope (SEM), FEI Quanta 2000 ESEM operating at an accelerating voltage of 30 kV and spot size of 5. Prior to examination, the fractured specimens were gold coated using the SPI module sputter coater.

3.3. Results and Discussion

3.3.1. Epoxy/micro-PCMs composites

Fig. 3-1 illustrates the variation in specific tensile and compression moduli and strength of micro-PCMs-reinforced epoxy composites as a function of the weight fraction of PCMs microcapsules. It can be seen that the introduction of microcapsules resulted in a reduction of the specific strength and moduli under tensile and compression loading.

(a)

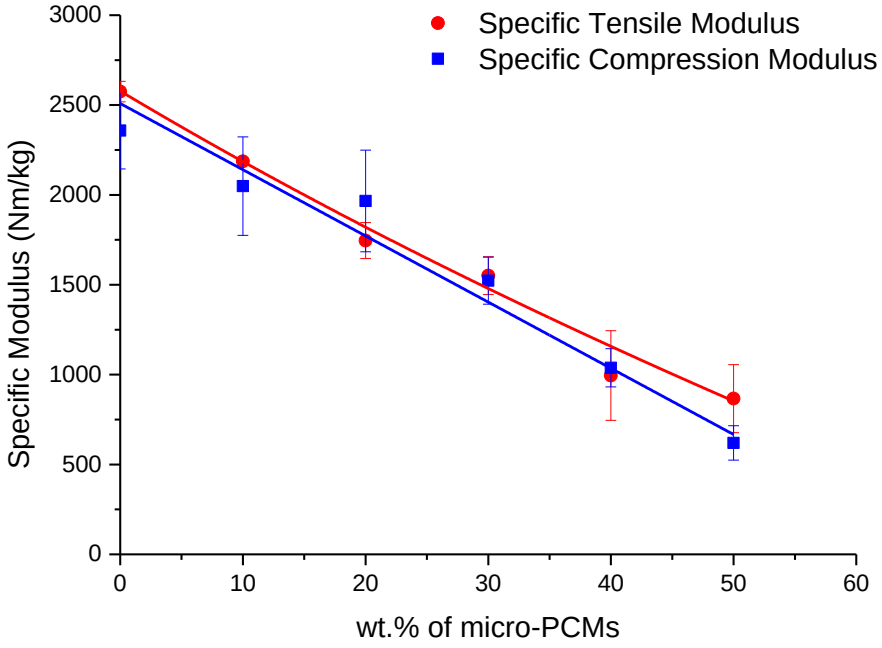

(b)

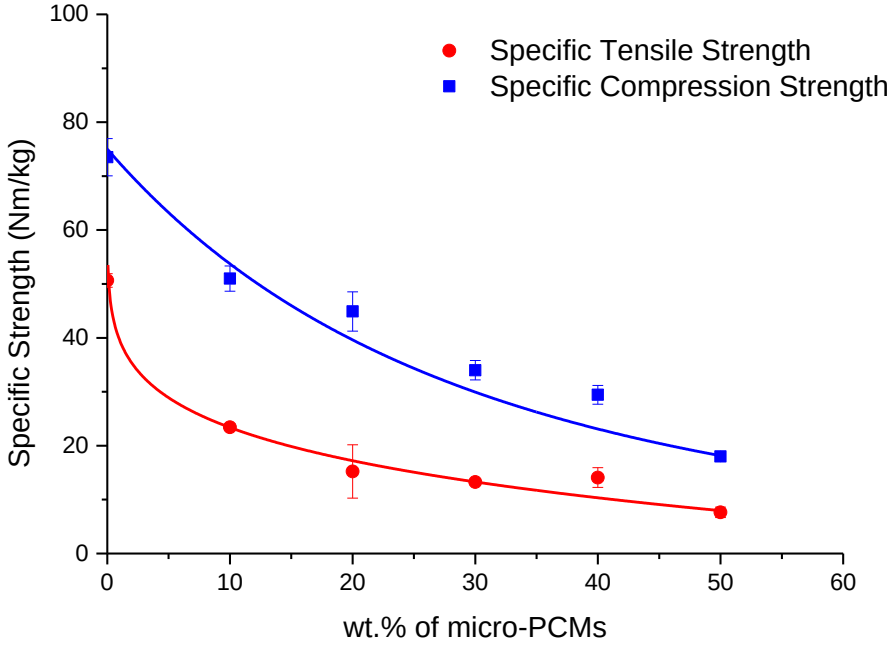

Figure 3-1 Effect of micro-PCMs loading on the (a) specific modulus and (b) specific strength of epoxy/ micro-PCMs composites

While the reduction of modulus is linearly proportional to the amount of microcapsule loading, the tensile and compression strength showed an exponential decay. Similar behaviour for other types of micro-PCMs-polymer composites was reported in [67, 92]. The reduction in elastic modulus can be explained by the fact that the variation of modulus in particulate-polymer composites is mainly controlled by the modulus of constitutive components and particle loading [48]. Since the modulus of micro-PCMs used in this study was not known an indirect approach was implemented to explain the elastic modulus reduction which was noticeably high in these composites.

Previous studies have shown that relative stiffness of the particle to that of the host epoxy plays a significant role in the fracture behaviour of the composite [48, 62, 67, 106, 107]. White *et al.* [62] investigated the effect of the relative stiffness of the microcapsule and epoxy matrix on the crack propagation of composites under tensile loading. They found that the crack was attracted towards the microcapsules in the case of compliant spherical inclusion. In addition, in a series of work by Guild and Young [114, 115], using a predictive model for particulate-filled composites, it was shown that the maximum stress concentration occurs at the interface close to the "equator" of soft particles (i.e. rubber spheres) while for hard particles such as glass beads, the stress concentration site is above the "pole".

To investigate the failure pattern of microcapsules used in this study, the tensile fracture surfaces of composites having 10 wt.% and 50 wt.% micro-PCMs were examined using the SEM. As it can be seen from Fig. 3-2, the crack path was mainly through the "equator" of the micro-PCMs while debonding occurred between the matrix and microcapsules. Based on these observations, it can be concluded that the Young's modulus of microcapsules used in this study was lower than that of the epoxy, which led to a reduced modulus of the composites. It is also worth pointing out that the density of voids in composite specimens

with 50 wt.% is higher than those with 10 wt.% of micro-PCMs, as evident from the SEM images.

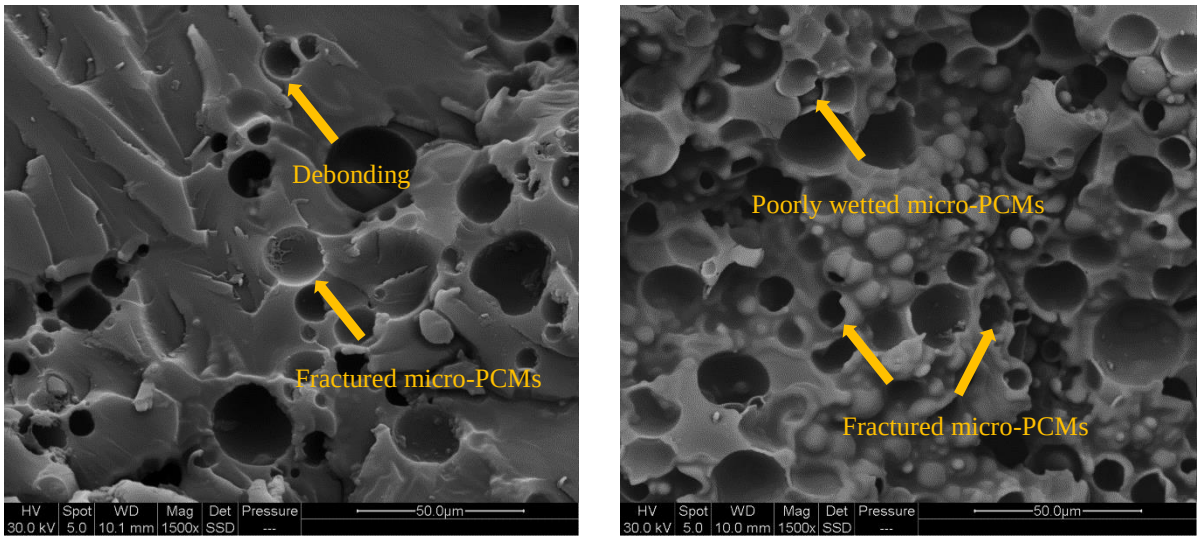

(a) (b)

Figure 3-2 Micrographs of the tensile fracture surfaces for epoxy/ micro-PCMs composites with (a) 10 wt.% and (b) 50 wt.% micro-PCMs

From Fig. 3-1b, it can be seen that increasing the concentration of micro-PCMs results in decreased compression and tensile strength of the composite specimens. The strength of particulate composites strongly depends on the efficiency of stress transfer between constitutive components [48] which is controlled by the interfacial bonding [116]. A weak bonding between the matrix and the filler will promote crack propagation that would result in the reduction of strength in particulate-filled composites. Fig. 3-2a shows few instances of debonding between micro-PCMs and epoxy even at low concentration of 10 wt.% of micro-PCMs. The vast extension of weak interfacial bonding for composites with higher wt.% of micro-PCMs can be attributed to the increasing apparent viscosity of micro-PCMs slurry during fabrication that deteriorates the wetting of microcapsule by the matrix. In fact, it was previously demonstrated that the micro-PCMs slurry behaves as a Newtonian fluid only up to a weight fraction lower than 20 % [117]. Therefore, the increasing viscosity in composites

with the high percentage of micro-PCMs can influence the interfacial bonding and consequently affect the strength of the composites.

3.3.2. Glass/Epoxy/micro-PCMs composites

3.3.2.1. Fibre volume fraction

As the density of the matrix varied due to the addition of micro-PCMs, it resulted in the different fibre volume fraction of the composite. The fibre volume fractions were determined from matrix burn-off test according to ASTM D3171-15. The furnace was preheated at 500 °C and then samples were subjected to a higher temperature of 600 °C for an hour. The weight fraction of fibre was calculated by measuring the weight of the sample before and after combustion. Using equation (3-2) the volume fraction of the fibre was then determined:

$$V_f = \frac{\rho_m W_f}{\rho_f W_m + \rho_m W_f} \qquad (3\text{-}2)$$

where V_f and W_f are the fibre volume and weight fractions, ρ_f is the density of fibre (2.54 g cm^{-3}) and W_m and ρ_m are the corresponding properties of the matrix. The results are shown in Table 3-1. It should be noted that the density of the matrix in equation (3-2) was adopted from the values obtained for the cured epoxy/micro-PCMs composites, described in Section 3.3.1. To ensure a fair comparison of mechanical properties, the measured modulus and strength of composite specimens were normalised at a fibre volume fraction of $\boldsymbol{V_f}$ **= 40 %** for all concentrations of micro-PCMs.

Table 3-1 The thickness and density of micro-PCMs-enhanced laminates

Micro-PCMs weight fraction /%	ρ_m /g cm^{-3}	ρ_c /g cm^{-3}	V_f /%
0	1.134	1.7 ± 0.0	43.5 ± 0.2
4	1.110	1.6 ± 0.0	42.6 ± 0.1
12	1.013	1.5 ± 0.1	36.7 ± 0.7
20	0.917	1.4 ± 0.1	33.2 ± 1.6

3.3.2.2. Tensile properties of micro-PCMs-enhanced FRP composite

Fig. 3-3 shows that the effect of microcapsule loading on the tensile modulus and strength of cross-ply and quasi-isotropic glass/epoxy/micro-PCMs composites. As it is expected, cross-ply laminates demonstrate higher strength and stiffness compared to the quasi-isotropic composites. Increasing the micro-PCMs concentration had an adverse effect on both the tensile modulus and strength of laminates used in this study. However, the tensile stiffness of cross-ply and quasi-isotropic laminates showed no sensitivity to increased micro-PCMs concentration after an initial drop of 11 % due to incorporating 4 wt.% of micro-PCMs. The tensile strength of both laminates, on the other hand was decreased almost linearly by increasing micro-PCMs weight percentage. The rate of reduction in tensile strength (≈ 0.065 MPa /wt.% micro-PCMs) was independent of the laminate configuration.

(a)

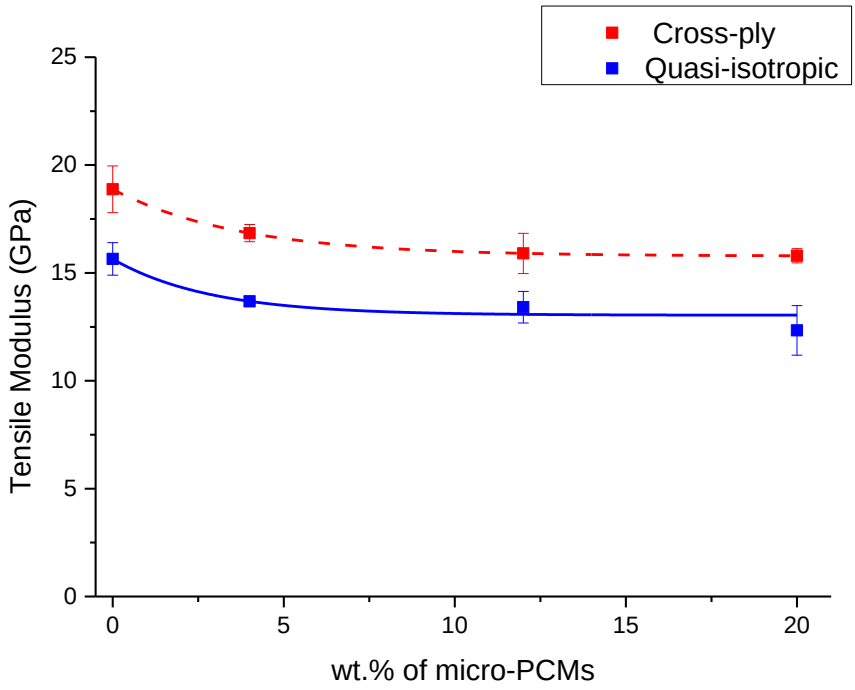

(b)

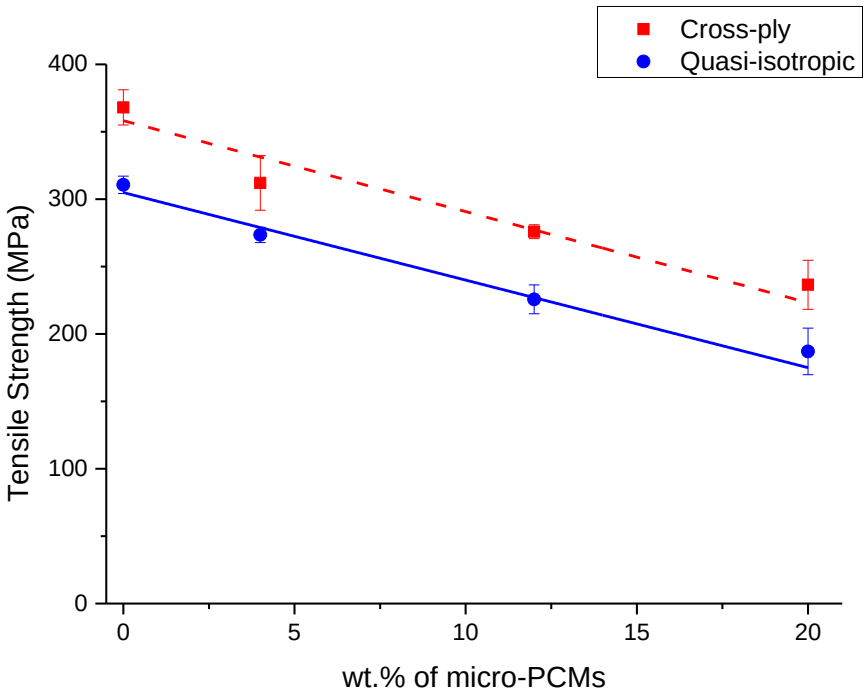

Figure 3-3 The variation of tensile modulus and strength with weight fraction of micro-PCMs

Visual inspection of the failed specimens, as shown in Fig. 3-4 revealed two dominant failure mechanisms depending on PCM concentration. For glass/epoxy specimens without any micro-PCMs and for those with 4 wt.% of micro-PCMs, a similar behaviour of fibre/matrix splitting -'brush-like' failure - was observed as shown in Fig. 3-4a and 3-4b. However, increasing the micro-PCMs concentration to 12 and 20 wt.% caused 'edge delamination' throughout the specimen (Fig. 3-4c and 3-4d). The observed fracture behaviour of glass/epoxy/micro-PCMs composites can be explained by taking into account the interfacial bonding between epoxy and PCM microcapsules.

(a) 0 wt.% (b) 4 wt.% (c) 12 wt.% (d) 20 wt.%

Figure 3-4 Tensile fracture patterns observed in glass/epoxy/micro-PCMs composites.

Several studies [118-121] have shown that the quality of adhesion at the interface of constitutive components is of crucial importance to the behaviour of composite laminates. The adhesion strength at the interface determines the load transfer capability between the components and eventually controls the strength and toughness of the composite. The elastic modulus, however, is not affected by interfacial adhesion because, for small loads or displacements, there is insufficient dilation to cause interface separation. It is worthwhile to note that filler loading also affects the strength of particulate composites, as discussed in Section 3.3.1.

To investigate the quality of adhesion between constitutive components in micro-PCMs-enhanced composites, fracture surfaces of cross-ply laminates were examined using the SEM.

Fig. 3-5 shows micrographs of the failed surfaces for laminates with micro-PCMs concentration between 0 and 20 wt.%.

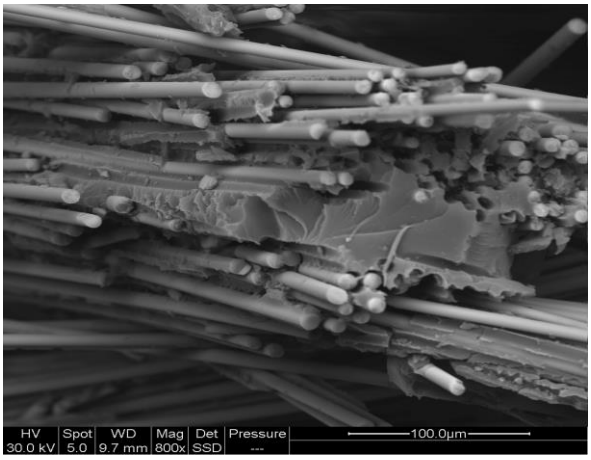

(a) 0 wt.%

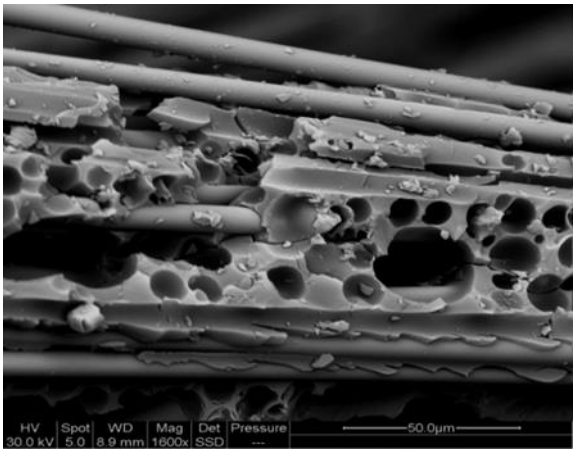

(b) 4 wt.%

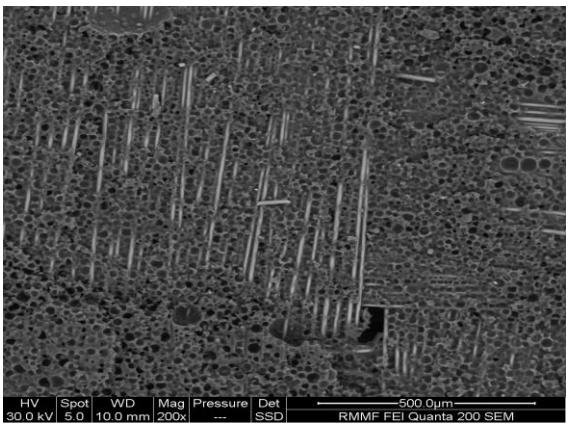

(c)12 wt.%

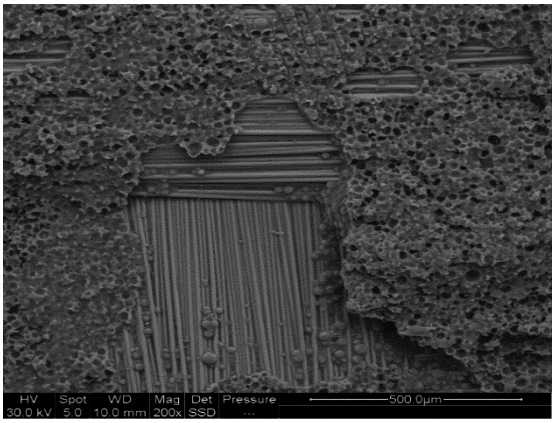

(d) 20 wt.%

Figure 3-5 Variation of the fracture mode by increasing micro-PCMs loading

The glass/epoxy composites with 0 wt.% of micro-PCMs (Fig. 3-5a) exhibit some degrees of fibre/matrix interfacial failure that is evident from clear fibre surfaces and little matrix material on the fibre surfaces. This micro-failure mode is responsible for creating a 'brush-like' fracture pattern as seen in Fig. 3-4a. Adding the micro-PCMs to composites introduces a new interface between epoxy and microcapsules. The quality of this interfacial bonding has a prominent effect on the strength of micro-PCMs composites. A strong interfacial bonding

between the micro-PCMs microcapsules and epoxy is critical for effective stress transfer leading to high composite strength.

Examinations of the fracture surfaces of composite specimens with different percentage of micro-PCMs show extensive damage due to poor microcapsule/epoxy adhesion (Fig. 3-5). Owing to the weak micro-PCMs /matrix bonding, the damage evolution occurs at early stages of loading, and the stress transfer from critically stressed fibres to lower-stressed regions cannot be done properly. Consequently, the laminate is cumulatively weakened and cannot sustain the same loads as that of composites with 0 wt.% micro-PCMs. By increasing the concentration of micro-PCMs, the weak interface between polymer matrix and microcapsules becomes dominant and controls the global failure of the specimen. In specimens with 20 wt. % of micro-PCMs, large areas of clean fibres at the ply boundary can be observed (Fig. 3-5d). The addition of micro-PCMs to the epoxy matrix increases its viscosity and reduces the amount of epoxy that is required for adequate wetting of the fibres. In a wet lay-up manufacturing method, this may result in reduced fibre impregnation and degraded fibre/matrix interfacial coupling [63]. Increasing the percentage of un-wetted fibres due to high micro-PCMs loading, promotes interlaminar delamination that results in early failure of the composite laminate.

3.3.2.3. Compressive properties of micro-PCMs-enhanced FRP composite

Fig. 3-6 illustrates the effect of micro-PCMs loading on the compression properties (modulus and strength) of glass/epoxy/micro-PCMs composites. The compressive moduli of cross-ply and quasi-isotropic laminates were reduced by increasing the weight percentage of micro-PCMs.

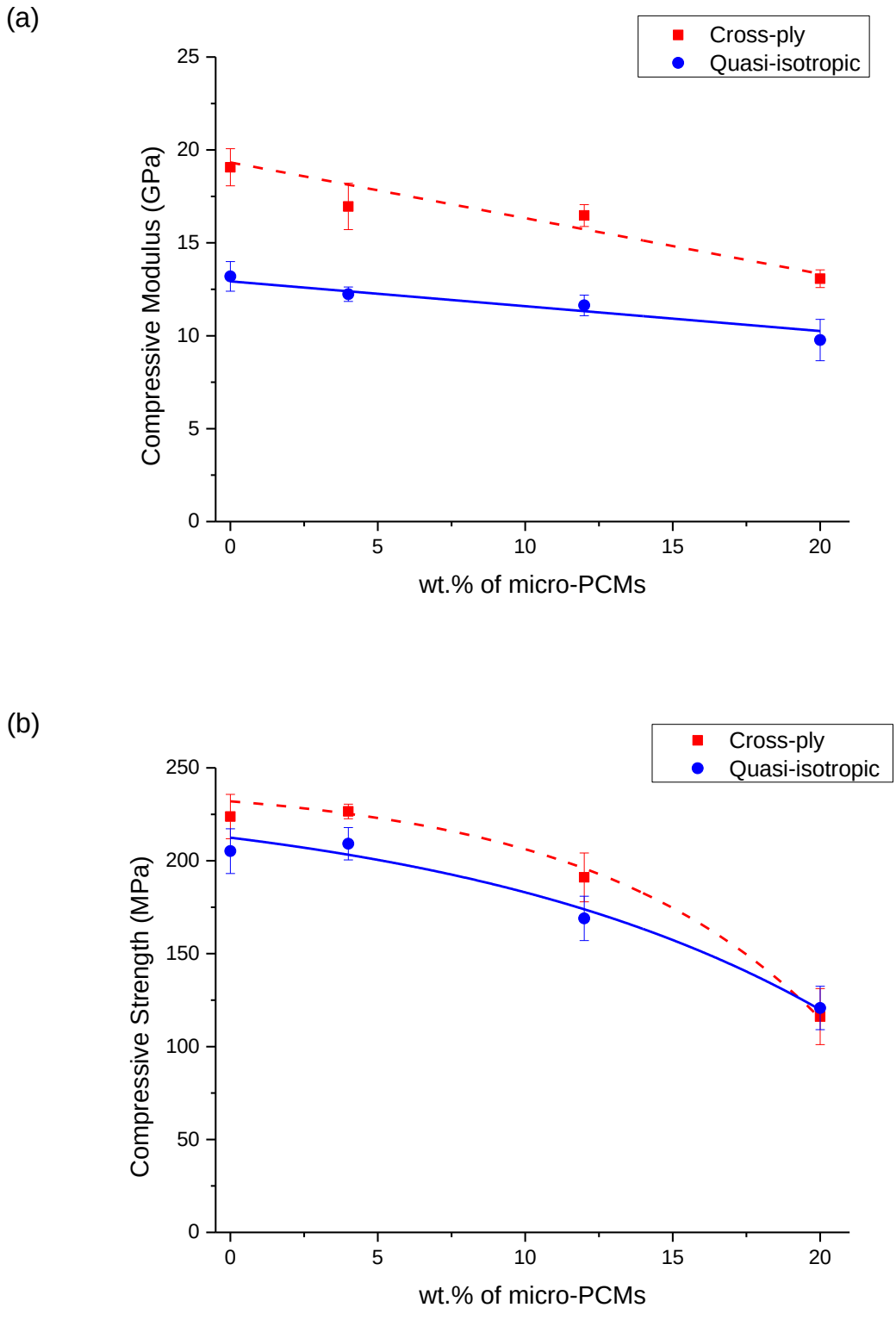

Figure 3-6 The variation of compressive modulus and strength with weight fraction of micro-PCMs.

The inverse linear proportionality between micro-PCMs concentration and compression modulus suggests that the adhesion between matrix and microcapsules was not strong enough to effectively transfer the applied stress without considerable deformation. It is worthy to note that the rate of reduction in the elastic modulus appears to be dependent upon the laminate configurations. As expected, in cross-ply laminates the compressive modulus was reduced at a higher rate (≈ 0.36 GPa/wt.% micro-PCMs) compared to that of the quasi-isotropic laminates (≈ 0.13 GPa/wt.% micro-PCMs).

The presence of micro-PCMs in the interlaminar region may promote further matrix cracking and ply delamination. From the visual observations in Fig. 3-7, a kink band was observed in glass/epoxy composites with 0 and 4 wt.% of micro-PCMs. The kink band was induced by a fibre micro-buckling and is orientated approximately 45° to a loading direction. The extension of fibre/matrix splitting is greater in specimens with 4 wt.% of micro-PCMs compared to that of control samples with no microcapsules.

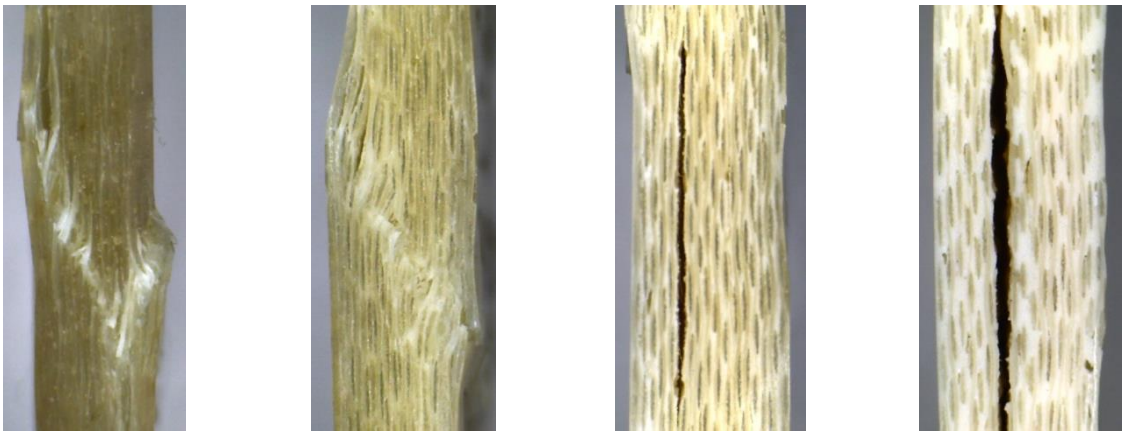

(a) 0 wt.% (b) 4 wt.% (c) 12 wt.% (d) 20 wt.%

Figure 3-7 Variation of the compression failure mode by micro-PCM loading

This phenomenon can be attributed to reduced fibre/matrix interfacial bonding due to the presence of micro-PCMs that may prevent a direct contact between fibre and matrix. Increasing the micro-PCMs concentration resulted in ply delamination failure in composites with 12 wt.% and 20 wt.% micro-PCMs, as illustrated in Fig. 3-7.

Due to poor interfacial properties between fibre/matrix and microcapsules/matrix in these specimens, fibres were easily separated from the matrix causing global delamination and final failure [122]. Unlike the tensile properties, the rate of reduction of compression strength in cross-ply laminates was greater than that of quasi-isotropic laminates for composites with 20 wt.% of micro-PCMs. This different behaviour is due to the fact that the amount of fibres supporting the compression loading in cross-ply laminates is less than that in quasi-isotropic laminates. Also, the different degree of transferring the applied external loading can be expected due to fibre orientation when micro-PCMs were located in the interfacial region. The influence of the applied loading in cross-ply is greater than that of quasi-isotropic laminate. Therefore, a greater reduction in the compression strength of cross-ply laminates is expected.

3.3.2.4. Flexural properties of micro-PCMs-enhanced FRP composite

The effect of micro-PCMs concentration on the flexural properties (modulus and strength) of glass/epoxy/ micro-PCMs composites is presented in Fig. 3-8. After an initial reduction of 12% due to incorporating 4wt. % micro-PCMs, the flexural modulus of quasi-isotropic composites was reduced only by further 5% after increasing the weight percentage of microcapsules to 20 wt. %. These results are not unexpected as the modulus is measured at low strains and the influence of the interfacial bonding (between fibre/matrix and matrix/micro-PCMs) will not be pronounced at these strains.

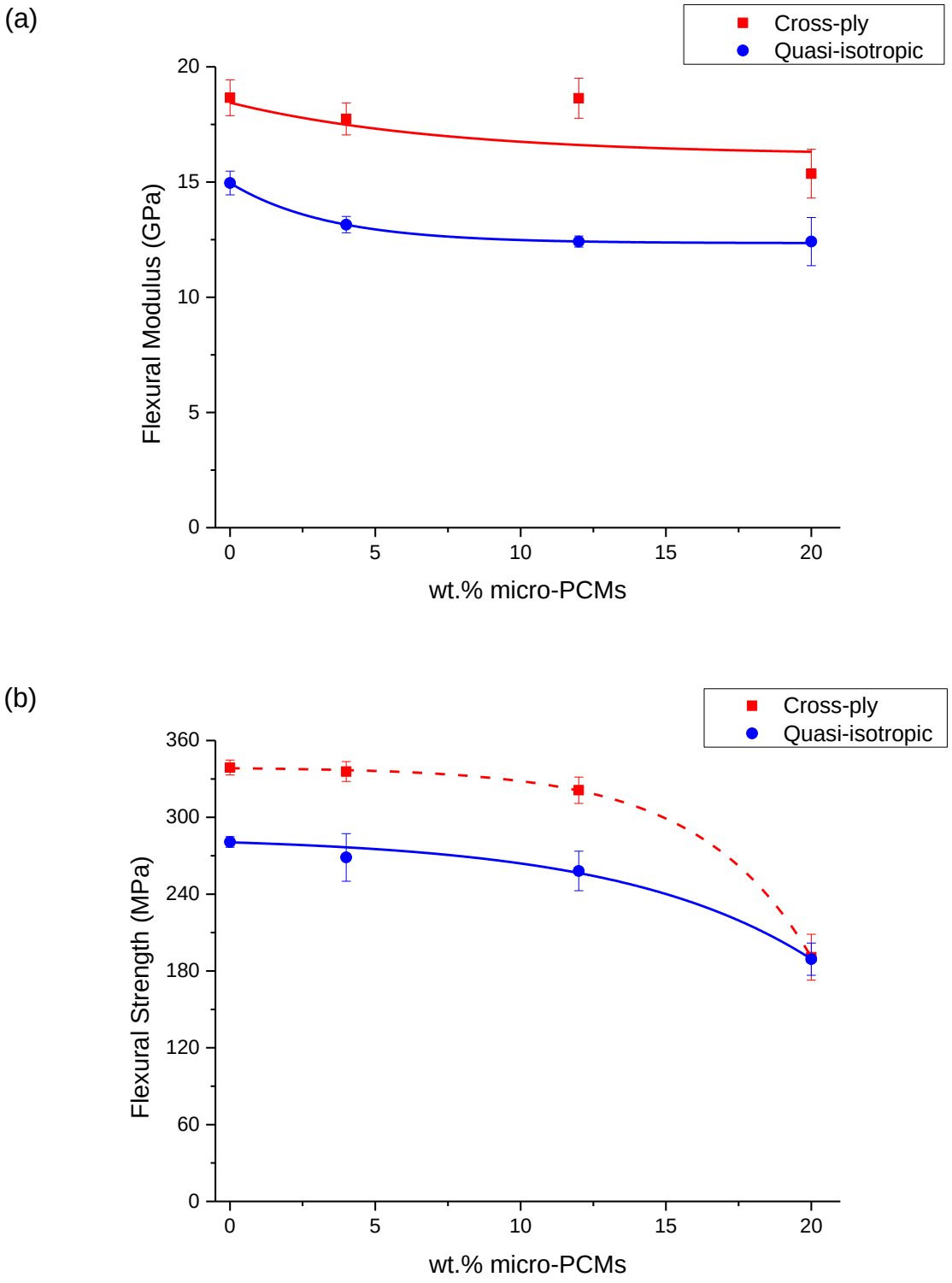

Figure 3-8 The variation of flexural modulus and strength with weight fraction of micro-PCMs.

However, as the weight percent of micro-PCMs increases and thus the interfacial area between epoxy and the micro-PCMs becomes larger, the contribution of the interface turns out to be significant. An unexpected change in the flexural modulus was observed for composites with 12 wt.% of the micro-PCMs. This might be attributed to an interlaminar sliding among different layers that reduces the axial strain in the outer fibres and results in higher flexural modulus in composites with poor fibre-matrix adhesion [122].

Similar to the compression strength, a significant decrease in the flexural strength of glass/epoxy/micro-PCMs composites was observed for specimens with 20 wt.% microcapsules. At this level of micro-PCMs loading, the flexural strength of cross-ply and quasi-isotropic laminates was reduced by 44 and 33 %, respectively. Such a significant reduction in the flexural strength can be attributed to dominant interlaminar failure in laminates with the micro-PCMs concentration of 20 wt.%.

3.3.2.5. Short beam shear strength of micro-PCMs-enhanced FRP composite

As discussed in previous sections, the tension, compression and flexural properties of FRP composites was reduced due to the integration of micro-PCMs. In addition, the interfacial bonding between fibre/matrix and matrix/microcapsules was introduced as a decisive parameter in promoting different failure modes that eventually led to the degradation of mechanical properties. To characterise the interfacial properties of micro-PCMs-enhanced FRP composites short beam shear tests were conducted. It should be noted that although shear is the dominant applied loading in this test method, the internal stresses are complex, and a variety of failure modes can occur [123]. To have a valid short-beam shear strength from this test, an interlaminar failure should occur at the mid-plane of the specimens.

(a)

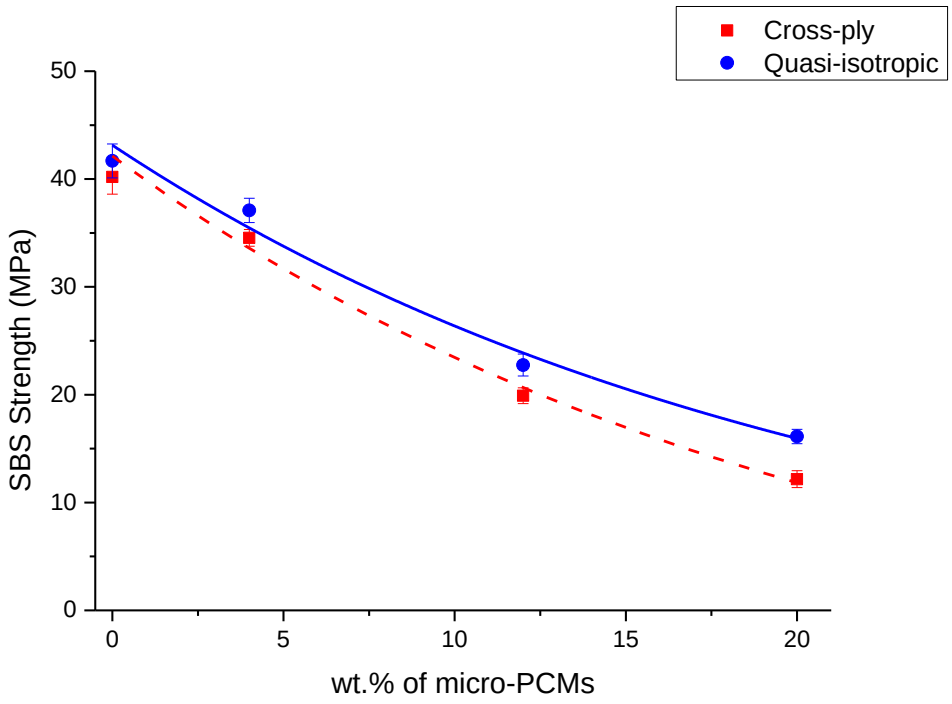

(b)

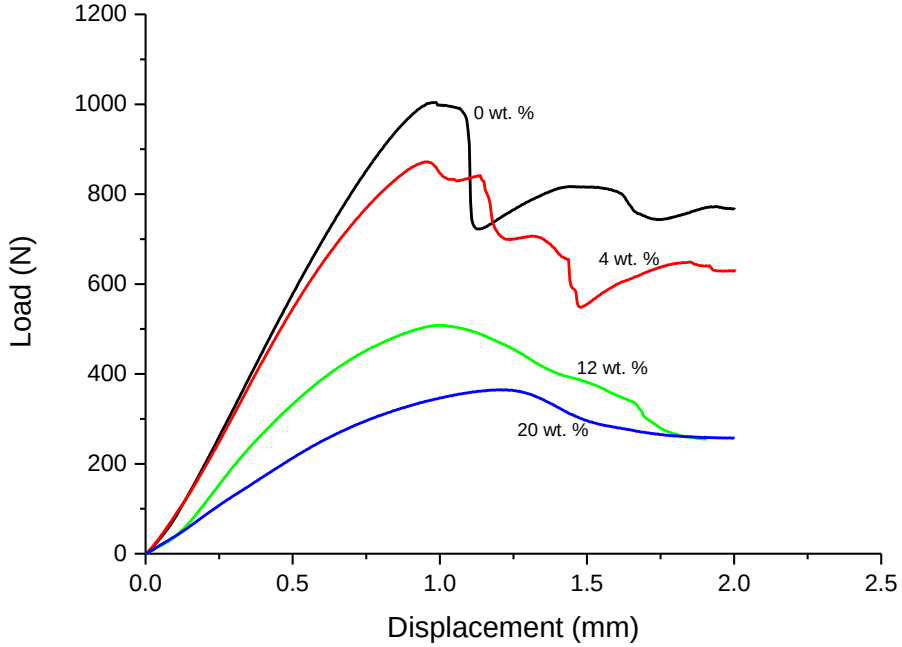

Figure 3-9 Influence of micro-PCMs loading on short-beam shear strength (a) and typical load-displacement curves for SBS tests (b)

Fig. 3-9 shows the short-beam shear strength for the various composition of glass/epoxy/micro-PCMs composites. As a general trend, by increasing the weight percentage of micro-PCMs the shear strength of cross-ply and quasi-isotropic laminates is deteriorated. At a micro-PCMs concentration of 20 wt.%, the short-beam shear strength decreased by 70 % and 61 % in cross-ply and quasi-isotropic laminates, respectively. Based on these observations, it can be concluded that the quality of interlaminar properties of glass/epoxy composites significantly degraded due to the incorporation of micro-PCMs.

SEM micrographs of the specimens tested under short-beam three point bending are shown in Fig. 3-10. For the control laminate with 0 wt.% micro-PCMs, compressive buckling near the loading nose accompanied with fibre/matrix debonding was observed, Fig 3-10a. Whitney and Browning [124] reporting the coupling of failure modes in short-beam tests, concluded that the compressive buckling is due to the fact that compression stresses suppress interlaminar shear failure modes. Thus, the appearance of compressive failure in the control laminate (Fig. 3-10a) was due to the combination of interfacial and matrix failure. This behaviour is also reflected in the load-displacement curve for the control specimens (see Fig. 3-9b). While a sudden drop in the load-displacement was observed for control specimens, relatively a constant load was noticed for other laminates with a micro-PCMs concentration of 12 and 20 wt.%. Research [125] shows that under short-beam testing, low shear strength in load-displacement behaviour is associated with the delamination while high shear strength is an indication of compressive fibre failure. From SEM micrographs, the interlaminar delamination was observed in specimens with 4 wt.% micro-PCMs, as shown in Fig. 3-10b. The extension of delamination was larger in specimens with increased micro-PCMs loading (Fig. 3-10c and 3-10d) due to inadequate fibre/matrix and matrix/microcapsule interfacial properties.

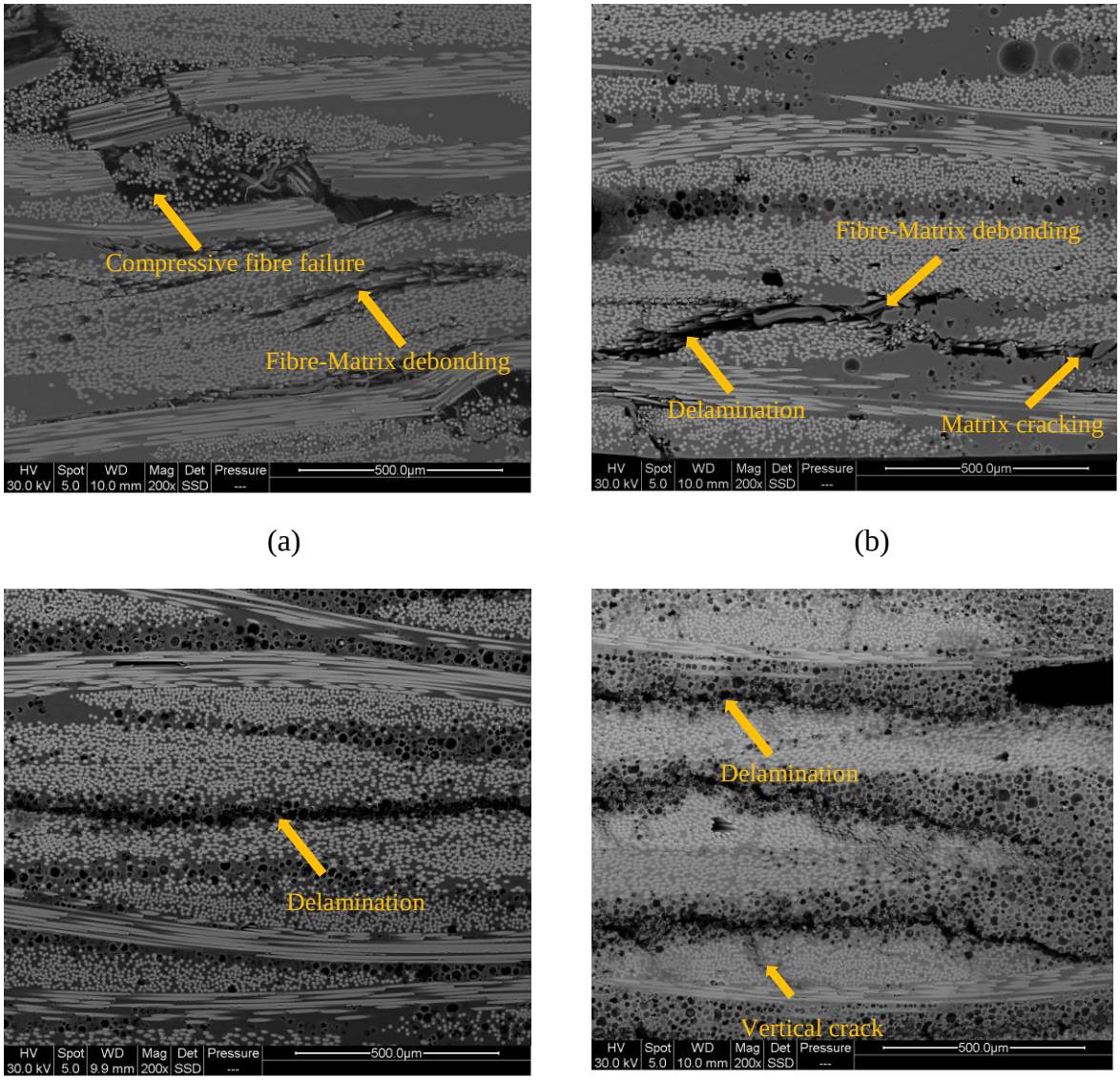

(a) (b)

(c) (d)

Figure 3-10 Micrographs of SBS tests illustrating various fracture modes for different micro-PCMs loading

3.3.2.6. Mode I interlaminar fracture toughness

Fig. 3-11 illustrates the delamination resistance (R-curve) versus crack length as a function of wt.% micro-PCMs. The G_{Ic} increased over the first 10 mm except for the specimens with micro-PCMs weight concentration of 20 wt.%. The mode I critical strain energy release rates for crack initiation (G_{Ii}) and steady-state propagation (G_{Ic}) are reported in Table 3-2. The G_{Ii} is corresponding to the crack initiation (a < 51 mm) while the G_{Ic} is the average value during

steady-state crack propagation (a > 65 mm). The main energy absorbing mechanism during the steady-state crack propagation in glass fibre reinforced composites is fibre bridging [126].

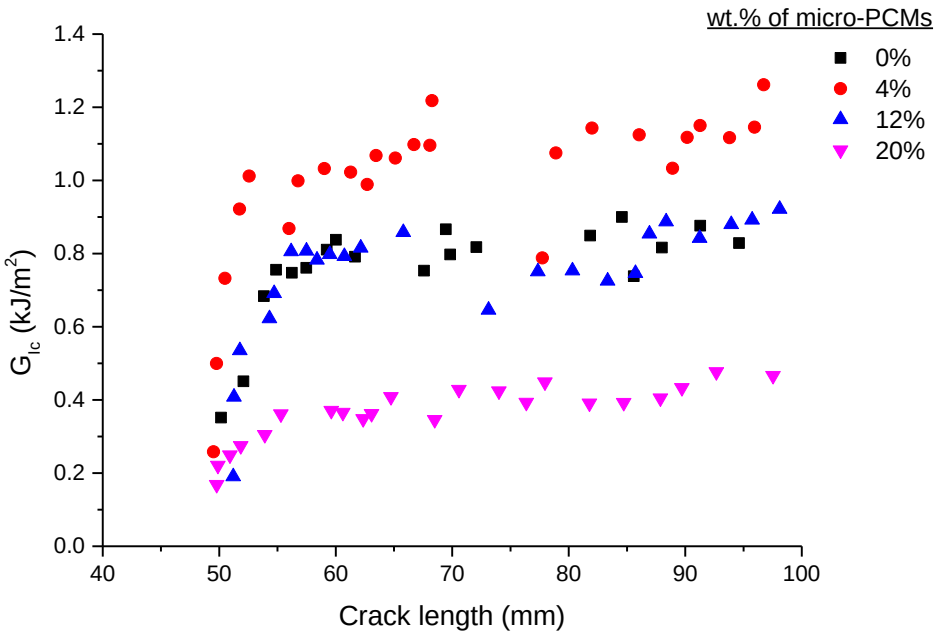

Figure 3-11 A delamination resistance (R-curve) as a function of wt.% micro-PCMs.

Previous research [127] shows that while G_{Ii} is independent of the fibre volume fraction, the critical strain energy release rate at steady-state crack propagation, G_{Ic}, changes with fibre volume fraction [128]. Both the initial and steady-state interlaminar fracture toughness of the laminates containing 4 wt.% of micro-PCMs was increased by 2 and 17 %, respectively, when compared to that of the control specimens. On the other hand, the corresponding values for composite laminates with higher PCM concentration show an opposite trend. This observation indicates that there is a transition point where for micro-PCMs concentration higher than a particular threshold, a different toughening mechanism is activated in the composite laminate. The initial increasing in interlaminar toughness in specimens with 4 wt.% of microencapsulated PCMs is attributed to the crack pinning and micro-cracking, primary mechanisms observed for particle toughening [60]. However, at higher micro-PCMs concentration, the poor wetting of the filler results in variation of the failure mechanism [60].

Therefore, it can be said that the reduction of G_{Ic} in laminates with a weight fraction of 12 and 20 % is due the poor particle-matrix adhesion.

Table 3-2 Mode I interlaminar fracture toughness for crack initiation and steady-state propagation as a function of wt.% micro-PCMs

Micro-PCMs weight fraction /%	G_{Ii} /kJ m^{-2}	G_{Ic} /kJ m^{-2}
0	0.466 ± 0.022	0.865 ± 0.080
4	0.474 ± 0.077	1.012 ± 0.069
12	0.387 ± 0.026	0.836 ± 0.006
20	0.213 ± 0.011	0.445 ± 0.021

Fig. 3-12 illustrates the micrographs of fractured surfaces for DCB specimens at crack initiation region. The pre-crack is located at the right hand side and the crack growth direction was from right to left. It was found that the initial crack growth in control specimens and composites with a micro-PCMs concentration of 4 wt.% was mainly associated with the matrix failure and fibre-matrix interface, as shown in Fig. 3-12a and 3-12b, respectively. For specimens with higher micro-PCMs loading, however, the crack propagation was through the matrix with little to no fibre bridging (Fig. 3-12c and 3-12d).

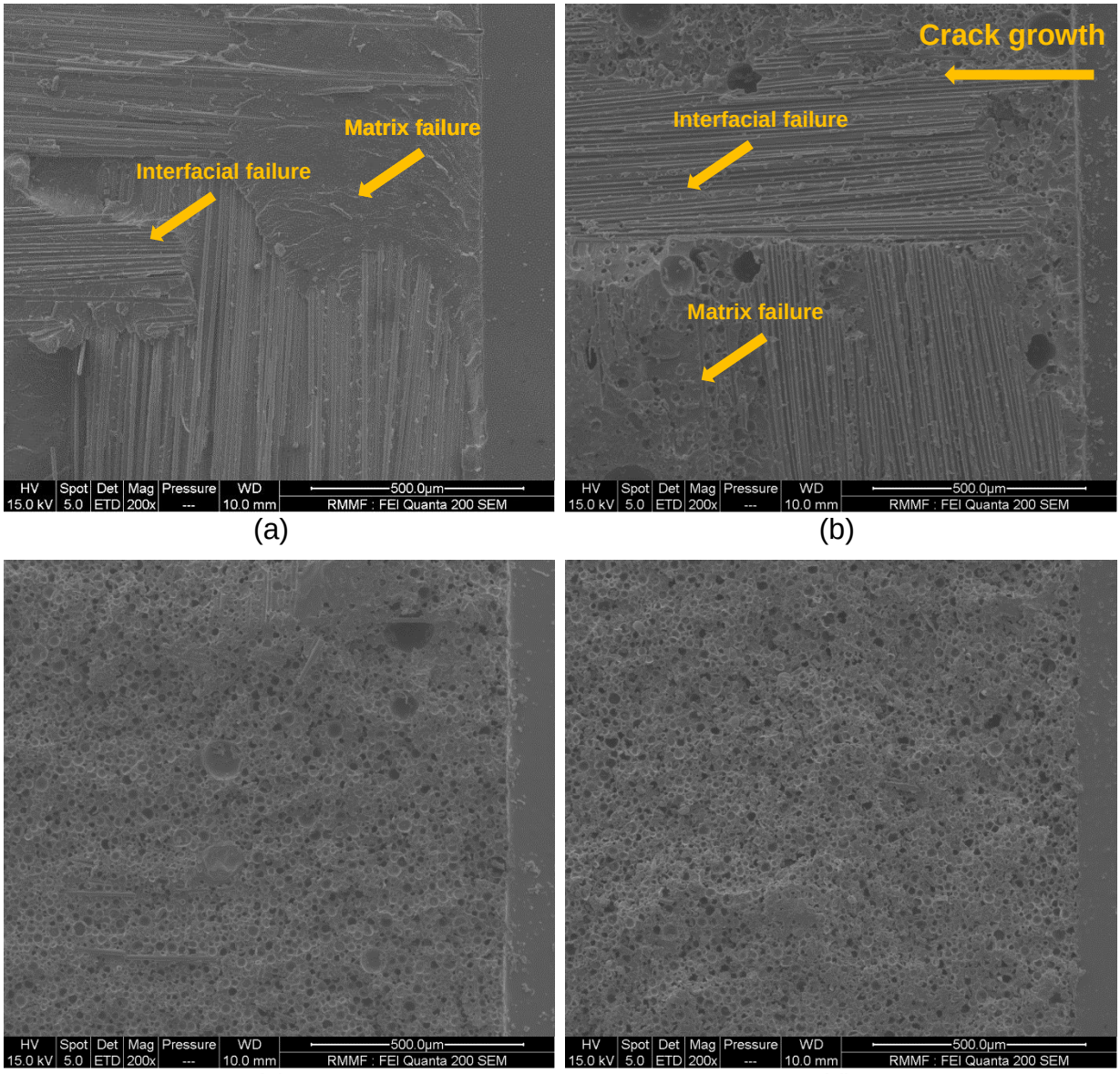

Figure 3-12 The micrographs of fracture surface of mode I fracture surfaces in the initiation region as function of weight fraction of micro-PCMs

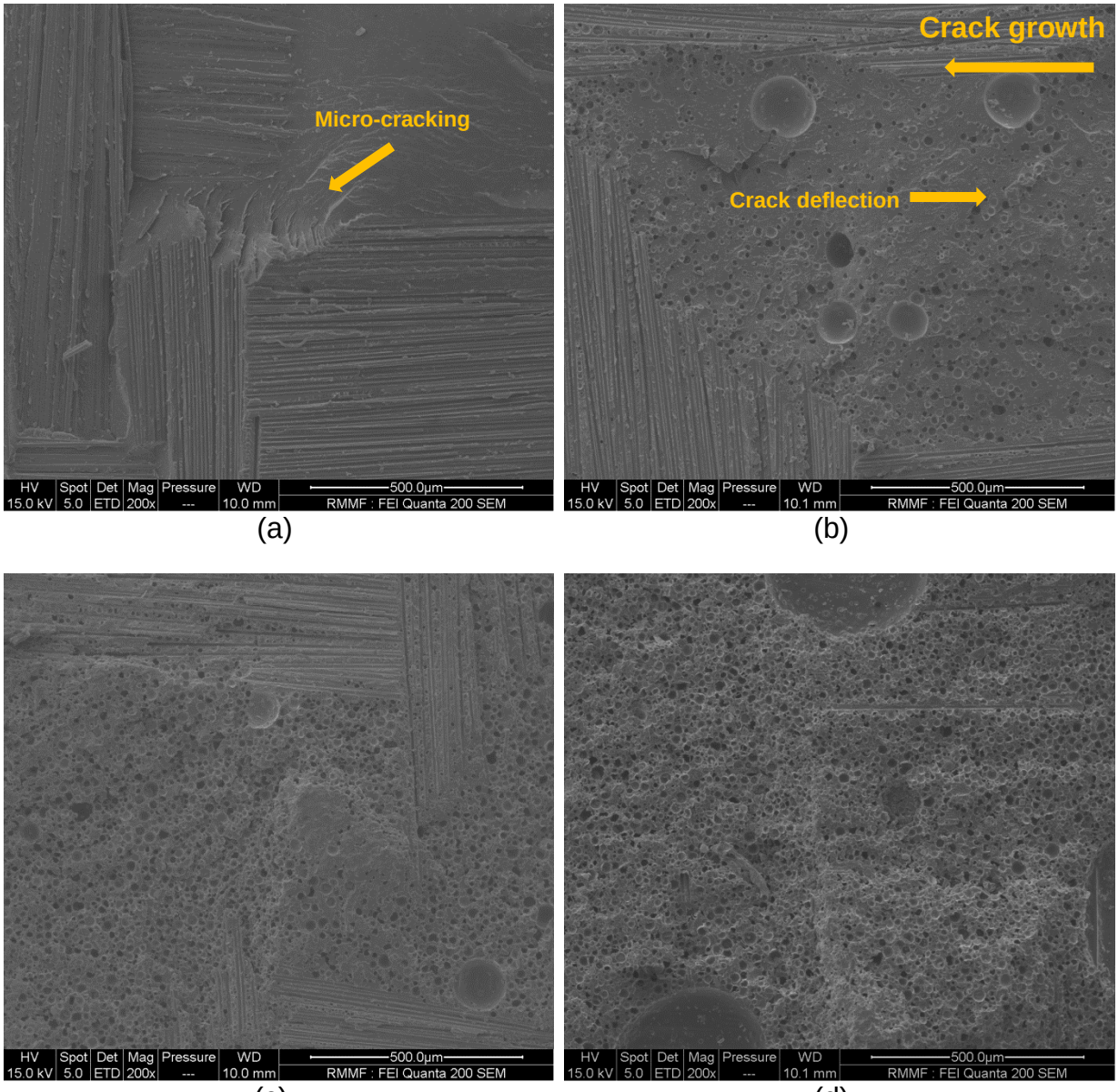

(a) (b)

(c) (d)

Figure 3-13 The micrographs of fracture surface of mode I fracture surfaces in the steady-state region as function of weight fraction of micro-PCMs

Fig. 3-13 shows the micrographs of the fractured surface along steady-state crack propagation region. A combination of adhesive failure at the fibre-matrix interface and cohesive failure at the matrix was the main toughening mechanism when micro-PCMs weight faction of 0 and 12 % were used (Fig. 3-13a and 3-13c). Fig. 3-13b shows the crack path deflection that was observed in composite laminates with 4 wt.% of micro-PCMs. Such crack deflection, results in higher energy requirement for crack propagation. A clear debonding of micro-PCMs can be observed through examining the same specimens under higher magnification in Fig. 3-14. Therefore, the improved fracture toughness in composite laminates incorporating 4 wt.% micro-PCMs is due to the activation of crack pining and debonding mechanisms.

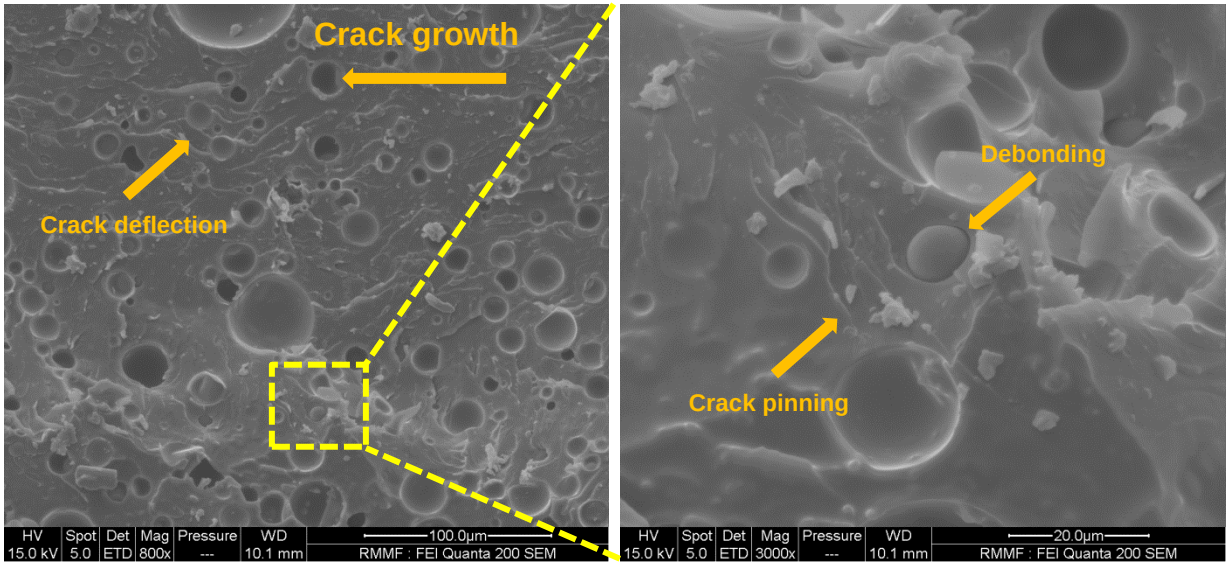

Figure 3-14 The micrograph of the composite contains 4 wt.% micro-PCMs in the higher magnification (3000×)

3.4. Summary

Due to their high efficiency, micro-PCMs -based thermal storage systems have attracted more attention in recent years from the research community as well as the industry. Employing microencapsulated PCMs in FRP composites leads to the development of multifunctional laminates that can simultaneously carry structural loads and have thermal management capability. As a first step in developing such a multifunctional laminate, the effects of micro-

PCMs inclusion on the mechanical properties of glass/epoxy laminates were investigated. After fabricating test specimens with varying weight percentage of micro-PCMs, mechanical tests including tension, compression, flexure and short beam strength were conducted. The introduction of micro-PCMs into epoxy resin led to a reduction in the density of the resultant composite specimens due to the lower density of the former. While the specific tensile and compression strength of epoxy/micro-PCMs composites decreased significantly after introducing 10 wt.% of microcapsules, the rate of the reduction was not high for further micro-PCMs loading. However, a linear reduction was observed for both tensile and compression specific moduli as a function of microcapsules are loading. Using SEM micrographs, it was found that relatively low stiffness of the microcapsules, the existence of voids and debonding of the microcapsules from matrix due to weak interfacial adhesion are responsible for the reduction of mechanical properties.

The tensile modulus of glass/epoxy/ micro-PCMs composites decreased by 11 % in both cross-ply and quasi-isotropic laminates after introducing 4 wt.% microcapsules. A further increment of micro-PCMs fillers did not have any noticeable effect on the tensile modulus. The compression modulus, on the other hand, was sensitive to the laminate configuration and in cross-ply composites the compression modulus was degraded continuously by incorporating more micro-PCMs. A similar behaviour was also observed for the tensile and compression strength of glass/epoxy/micro-PCMs composites. The compressive strength of cross-ply laminates was rapidly deteriorated when a high concentration of microcapsules (20 wt.%) was used in the laminate. Examining the failure modes, it was revealed that the matrix cracking, fibre/matrix splitting and interlaminar delamination increased with increasing the micro-PCMs loading. Furthermore, debonding of microcapsules from the matrix was also observed in all laminates.

Considering the above mentioned failure modes, SBS tests were conducted to quantify the interfacial bonding between fibre/matrix and micro-PCMs/matrix in the fabricated composites. The results revealed that the interlaminar properties of micro-PCMs-enhanced glass/epoxy composite laminates decreased by 70 % and 61 % in cross-ply and quasi-isotropic laminates, respectively, at a micro-PCMs concentration of 20 wt.%. This significant reduction was due to reduced volume fraction of the matrix as well as increased viscosity that leads to poor wetting of fibres during hand lay-up fabrication. Furthermore, the steady-state mode I interlaminar fracture toughness of micro-PCMs-enhanced FRP composites was increased by 17 % due to the inclusion of 4 wt.% of micro-PCMs. However, increasing the micro-PCMs loading in composite specimens resulted in the reduction of fracture toughness.

4. EFFECT OF MICRO-PCMS ON THERMOPHYSICAL PROPERTIES OF MULTIFUNCTIONAL COMPOSITE

4.1. Introduction

In addition to mechanical properties, incorporating micro-PCMs in FRP composites also influences the thermophysical behaviour of the host composite. A survey of open literature shows that the majority of available studies are focused on the thermophysical characterisation of microcapsules including phase change properties, thermal stability [129-132] and thermal conductivity [133-135]. However, a possible synergetic thermophysical effects due to the interaction between micro-PCMs and host FRP composites has not been fully understood. For adaptation of multifunctional composites with thermal storage capability it is therefore necessary to investigate such properties. This chapter presents an experimental investigation on the thermophysical properties of novel multifuctional FRP composites incorporating micro-PCMs. The influence of micro-PCMs inclusion on the thermophysical properties of FRP composites including phase change properties, thermal conductivity, and thermal and dimensional stability are reported.

4.2. Materials & Methods

4.2.1. Materials

The same materials and fabrication methods, as presented in Chapter 3, were used to fabricate different specimens for thermophysical analysis.

4.2.2. Characterise techniques

4.2.2.1. Differential scanning calorimetry (DSC)

A PerkinElmer DSC 8000 equipped with an Intra-cooler II was used to determine the melting and crystallisation properties of FRP composites incorporating micro-PCMs. DSC scans were

conducted under nitrogen purge with a flow rate of 20 mL min^{-1}. Samples, with a weight of approximately 5 mg, were encapsulated in 10 μL aluminium pans and heretically sealed. The melting and crystallisation scans of samples were obtained at the heating/cooling rate of 2 K min^{-1} over a temperature range of 5°C to 50°C. The scan cycle was conducted as follows: heating from 5°C to 50°C → holding at 50°C for 3 min → cooling from 50°C to 5°C → holding at 5°C for 3 min → heating from 5°C to 50°C. The first melting cycle was performed to erase the thermal history of the composite and remove self-seeding nuclei of the samples. It should be noted that DSC scans were repeated six times to obtain averaged values.

4.2.2.2. Heat flux apparatus

In-house experimental set-up was developed to measure the heat flux (φ) exchanged over the period time during the phase transition (solid ↔ liquid) of micro-PCMs. Fig. 4-1 illustrates the schematic of the heat flux measurement apparatus. The composite specimen was sandwiched between two heat flux meters (Model B-HT with Type K thermocouple, from International Thermal Instrument Company, USA.), and the heat mats (12V, 3.75 W, 50 x 75 mm, from RS Components, Australia) were placed on both ends. The temperature of heat mats was controlled using a DC power supply. The whole set-up was then insulted using the insulation materials (Fiberfrax®, k = 0.08 W m^{-1} K^{-1}, from Unifrax, Australia) to reduce the thermal transmission through the surrounding. The lateral sides of the aperture were insulated by approximately 50 mm thickness of insulating materials so that a one-dimensional heat transfer problem can be assumed with negligible heat loss. In order to minimise the thermal contact resistance [136], the thermal grease (zinc oxide filled silicone, from GC Electronics, USA) was applied between surfaces.

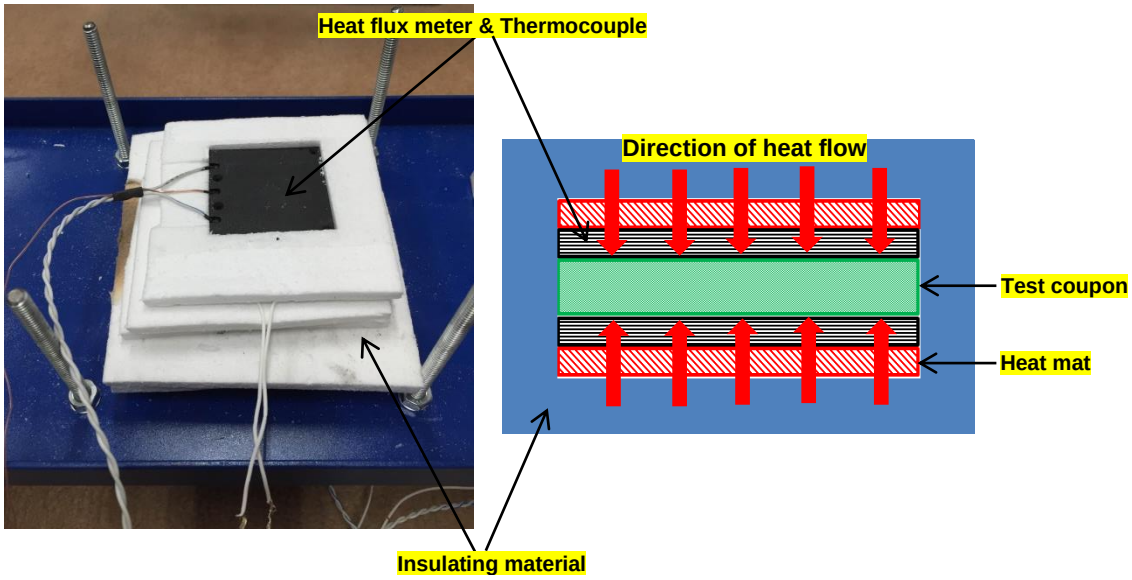

Figure 4-1 A half bottom view and schematic drawing of the heat flux apparatus

This experiment allows measuring the heat of fusion (ΔH) through two different iso-thermal conditions, which correspond to the variation of the internal energy of the system. In addition, the specific heat (C_p) can be simultaneously estimated. Before beginning the experiment, the test rig was allowed to reach a steady state at room temperature ($\Delta\varphi = 0$). The initial temperature was set to 30°C, and gradually increased to the final temperature of 50°C on both side. It should be noted that the time required to reach the steady-state condition was approximately 4 hrs for each step. Heat flux and corresponding temperature simultaneously were recorded via TC-08 data logger (Pico Technology, UK). The apparent heat of fusion, ΔH and specific heat capacity were then estimated as following equation (4-1) [76, 137].

$$\Delta H = \frac{1}{\rho \cdot e}\int_{tini}^{t_{end}} \Delta\varphi \cdot dt = C_p \cdot (T_{end} - T_{ini}) \qquad (4\text{-}1)$$

where ΔH is the integral of the heat flux difference ($\Delta\varphi$) from initial time (t_{ini}) to final time (t_{end}). T_{end} and T_{ini} are corresponding temperatures to the initial and final times, ρ is the density, e is the thickness, and, C_p is the specific heat.

4.2.2.3. Thermal conductivity

The hot disk thermal constants analyser TPS 2500S from Hot Disk AB was used to measure the through-thickness thermal conductivity. The instrument is based upon transient plane source (TPS) method to determine thermal conductivity, thermal diffusivity and volumetric specific heat capacity. Further information about the measurement principles of TPS can be found in the literature [138, 139]. A Kapton insulated disk sensor (Hot disk 7577) with a radius of 2 mm was sandwiched between two specimens. The specimens were cut to a coupon size of 30 mm × 30 mm. A heating power of 0.02 W with a pre-determined measurement time (10 s) was used to obtain 200 resistance data points at room temperature. Points between 50 and 200 were then used for analysis in order to reduce the effect of initial thermal-mass from the sensor [140]. The thermal conductivity was measured at least three times.

4.2.2.4. Thermogravimetry Analysis (TGA)

The composition of the specimens were analysed using TGA 7 (PerkinElmer, USA). Samples with a weight range of 4 - 5 mg were heated from 30 °C to 600 °C under a nitrogen purge and then heated to 850 °C under an air purge. The heating rate of 20 K min^{-1} was maintained throughout the scans.

4.2.2.5. Modulated Temperature Thermomechanical analysis (mT-TMA)

The linear coefficient of thermal expansion (α), before and after glass transition temperature was measured using a TMA Q400EM (TA Instruments, USA). The modulated-temperature thermomechanical analysis resolved dimension changes that were in-phase (reversing) and out-of-phase (non-reversing) with the modulated temperature programme [141]. Specimens (5 mm × 5 mm) were heated from 25 °C to 140 °C at a rate of 0.5 K min^{-1} under a nitrogen gas with a flow rate of 50 mL min^{-1}. A sinusoidal temperature modulation with amplitude of

5 °C and period of 300 s was superimposed on the temperature ramp. Neat epoxy resin and micro-PCMs were also analysed for comparison purposes.

4.3. Results and discussion

4.3.1. Phase change properties

Fig. 4-2 shows the heating and cooling DSC curves for micro-PCMs-enhanced composite laminates, and Table 4-1 summarises the results for the phase transition properties and latent enthalpy determined from the heat flow measurements. A peak melting temperature of 36.6 ± 0.1 °C with a latent heat capacity (enthalpy) of 184.5 ± 0.6 J g^{-1} was measured for pure micro-PCMs. The measured heat of fusion was slightly lower than the manufacturer reported value of 190 – 200 J g^{-1}. This small difference may be due to a different integration range being used to calculate the area under the heat capacity-temperature curves.

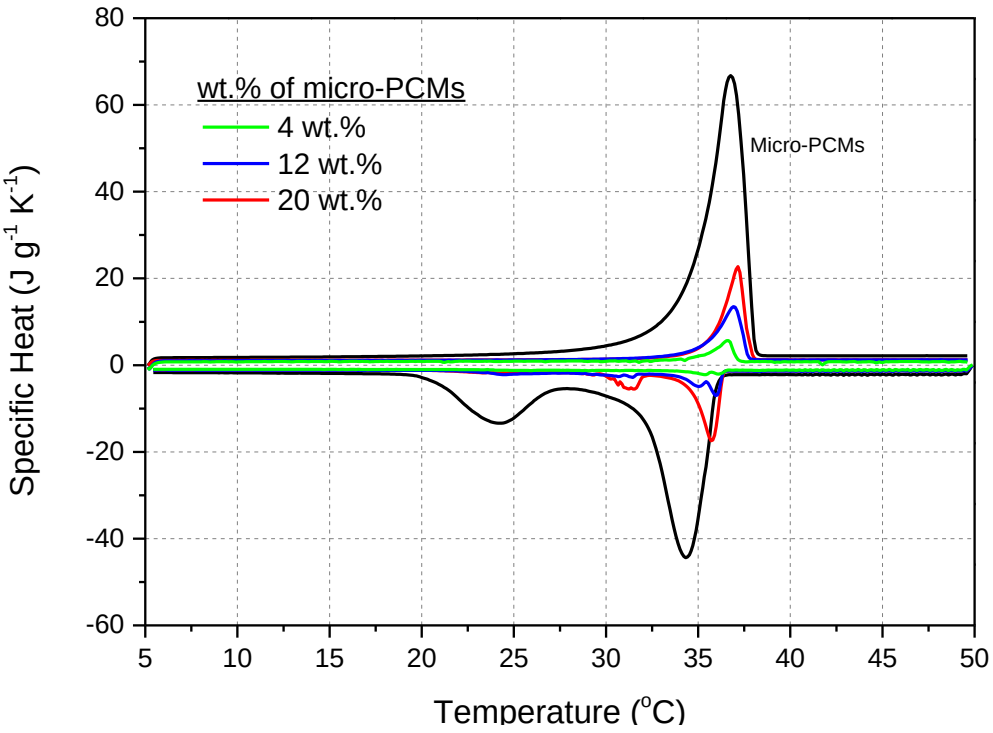

Figure 4-2 Heat capacity melting and crystallisation curves with scanning rate of 2 K min^{-1}

Regardless of the micro-PCMs weight fraction, one endothermic and two exothermic peaks were identified on the melting and crystallisation curves, respectively. The crystallisation behaviours of microencapsulated *n*-alkanes (C_nH_{2n+2}) were equivalent to that of bulk *n*-alkanes, which depended on the number of carbon atoms (odd or even) [142]. The *n*-eicosane (even numbered alkanes) shows rotator phase only on crystallisation process while odd numbered alkanes between C_9 and C_{21} exhibit on both melting and crystallisation process, and a solid-solid transition of bulk *n*-eicosane occurred via a metastable rotator phase [71].

Table 4-1 Summary of DSC results of micro-PCMs-enhanced laminates

	Melting			Crystallisation		
Micro-PCMs weight fraction/%	Onset Tm /°C	Peak Tm /°C	Δ*H*m /J g-1	Onset Tc /°C	Peak Tc /°C	Δ*H*c /J g-1
4	35.2±0.2	36.5± 0.2	6.7±2.2	36.1±0.5	35.3±0.1	6.5±1.6
12	35.3±0.4	36.9± 0.3	19.8±3.6	36.3±0.1	35.8±0.4	21.2±3.3
20	35.2±0.3	37.0± 0.2	40.9±6.0	36.2±0.2	35.3±0.4	40.0±4.1
	34.7±0.2	36.6± 0.1	184.5±0.6	36.0±0.0	34.4± 0.1	184.5±0.7
Micro-PCMs	* Based on homogeneous crystallisation process		26.6±0.4*	24.1±0.0*		31.1±0.2*

The second exothermic peak is an indication of homogeneous nucleation in liquid-crystal transition that has been observed in other investigations [143-147]. The heterogeneous nucleation induced by the surface freezing is governing the phase transition from liquid to solid of microencapsulated *n*-alkane [148]. The existence of two exothermic peaks in all specimens studied in this project suggests that the integrity of micro-PCMs was conserved although they have been incorporated into glass fibre/epoxy composite laminates. Furthermore, it was observed that the enthalpy of micro-PCMs-enhanced composite laminates is linearly proportional to the weight fraction of micro-PCMs, as shown in Fig. 4-3,

where the rule of mixture has been used to calculate the theoretical heat of fusion. This observation confirms that the phase change properties and physical integrity of micro-PCMs were preserved during the manufacturing process, as reported in similar studies [73].

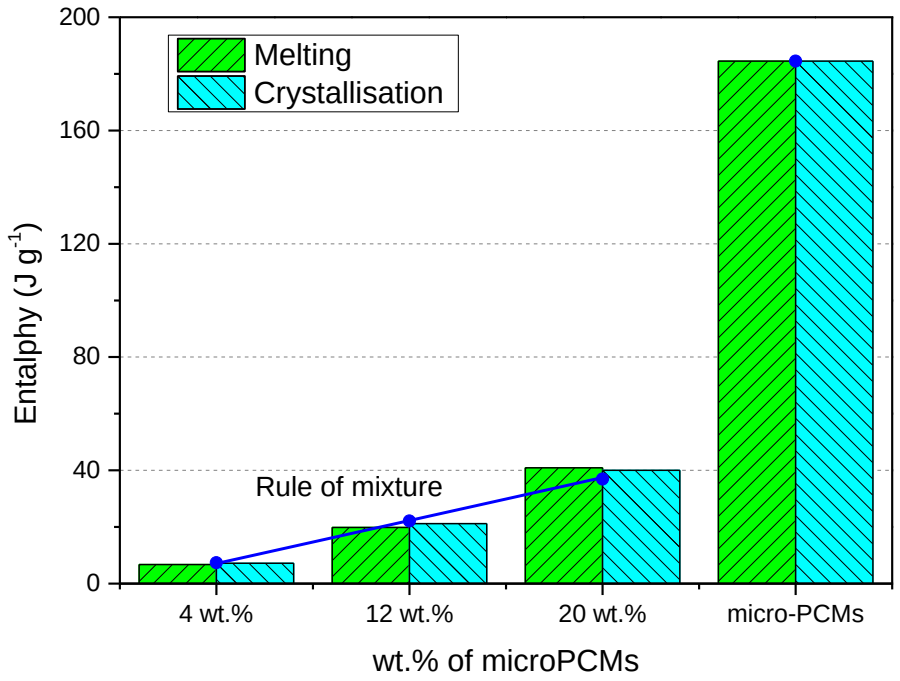

Figure 4-3 Melting and crystallisation enthalpy versus weight fraction of micro-PCMs

4.3.2. Apparent heat capacity

Fig. 4-4 illustrates the variation of heat flux as a function of time between 10,000 and 20,000 seconds. The apparent heat of fusion (ΔH) and specific heat (C_p) were then calculated using equation (4-1), and reported in Table 4-2. Considering the melting temperature of micro-PCMs at 37 °C, the integral of heat flux between t_{ini} = 10,000 and t_{end} = 20,000 seconds provides the total energy stored (ΔH) during the solid to liquid phase-change process. It can be seen that the area under the graph (the integral of heat fluxes over the time) was increased with increasing the micro-PCMs weight concentration.

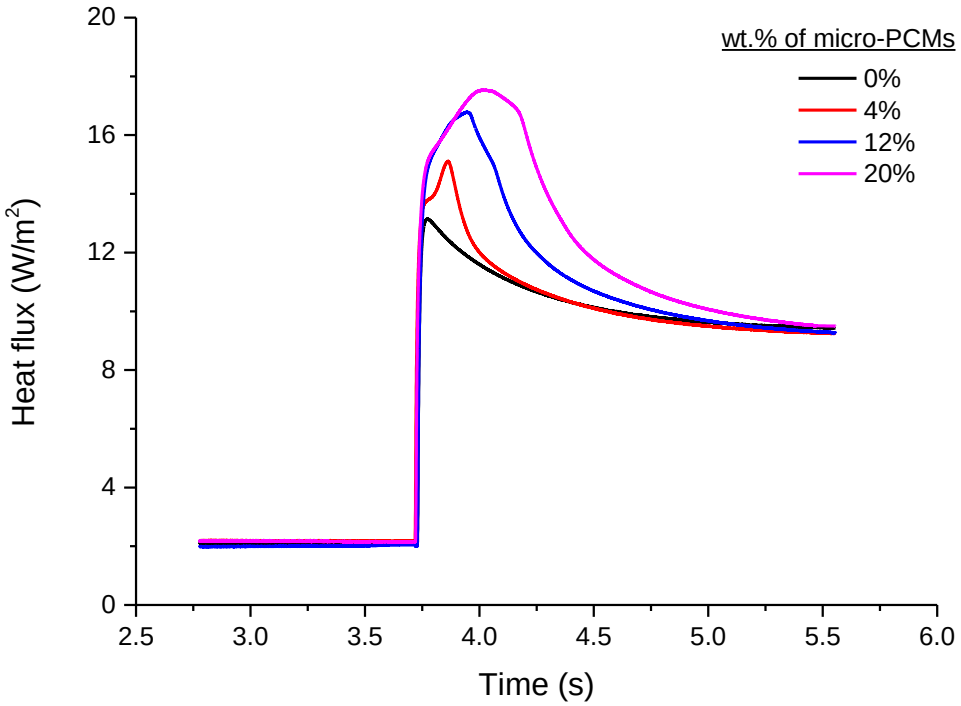

Figure 4-4 The measured heat flux as a function of time when the temperature increases from 30 to 50°C

Compared to the control laminates, the variation of ΔH was proportional to the fraction of micro-PCMs in the composites, as summarised in Table 4-2. This observation suggests that the experimental set-up used in this study was able to correctly characterise the behaviour of micro-PCMs during solid to liquid phase transition.

Table 4-2 Apparent heat of fusion and specific heat capacity

Micro-PCMs weight fraction/%	P /kg·m^{-3}	e /m	ΔH /kJ·kg^{-1}	C_p /kJ·kg^{-1}·°C^{-1}	ΔH* /%	ΔC_p* /%
0	1696	0.00268	14.27	0.643	-	-
4	1628	0.00286	14.88	0.657	4.12	2.09
12	1490	0.00323	16.31	0.682	12.53	5.65
20	1364	0.00363	17.70	0.797	19.39	19.23

*compare to the laminate 0 wt.% of micro-PCMs

However, the variation of the specific heat, C_p, was not proportional to the weight fraction of micro-PCMs. This discrepancy can be contributed to the fact that the thermocouples used in the study were embedded in the mid-plane of the heat flux meters. In this case, the laminate's temperature might not be accurately measured owing to different thermal conductivities of the heat flux meter and the laminate.

Fig. 4-5 shows the temperature profiles of various specimens as a function of time. While for the composite laminates without micro-PCMs, the temperature was exponentially increased during the experiment, however, for the specimens with embedded micro-PCMs, the change of the temperature was compliant when approaching to the melting temperature of micro-PCMs.

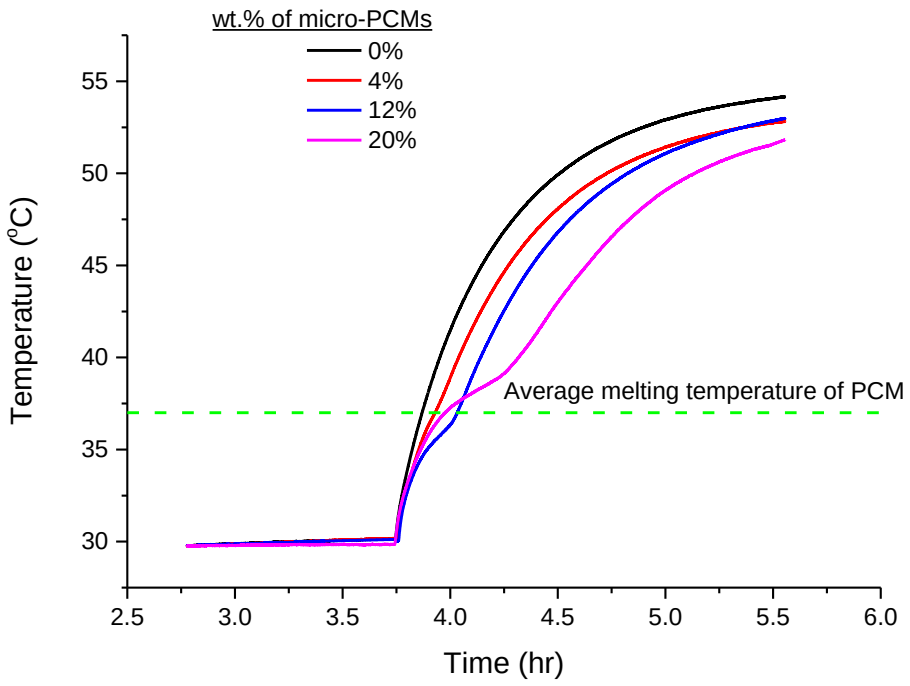

Figure 4-5 The temperature profile (30-50°C) as function of time

It is expected that the temperature remains at fairly constant level during PCMs melting. The levelling of the temperature implies that the host composite is exhibiting some degree of the latent thermal storage capacity. It can be clearly shown that no time delay is observed in the

laminates without micro-PCMs, and the time delay due to the phase transition is increased with increasing the micro-PCMs weight concentration. This indicates that the heat capacity of the laminates is increased by increasing the weight fraction of micro-PCMs. The time delay, observed in these experiments is one of the most important features of the integration of micro-PCMs in thermal management systems [149].

4.3.3. Thermal conductivity

The through-thickness thermal conductivity of micro-PCMs-incorporated composite laminates was measured experimentally using transient plane source (TPS) technique. Fig. 4-6 shows the variation of thermal conductivity as a function of micro-PCMs weight fraction.

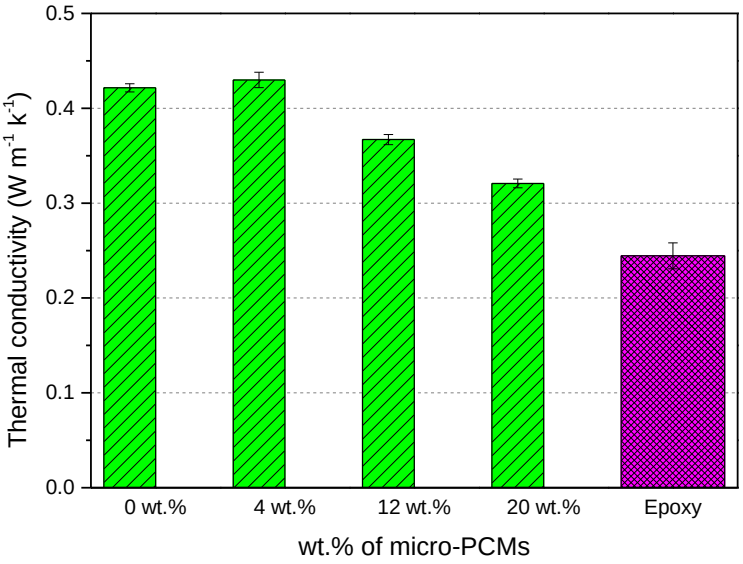

Figure 4-6 The through-thickness thermal conductivity of multifunctional composites versus micro-PCMs concentration

It was found that the thermal conductivity of composite laminates decreased with increasing the micro-PCMs loading. This phenomenon is attributed to the relatively lower thermal conductivity of micro-PCMs that was measured as 0.09 W m^{-1} K^{-1} in this study. It is also noteworthy that the thermal conductivity of melamine-formaldehyde microcapsules (similar to those used in this study) depended on the chemical composition of the shell material [93].

Therefore, adding micro-PCMs with a low thermal conductivity will adversely affect the thermal properties of PCM-enhanced polymer composites [70, 137]. A careful consideration such as an appropriate sample/sensor size is needed to obtain the optimal response in TPS technique. The accuracy can be improved by fulfilling two conditions. Firstly, the geometric constraints, "probing depth" (*D*), must not be larger than the sample size so that the heating from the sensor does not excessed any one of the material's boundaries from the sensor edge. The *D* can be estimated using the equation (4-2). Secondly, an adequate experimental time should satisfy the dimensionless relation given from equation (4-3). When both equations are satisfied, the measurement is highly optimal and accurate [140, 150]. It should be noted that the tests were iterated until two equations satisfied.

$$D = 2(\alpha t)^{1/2} \qquad (4\text{-}2)$$

$$0.3 \leq \alpha t / r^2 \leq 1 \qquad (4\text{-}3)$$

where α is the sample thermal diffusivity ($mm^{-2}\ s^{-1}$), *t* is the time (s), and *r* is the sensor radius (mm). Given the sensor radius (2 mm), the probing depth (*D*) was measured from 3.1 mm to 3.7 mm. These results are smaller than any dimension of the specimen used in this work. Thus, the combination of specimen size and sensor radius is appropriate, and the solution can be considered as semi-infinite. Also, the relation between length of the time (10 s) and sensor radius was fulfilled by the requirement from equation (4-3). It can be then concluded that the collected data was highly accurate. Furthermore, the measurement on the thermal conductivity of composites is strongly influenced by their density, temperature and moisture as well as the microstructure and anisotropy [140]. In this work, composite specimens were highly anisotropic. Thus, it can be said that the scatter in the thermal conductivity measurement is due to non-uniform distribution of micro-PCMs in the interlaminar region of the composite laminates rather than the accuracy of the test condition.

4.3.4. Thermal stability

Fig. 4-7 illustrates the weight loss (%) of micro-PCMs-enhanced glass fibre/epoxy composites as a function of temperature. The decomposition temperature for each case was calculated from the onset of weight loss and it is reported in Table 4-3.

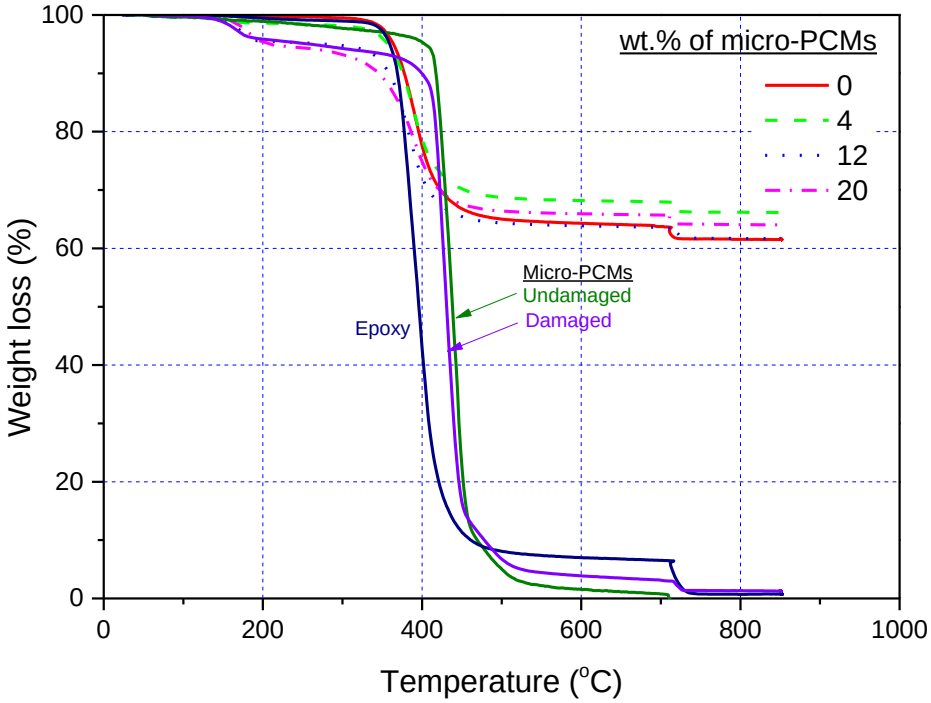

Figure 4-7 Representative weight loss curves of micro-PCMs-enhanced glass/epoxy composite as a function of temperature

From the thermogravimetry curves (Fig. 4-7) it can be seen that incorporating 4 wt.% of the micro-PCMs did not affect the thermal stability of the composites. Further inclusion of micro-PCMs (12 and 20 wt.%) led to a reduction of the decomposition temperature due to the weak adhesion between the filler and matrix. On the other hand, the stronger interface can limit the continuous decomposition [151], and the influence of the adhesion on decomposition temperature was also reported in Ref. [64, 83].

Table 4-3 Thermal stability of micro-PCMs-enhanced glass/epoxy composites

Micro-PCMs weight fraction /%		Decomposition temperature /°C
0		357 ± 7
4		355 ± 5
12		346 ± 6
20		346 ± 3
Micro-PCMs	Undamaged:	416 ± 3
	Damaged:	410 ± 2
Epoxy		365 ± 2

Furthermore, those laminates with a higher micro-PCMs loading experienced an early weight reduction of about 5% at a temperature around 140°C. It is hypothesised that the weight loss at this low temperature is attributed to the leakage of the core material from micro-PCMs. The leakage of *n*-octadecane from similar microcapsules was reported in the literature [82] and adversely affected the thermal stability of the system [152, 153]. In order to confirm the cause of this initial weight loss, the micro-PCMs were damaged by squashing between two sliding glass plates for 2-3 minutes. As shown in Fig. 4-7, the initial weight loss for the damaged micro-PCMs was consistent with the observed weight loss at 140°C for composites with 12 and 20 wt.% of micro-PCMs. Therefore, it can be concluded that the damage of micro-PCMs during sample preparation may have been contributed to the initial weight loss. The epoxy was thermally stable until 365°C, as shown in Fig. 4-7, but was completely decomposed by 720°C. When the purge gas changed from nitrogen to air at 600°C, the carbon residue from epoxy was burned off. Thereby, the thermogravimetry curves were used to determine the fibre weight fraction of the composites. The final residual weight of all composite samples was close to 60 %, which is the weight fraction of glass fibre used during the manufacturing process. This behaviour was observed for all micro-PCMs-enhanced glass fibre/epoxy laminates regardless of the micro-PCMs loading.

4.3.5. Dimensional stability

The coefficient of thermal expansion (CTE) is an important material property that defines the dimensional stability of engineering structures subjected to temperature variations. The modulated-temperature programme used in this study is capable of resolving the reversing changes from the irreversing effects such as relaxation, stress relief and post-cure of the specimen under external loading [154]. The linear coefficient of thermal expansion was calculated from the slope of the reversing dimension change versus temperature curve using equation (4-4):

$$\alpha = \frac{dL}{dT}\frac{1}{L_0} \qquad (4\text{-}4)$$

where dL is the change in dimension, *dT* is the change in temperature and L_0 is the initial length of the specimen. The CTE was determined both below (α_1) and above (α_2) the *Tg*, although the former is generally considered to be more useful since polymers lose most of their mechanical properties above the *Tg* [155].

The reversing curves of epoxy, micro-PCMs and composite laminates are shown in Fig. 4-8 while coefficient of thermal expansion and *Tg* of the materials are summarised in Table 4-4. The reversing (in-phase) curve displays only the thermal expansion component of the material, removing non-reversing phenomena such as creep and flow. The below-*Tg* coefficient of thermal expansion of the control specimen was 30% lower than that of the neat resin owing to the relatively low CTE of glass fibre (about 5×10^{-6} / K^{-1}). This occurrence was also visually noticeable by a decrease in the curve gradient shown in Fig. 4-8. However, the CTE values above the *Tg* for the same specimens were higher than that of the neat epoxy. The change in the coefficient of thermal expansion below and above *Tg* is attributed to the mobilization of molecular segments that adhere to rigid fibres and only become more compliant upon epoxy softening [156].

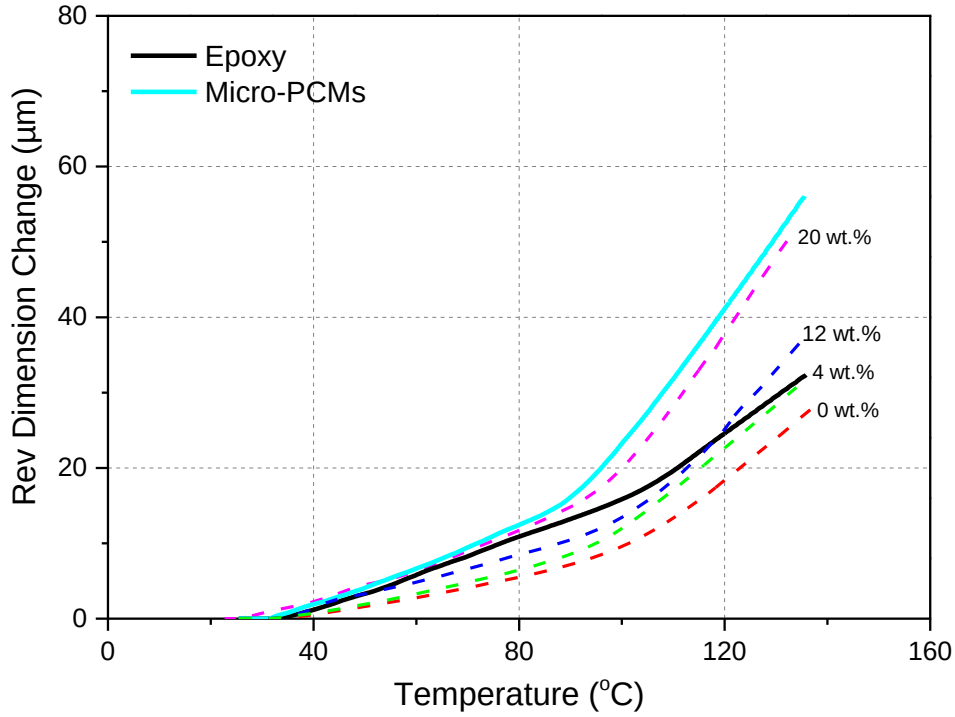

Figure 4-8 The temperature dependence of reversing dimension change with variable weight fraction of micro-PCMs

Table 4-4 The coefficient of thermal expansion and glass transition temperature

Micro-PCMs weight fraction/%	α_1 /$10^{-6}K^{-1}$	α_2 /10^{-6} K^{-1}	T_g^* /°C
0	45	200	98
4	54	209	99
12	59	258	98
20	63	263	96
Epoxy	67	133	104
Micro-PCMs	63	233	93

*T_g was determined from the inflection on the CTE curves.

Incorporating micro-PCMs into composite laminates increased the coefficient of thermal expansion below and above the *Tg*. The increase in CTE is due to the micro-PCMs/matrix interaction that influenced the conformational changes of the epoxy polymer chain segments [157]. The thermal expansion of the micro-PCMs-enhanced composite laminates depends on both the epoxy and micro-PCMs, and the interfacial properties between the two components. At micro-PCMs weight concentrations of 0, 4 and 12 %, the variation of the CTE was dominated by the epoxy whereas the reversing curve of composites with higher micro-PCMs loadings (weight fraction of 20 %) almost followed that of the micro-PCMs. It is believed that the thermal expansion of micro-PCMs below the T_g was supressed by the epoxy and then relaxed under a rubbery matrix.

It has been demonstrated that thermophysical properties, including the CTE and *Tg*, can be significantly affected by the interfacial properties of modified epoxy/particulate composites [158]. A strong interaction between filler and polymer will promote better thermophysical properties. It should be noted that the weight fraction of micro-PCMs plays a significant role on determining the interfacial properties between microcapsules and epoxy. A poor wetting of microencapsulated PCMs by epoxy resin can result in a weak interfacial bonding. Based on the results presented in Fig. 4-8 and Table 4-4, when micro-PCMs are fully wetted, i.e. at lower weight fractions, the epoxy controls the thermal expansion coefficient of the composite laminates. In comparison, a higher loading of micro-PCMs (20 wt.%) results in a high viscosity system [159] that leads to poor impregnation of microcapsules as shown in Fig. 4-9. The lower thermophysical properties are consequently expected due to the weak adhesion.

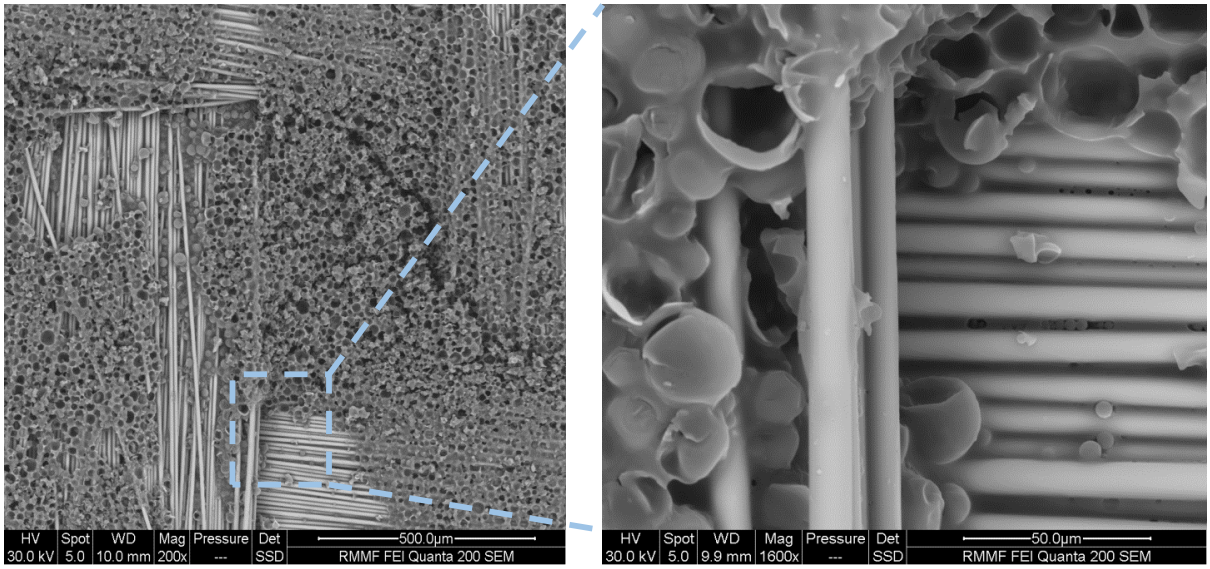

Figure 4-9 SEM micrographs of glass fibre/epoxy composites with 20 wt.% of micro-PCMs at low and high magnifications

4.4. Summary

Thermophysical properties of woven glass fibre/epoxy laminates incorporating micro-PCMs were investigated with various microencapsulated PCM concentrations. DSC was used to investigate the phase change characteristics of the micro-PCMs-enhanced composites. It was found that the enthalpy of the composite laminates, studied in this work, is proportional to the weight fraction of the embedded micro-PCMs. In addition, the glass transition temperature of the composite laminates was not significantly changed due to the introduction of micro-PCMs. The overall thermal conductivity of micro-PCMs-enhanced glass fibre/epoxy composite laminates was decreased due to the lower thermal conductivity of the microcapsules. Reduction of the thermal conductivity was caused by a non-uniform distribution of micro-PCMs in the interlaminar region.

Thermal stability was also investigated using TGA, and it was revealed that the inclusion of micro-PCMs reduced the thermal decomposition temperature due to the weak interface between microcapsules and the host epoxy resin. The microencapsulated PCMs can be thermally stable up to about 415 °C with the assistance of its shell material, however, it was

found that the thermal decomposition temperature was significantly reduced to approximately 140 °C due to the leakage of PCMs from the microcapsules.

Dimensional stability of the composite laminates incorporating micro-PCMs was investigated by measuring the through-thickness coefficient of thermal expansion using a modulated temperature programme. It was found that the CTE of micro-PCMs-enhanced glass fibre/epoxy composite was increased with increasing of the weight fraction of micro-PCMs. The SEM micrographs of composite laminates with a higher weight fraction of micro-PCMs revealed a poor wetting between the epoxy and micro-PCMs. It can be concluded that the weak interfacial properties between the epoxy resin and microcapsules are responsible for the reduction in thermophysical properties of the composite laminates.

5. EFFECT OF MICRO-PCMS ON VISCOELASTIC PROPERTIES OF MULTIFUNCTIONAL COMPOSITE

5.1. Introduction

Amongst thermophysical characteristics, viscoelastic properties over a wide range of frequency and temperature are crucial to adaptation of FRP composites incorporating micro-PCMs in engineering applications. Furthermore, thermal management capabilities are strongly influenced by not only the filler but also thermo-mechanical properties of the matrix. The characterisation of viscoelastic properties on a newly introducing composite is crucial due to the viscoelastic nature of the polymer based matrix. The physical and mechanical properties of the polymer are drastically changed at T_g due to the glass-rubber phase transition. Thus, a maximum operating temperature for polymer-based composites is determined based on T_g [160]. Therefore, characterising all effective parameters that may affect the T_g is essential for successful adaptation of micro-PCMs-incorporated composite laminates. Although the influence of micro-sized particles on the glass transition temperature of the host polymer has been reported in the literature [107, 161, 162], the glass-rubber relaxation behaviour of FRP composite incorporating micro-PCMs is still unknown. In this chapter, the viscoelastic behaviour of FRP composites incorporating micro-PCMs is presented.

5.2. Materials & Methods

5.2.1. Materials

The same materials and same fabrication methods were used as presented in Chapter 3.

5.2.2. Dynamic mechanical analysis

Dynamic mechanical analysis (DMA) was performed in single cantilever mode using a Pyris Diamond DMA (PerkinElmer, USA). Constant strain amplitude of 10 μm was used with a frequency of 1 Hz, while the temperature scan range was from 0 °C to 150 °C at a heating rate of 2 K/min. Micro-PCMs-enhanced glass–epoxy composite laminates with eight layers were manufactured using the method described in Chapter 3 to suit the single cantilever mode. DMA test specimens of 20 mm × 8 mm × thickness were then cut from these laminates using a diamond saw. A neat resin epoxy with a thickness of 2 mm was prepared as a reference. Storage modulus, loss modulus and tan δ were obtained as a function of temperature. In addition, a synthetic-frequency multiplexing mode (0.5, 1, 2, 5 and 10 Hz) was used to assess glass transition relaxation. Dynamic mechanical analysis of micro-PCMs capsules was also conducted for comparison purposes. To this end, DMA was performed using compression mode with a frequency of 1 Hz and modulation force of 0.5 N using a Q400EM (TA instruments, USA). The storage modulus (E'), loss modulus (E'') and tan δ (E''/E') of PCM microcapsules were obtained in a temperature range of 25°C to 140°C with a heating rate of 2 K min^{-1}. Furthermore, compression tests to assess the influence of melting transition of micro-PCMs on the mechanical properties of multifunctional composites were performed. All these tests were conducted using a Q800 DMA (TA instruments, USA) under a constant strain of 1 % while the temperature was ramped from 30°C to 50°C. The sample size for these compression tests was 5 mm × 5 mm.

5.2.3. Mechanical tests

Short beam strength (SBS) tests were performed at below and above the melting temperature of PCMs (about 37°C) to assess how the solid ↔ liquid phase transition influences the mechanical properties of the multifunctional composites. Short beam strength of micro-

PCMs-enhanced glass/epoxy composite was determined according to ASTM D2344-13.Test coupons (18 mm length × 6 mm width) were prepared using a diamond saw corresponding to a loading span length-to-specimens thickness ratio of 4.0. Tests were conducted using an Instron 5569 with an environmental chamber (3119-605) at a loading rate of 1 mm min^{-1} under room (25°C) and elevated temperatures (50°C). All tests were repeated at least five times and the average values are reported.

5.3. Results and discussion

5.3.1. Dynamic mechanical analysis

5.3.1.1. Transitions and relaxations temperature dependence

The viscoelastic behaviour of micro-PCMs-enhanced glass/epoxy composite laminates was investigated through DMA. Fig. 5-1 illustrates differences in the temperature dependence of storage modulus as a function of micro-PCMs concentration. The storage modulus of glass/epoxy laminates was significantly higher than that of the neat epoxy resin. Introducing micro-PCMs, however, had an adverse effect on the storage modulus of composites, as shown in Fig. 5-1. A micro-PCMs loading of 4 wt.% resulted in 13 % reduction in the storage modulus of the multifunctional composites.

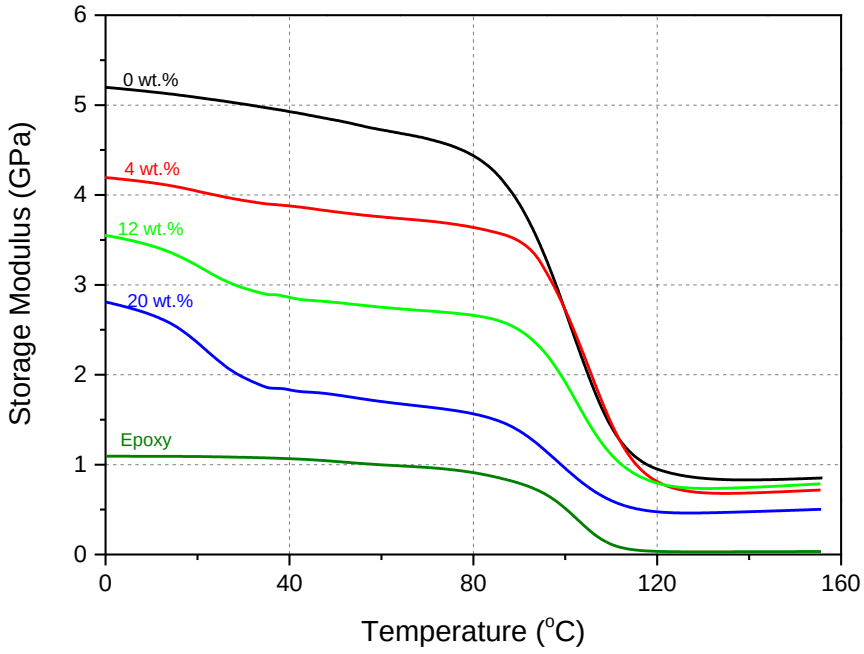

Figure 5-1 Temperature dependence of glass/epoxy laminates incorporating micro-PCMs on the storage modulus

The reduction of storage modulus can be related to the crosslinking density in the composite [83, 102]. The apparent crosslinking density can be determined from the storage modulus at rubbery plateau region, E'_r using equation (5-1) [163]:

$$E'_r = 3qnRT \qquad (5\text{-}1)$$

where q is the concentration of inactive chains, a variable with an unknown value that is considered to be close to unity as a first approximation [164], n is the apparent crosslinking density, R is the gas constant (8.314 J K^{-1} mol^{-1}) and T is temperature (K). The storage modulus at rubbery plateau region was determined at $T = T_g + 30$ °C.

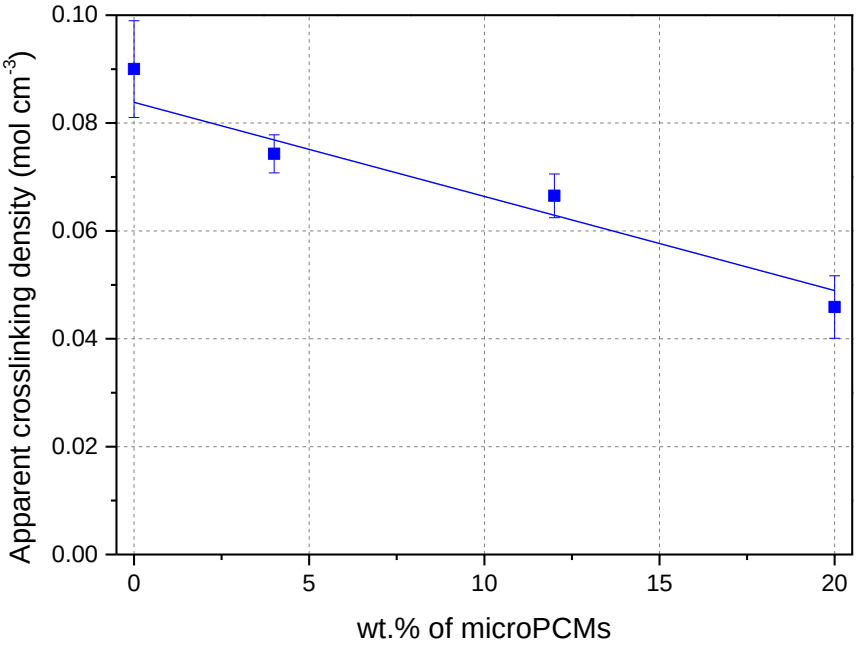

Figure 5-2 Apparent crosslinking densities as function of micro-PCMs weight concentration evaluated from storage modulus in rubbery phase (E'_r at 130°C)

The apparent crosslinking density for composite laminates, with various loading fraction of micro-PCMs, was calculated using equation 5-1 and results are shown in Fig. 5-2. A linear relationship between the apparent crosslinking densities and micro-PCMs loading is evident. Therefore, it is expected that the stiffness of the laminates will be significantly lowered at high micro-PCMs concentrations. It is noteworthy that the melting of PCMs around 37°C also resulted in a further reduction of the storage modulus that is more pronounced for composites with 20 wt.% of micro-PCMs.

Fig. 5-3 shows the loss modulus as a function of temperature for the composite laminates with various weight fraction of micro-PCMs. The maximum loss modulus (peak height) was inversely proportional to the microcapsule's loading. This reduction can be attributed to the weak bonding between micro-PCMs and the epoxy resin.

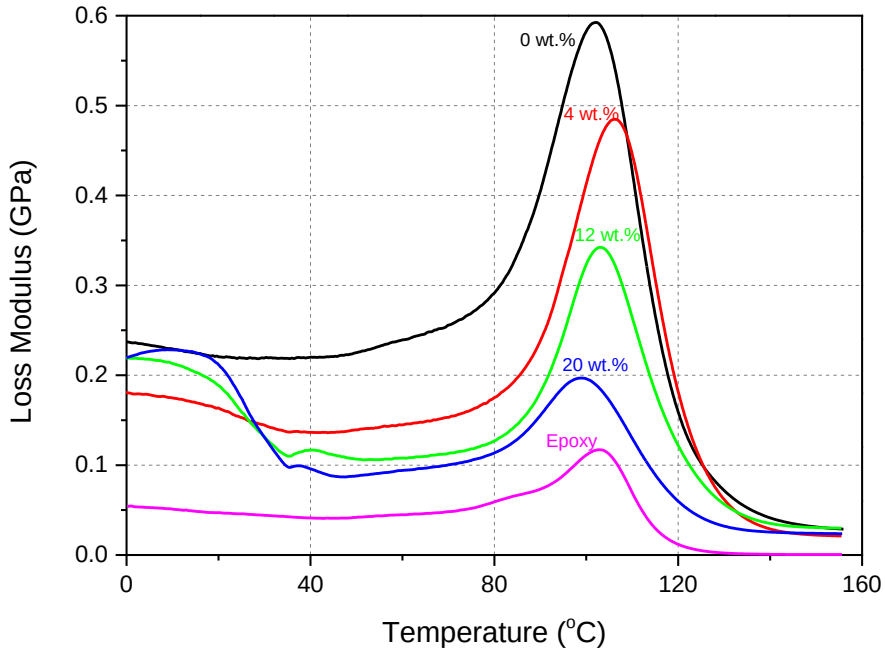

Figure 5-3 Temperature dependence of glass/epoxy laminates incorporating micro-PCMs on the loss modulus

Akay [165] reported that the evaluation of T_g from the maximum loss modulus was more consistent and precise in comparison with that from the maximum of tan δ. The glass transition temperature, T_g, determined using the loss modulus is presented in Table 5-1 together with the storage modulus of the glassy phase, (E'_g at 25°C) and rubbery phase (E'_r at 130°C) There were almost no changes in the glass transition temperature, T_g after addition of glass fibres when compared to that of the neat resin. At micro-PCMs concentration of 4 wt.%, the T_g was slightly increased from 102°C to 106°C (i.e. a 4% increment). This change in the glass transition temperature can be attributed to the variation of segmental motion restrictions

in the epoxy matrix. It was reported that the incorporation of micro-sized fillers could increase the T_g of a composite due to the immobilization of the polymer molecular chains near the surface of the filler [96, 166]. However, further addition of the filler will cause the separation of molecular chains and will increase the segmental motion. This observation suggests that there is a critical micro-PCMs concentration below which the segmental mobility is significantly restricted.

Table 5-1 Viscoelastic properties of micro-PCMs enhanced glass-epoxy composite

Micro-PCMs weight fraction/%	E'_g /GPa	E'_r /GPa	T_g /°C	E''_{max} /GPa	$\tan(\delta)_{max}$
0	5.1	0.85	102	0.58	0.298
4	4.0	0.69	106	0.48	0.309
12	3.1	0.73	103	0.34	0.243
20	2.1	0.46	99	0.2	0.218
Epoxy	1.1	0.03	103	0.18	0.634

The interfacial bonding between composite constituents can also play a significant role in the variation of glass transition temperature. Some studies have suggested that the interfacial bonding between a filler and host polymer can be correlated to the measured peak tan δ [118, 167, 168]. In this case, a high maximum tan δ is an indication of poor interfacial bonding. To examine the validity of this hypothesis in composites with more than one type of filler (glass fibres and microencapsulated PCM in this study), the temperature dependence of tan δ was analysed and shown in Fig. 5-4.

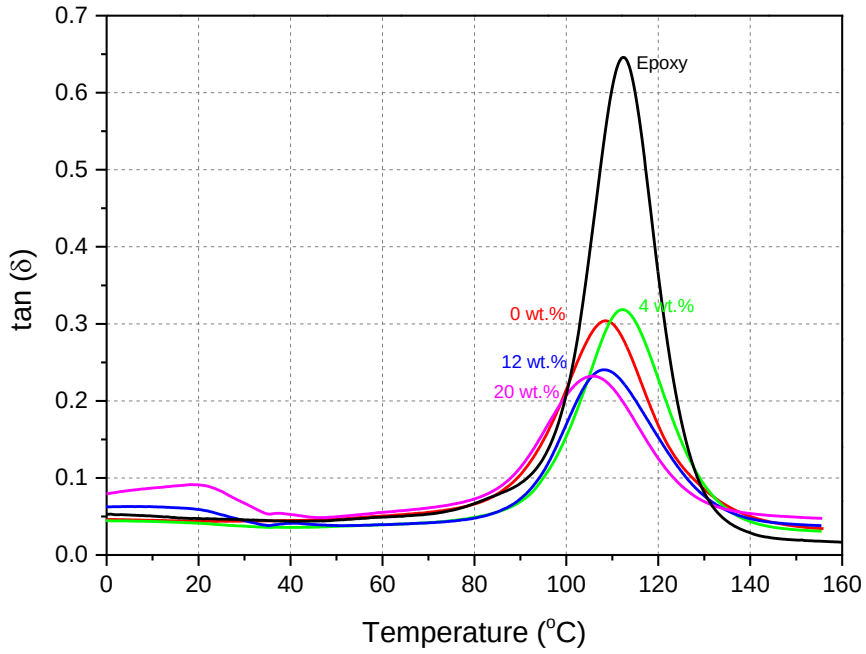

Figure 5-4 Temperature dependence of glass/epoxy laminates incorporating micro-PCMs on Tan δ

Incorporating 4 wt.% of micro-PCMs did not result in a significant variation of the peak tan δ for multifunctional composites. In other words, the rate of the reduction of the storage and loss moduli due to addition of micro-PCMs was very close. Therefore, the increment in *T*g after embedding 4 wt.% of micro-PCMs can only be attributed to the segmental motion restrictions. For higher concentration of micro-PCMs, although the maximum tan δ was decreased, this cannot be interpreted as an improvement in the filler/polymer interfacial bonding. In fact, the rate of the reduction for storage modulus due to the incorporation of micro-PCMs was much higher than the corresponding rate for the loss modulus.

Furthermore, the SEM images of fractured surface with revealed that the interfacial bonding is deteriorated with increasing weight fraction of micro-PCMs, as illustrated in Fig. 3-5 and 3-10. Therefore, it can be concluded that the maximum tan δ cannot be used to estimate the interfacial bonding for composites with more than one type of filler. The same conclusion has been reached for the case of hybrid composites [167, 168]. To further investigate the effect of

incorporating micro-PCMs on the glass transition temperature of multifunctional composites and in order to identify related mechanisms, the concepts of "apparent activation energy" and "free volume" can be utilised.

5.3.2. Apparent activation energy

The activation energy is considered as "the minimum activation barrier" that should be overcome so that a large-scale molecular motion can happen in a polymer. The activation energy, ΔE_a can be calculated using data collected from multi-frequency tests using Arrhenius equation (5-2) [169, 170]:

$$\Delta E_a = -R \frac{d[\ln(f)]}{d[\frac{1}{T_g}]} \qquad (5\text{-}2)$$

where f is the measuring frequency, *R* is the universal gas constant (8.314 J K^{-1} mol^{-1}) and *T*g is the glass transition temperature. Fig. 5-5 shows the tan δ of multifunctional composites over a range of frequencies from 0.5 to 10 Hz. It can be seen that the glass transition temperature determined from tan δ curves shifts to a higher temperatures as the measuring frequency increases, which is the general trend in solid polymers [100].

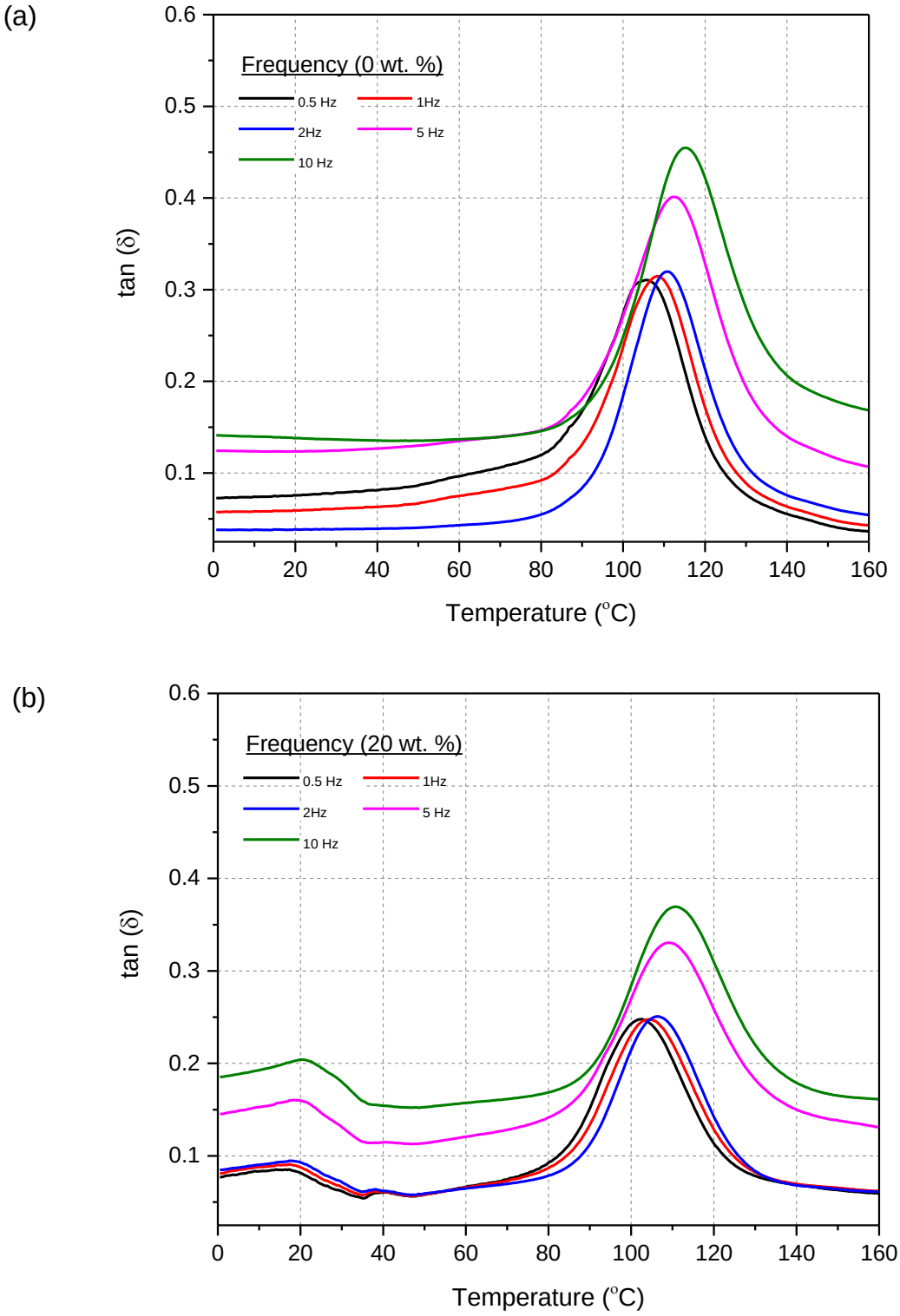

Figure 5-5 The a temperature scan as a function of tan δ at different frequencies across the T_g of glass/epoxy laminates incorporating micro-PCMs (a) 0 wt.% and (b) 20 wt.%

Using equation (5-2), the activation energy can be determined from the slope ($-\Delta E_a/R$) of linear regression equation from $\ln(f)$ versus $1000/T_g$ as shown in Fig. 5-6. The apparent activation energy for composite specimens was obtained by fitting a linear regression on the slope of Arrhenius plot, and the results are presented in Table 5-2. Introducing 4 wt.% of micro-PCMs resulted in an increase in the activation energy by 7 % while higher concentration of the micro-PCMs had an adverse effect. Several studies [171, 172] have reported that the variation of activation energy can be attributed to the interfacial properties between the filler and matrix. Thus, the decrease in ΔE_a involves reduced segmental constrains between micro-PCMs and epoxy that is happening in composites with micro-PCMs weight fraction of more than 4%.

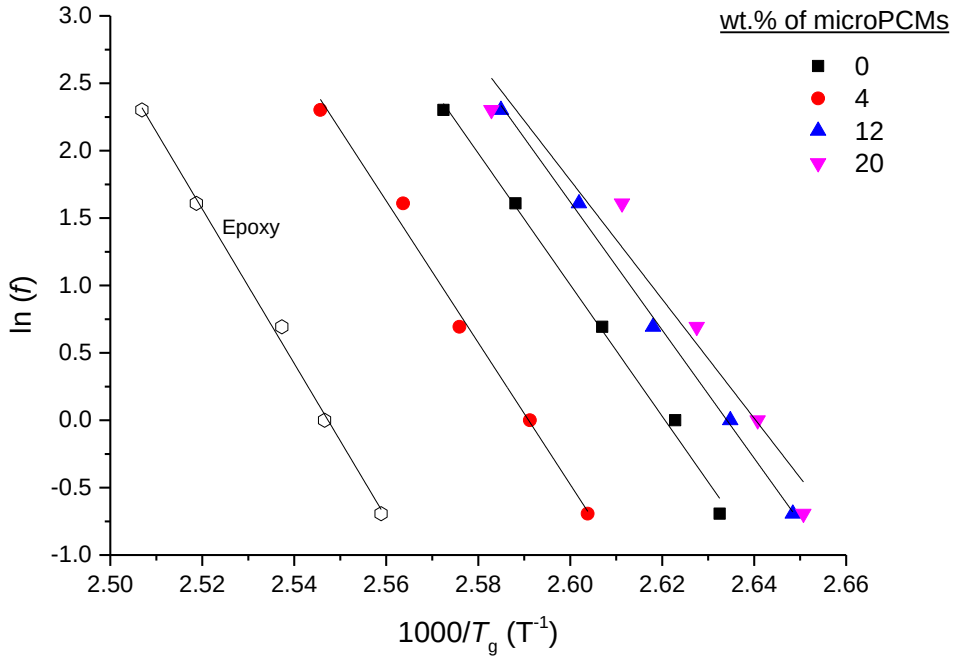

Figure 5-6 The variation of $ln(f)$ versus $1000/T_g$. The T_g was measured from the peak height of tan δ.

Table 5-2 The apparent activation energies (ΔE_a) with correlation coefficient (R^2) value

Micro-PCMs weight fraction/%	ΔE_a/kJ mol^{-1}	Slope	R^2
Epoxy	562.9	63.14	0.995
0	405.5	48.78	0.995
4	437.2	52.59	0.992
12	395.2	47.54	0.998
20	367.2	44.17	0.960

5.3.3. Free volume interpretation

The transitions of the polymer can also be described by the changes in free volume, which is the space between molecules for an internal movement. The glass transition is associated with the expansion of the free volume allowing greater chain mobility [100]. The fractional free volume fraction (f_g) at the T_g can be determined from the peak of tan δ using equation (5-3) [173]:

$$f_g = \left(\frac{\Delta\alpha \cdot \mathrm{B} \cdot \frac{C_2}{C_1}}{2.303} \right)^{\frac{1}{2}} \qquad (5\text{-}3)$$

where $\Delta\alpha$ is the difference between the CTE of below and above T_g, B is a numerical constant generally considered close to 1 if the Δα is entirely associated with free volume [174], and C_1 and C_2 are William-Landel-Ferry (WLF) constants. WLF constants were found with the equation (5-4) [173]:

$$\frac{1}{\log\left(\frac{f}{f_f}\right)} = \frac{C_2}{C_1}\left(\frac{1}{T_g - T_{gr}}\right) + \frac{1}{C_1} \qquad (5\text{-}4)$$

where r is the reference parameter at 1Hz. The WLF constants were found from the slope and the y-intercept of a linear regression line from a plot of $\frac{1}{log\frac{f}{f_r}}$ versus $\frac{1}{T_g - T_{gr}}$. A summary of the calculated fractional free volume is presented in Table 5-3. An introduction of 4 wt.% micro-PCMs into the glass/epoxy composites decreased the free volume by 10 %. Further incorporation of micro-PCMs in glass fibre/epoxy laminates resulted in an increment of the free volume. The decrease in the free volume indicates a strong interaction between the epoxy and micro-PCMs at low microcapsule concentration (i.e. 4 wt.%). This results indicates that there is a critical concentration where the micro-PCMs is favoured in terms of chain mobility with the epoxy as the free volume decreased at lower micro-PCMs concentration.

Table 5-3 Fractional free volume (f_g) and input parameters

Micro-PCMs weight fraction/%	α_1 /10^{-6} K^{-1}	α_2 /10^{-6} K^{-1}	$\Delta\alpha$ /10^{-6} K^{-1}	C_2/C_1 /K^{-1}	f_g
0	45	200	155	8.27	0.0236
4	54	209	155	6.61	0.0211
12	59	258	199	6.99	0.0246
20	63	263	200	7.89	0.0262
Epoxy	67	133	66	4.68	0.0116
Micro-PCMs	63	233	-		

5.3.4. The influence of phase transition

5.3.4.1. Micro-PCMs capsules

It is interesting to note that an unusual transition was observed on DMA results in the temperature range of 0 to 40 °C (see Fig. 5-1 and 5-3). To identify the cause of this supplementary transition, Fig. 5-7 shows the complex modulus (E^*) of micro-PCMs as a function of temperature, measured using DMA.

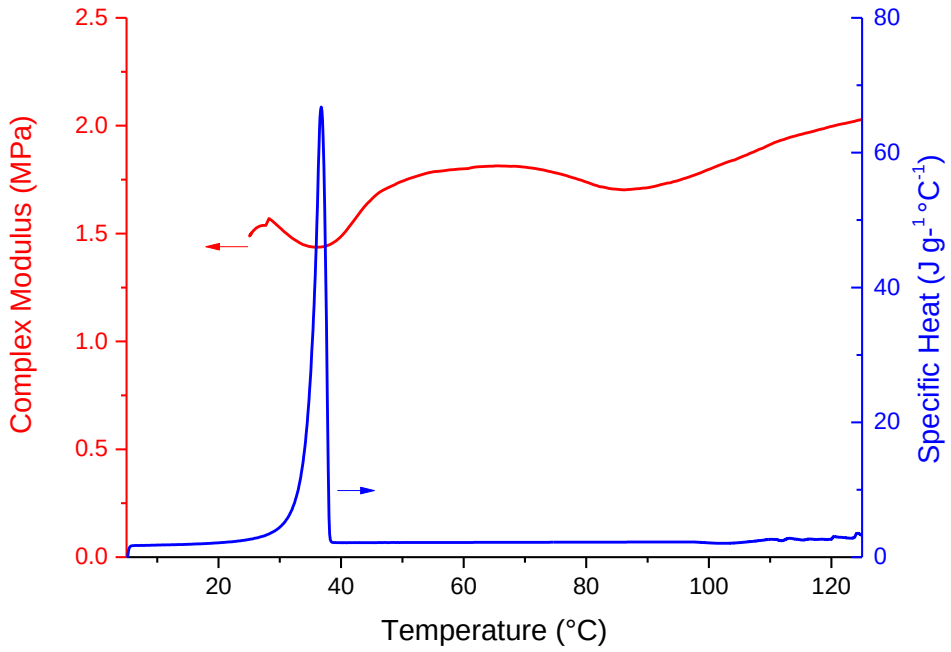

Figure 5-7 An overlay of DMA and DSC curves illustrating complex modulus and specific heat of micro-PCMs, respectively.

Considering the fact that the minimum complex modulus is reached at approximately 38 °C, corresponding to the melting temperature of PCMs, it is hypothesised that the supplementary transition is due to PCMs melting. This phenomenon can be indirectly confirmed by two observations: (1) melting is independent of the frequency as it is a thermodynamic event, unlike the T_g (see Fig. 5-5) and (2) an overlay between the complex modulus and DSC heat flow of micro-PCMs shows that the melting temperature is matched by the minimum

complex modulus, as illustrated in Fig. 5-7. The correlation of DMA and DSC curves has already been used to determine the melting and glass transitions of powders [175]. Considering above-mentioned observations, it can be concluded that the supplementary reduction of loss modulus is related to the melting of PCMs.

5.3.4.2. Short Beam Strength

In the previous section, the variation of storage and loss moduli in the low temperature range was related to the melting transition of PCMs. In other words, it was concluded that the liquid-phase of PCM influence the viscoelastic response of the specimens. To investigate the effect of the phase transition on mechanical properties, short beam strength tests were conducted at different temperature corresponding to solid and liquid phase of PCMs. The experiments were performed at room (T = 25°C) and elevated temperatures (T = 50°C) where no exothermic peak was observed in the DSC curve. The calculated shear strength of the multifunctional composites with different weight fraction of micro-PCM are summarised in Table 5-4. As it is expected, the short beam shear strength decreased with increasing the weight fraction of micro-PCMs under both temperatures. This behaviour can be related to the deterioration of interfacial strength in composites due to incorporating microcapsules, as discussed in Chapter 3. In addition, it can be seen from Table 5-4 that the shear strength at elevated temperature is lower than that of the room temperature. However, the difference is almost independent for the micro-PCMs loading up to 12 wt.%. Only in composites with 20 wt.% of micro-PCMs was a higher reduction of 19% observed.

Table 5-4 The effect of incorporating micro-PCMs on short beam shear properties as a function of temperature

Micro-PCMs weight fraction/%	SBS at 25°C /MPa	SBS at 50°C /MPa	The difference /%
0	43.76 ± 1.75	38.42 ± 0.99	12.2
4	36.82 ± 0.82	31.81 ± 0.77	13.6
12	18.28 ± 0.68	15.77 ± 0.88	13.7
20	10.11 ± 0.65	8.18 ± 0.54	19.1

Previous experimental results show that most of the micro-PCMs undergo a large volume change (~10 %) while melting [23, 142, 176]. As it is discussed in section 4.3.5, the CTE is dominated by the behaviour of epoxy for micro-PCM loadings up to 12 wt.% whereas for higher concentration of 20 wt.% it is the micro-PCM that controls the coefficient of thermal expansion. These results show that the epoxy suppress the volume change of micro-PCMs at low concentrations (4 and 12 wt.%), however, the restriction is compliant at micro-PCMs concentration of 20 wt.%. Thus, it can be said that the volume change in composites could influence the interfacial strength between microcapsules and the matrix. This is based on the fact that the CTE affects the stress transfer in the interfacial region [94]. Therefore, the effect of phase transition on the mechanical properties of multifunctional composites depends on dominant mechanism in determining the CTE.

It should also be noted that the volume fraction of the epoxy was reduced with increasing micro-PCMs concentration, as it is evident from SEM images of the fractured specimens (see Fig. 3-5.). At lower micro-PCMs concentrations, the epoxy with a relatively higher stiffness, can suppress the volume change of micro-PCMs. However, micro-PCMs can freely expanded due to the less amount of the epoxy used at higher concentrations, which is also reflected in the CTE values. Taking into account the CTE results, it can be concluded that the liquid phased micro-PCM influences the interfacial properties for the high loading rate of 20 wt.%.

This observation suggests that there should be a critical micro-PCMs concentration between 12 and 20 wt.% where the volume expansion of micro-PCMs could be restricted.

5.3.4.3. Through-thickness compression tests

The influence of PCM phase transition on the mechanical properties was discussed above. To verify the above observations, compression tests in the through-thickness direction were performed to explain the variation of viscoelastic properties over the PCMs melting transition. Fig. 5-8 shows the changes in normalised compression stress while the temperature was ramped from 30 to 50 °C at a rate of 2 K min^{-1}.

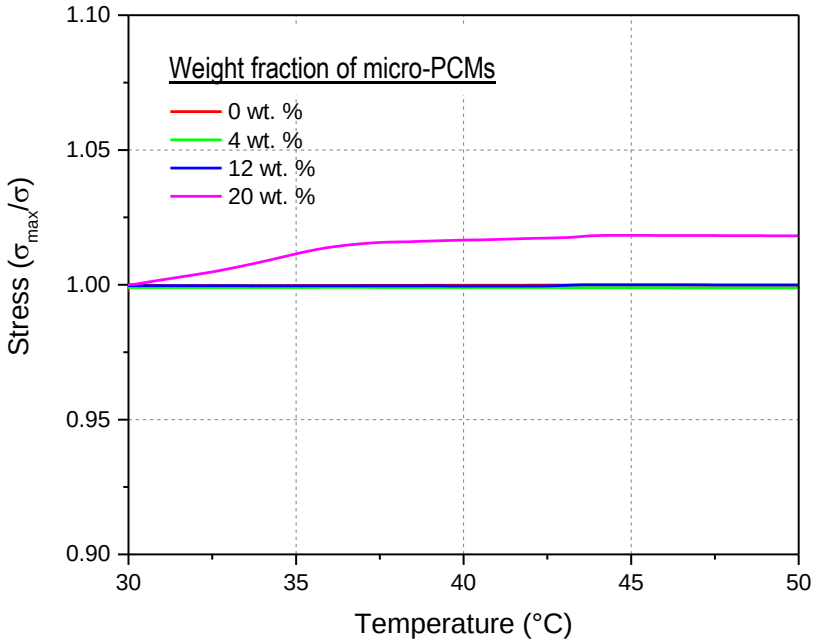

Figure 5-8 Temperature dependence of PCM enhanced composites under a constant 1 % strain

During the experiment, when the volume change was pronounced, the stress varied to maintain a constant strain of 1 %. It is interesting to note that the stress was increased only in the laminate containing 20 wt.% of micro-PCMs when the temperature was about 37°C. This temperature is corresponding to the melting temperature of the PCM used in this study. This observation indicates that the volume change of micro-PCMs took place during the melting

transition, and was pronounced when micro-PCMs concentration was 20 wt.%, which is consistent with the results from SBS tests (as discussed in section 3.3.2.5).

5.4. Summary

The viscoelastic properties of woven glass-epoxy laminates incorporating various concentrations of micro-PCMs were investigated using DMA scans. It was revealed that the storage modulus of the glassy phase (at 25°C) was decreased with increasing PCMs concertation (approximately 1.3 GPa per micro-PCMs wt.%) due to the prevention of potential crosslinking in the composite. The T_g was measured from the peak height of the loss modulus curves and it was increased at after incorporating 4 wt.% of micro-PCMs. The micro-PCMs occupied a free space between glass-fibres causing a decreasing trend of T_g with increasing micro-PCMs loading. Multi-frequency DMA scans was performed to understand how micro-PCMs affects the glass transition. Using "apparent activation energy" and "free volume" concepts the variation of glass transition temperature was explained. It was found that the additional loss peak observed in DMA results is due to the PCMs melting transition. The phase transition also affected the mechanical properties when a high concentration of 20 wt.% of micro-PCMs was used. Consequently, viscoelastic properties of micro-PCMs-enhanced glass-epoxy composites were significantly affected by the microcapsule weight fraction.

6. CONCLUSION & RECOMMENDATION

6.1. Conclusion

Multifunctional composites incorporating micro-PCMs is one of the promising solutions to develop material systems that exhibit thermal storage capability as well as load bearing competency. The main goal of this project was to characterise the inclusion effect in order to fully understand the interactions between embedded micro-PCMs and the host composite. This thesis demonstrated that the goal was successfully achieved as the experimental study conducted through Chapter 3-5. A detailed achievement summary for different aspects of the project is presented in each Chapter.

Herein, the key answers for the research questions from section 1.3 are given. In this project, micro-PCMs were integrated into glass Fibre Reinforced Polymer (FRP) composites and their mechanical, thermophysical and viscoelastic properties were investigated. It was found that the reduction of mechanical properties including tensile, compressive, and flexural was directly proportional to the weight fraction of micro-PCMs. The failure mechanisms changed from fibre/matrix failures to interlaminar delamination after incorporating 12 wt.% of micro-PCMs. It was observed that the interfacial bonding between micro-PCMs and epoxy controls the failure mechanism. The increased viscosity of matrix system due to incorporating micro-PCMs influences the wetting of the fillers during the manufacturing and consequently affects the interfacial bonding. Furthermore, mode I interfacial fracture toughness was investigated using DCB tests and toughening mechanisms were identified. It was found that the mode I fracture toughness at crack initiation is controlled by matrix-dominated properties. For the steady-state crack propagation, the mode I interfacial fracture toughness was initially increased due to the combination of fibre bridging and particle toughening (i.e. crack pinning

and debonding) at micro-PCMs weight fraction of 4 %. However, the trend was reversed at higher micro-PCMs concentrations due to the poor interfacial properties.

Regarding thermophysical properties, it was found that the enthalpy of the multifunctional composites was proportional to the weight fraction of micro-PCMs. The phase change properties of the microencapsulated PCMs were not affected after incorporating these materials in FRP composites. The enthalpy (heat of fusion/crystallisation) measured from DSC was linearly proportional to the weight fraction of micro-PCMs used in the composite. Furthermore, it was observed that the enthalpy from the heat flux apparatus were also proportional to micro-PCMs concentration used in the composite. These observations suggest that the integrity of micro-PCMs was preserved. The decomposition temperature was reduced due to the weak interface. Also, the leakage of paraffin-based core material from damaged PCMs caused significant degradation on thermal decomposition. The CTE of micro-PCMs-enhanced glass fibre/epoxy composite increased with increasing of the weight fraction of micro-PCMs. The CTE of multifunctional composites was dominated by that of the epoxy up to micro-PCM weight fraction of 12 %. For composites with higher weight fraction of micro-PCMs, the coefficient of thermal expansion was controlled micro-PCMs. This observation suggests that the CTE was strongly influenced by the interfacial properties.

In respect to viscoelastic properties, it was observed that the storage modulus was reducing due to the reduction in crosslinking density caused by the inclusion of micro-PCMs. The T_g determined from the peak of loss modulus was also changed as a result of incorporating micro-PCMs. At a micro-PCMs concentration of 4 wt.%, the T_g was initially increased because of the restriction in segmental motion of the epoxy matrix. However, further addition of micro-PCMs caused a reduction in $T_{g,}$ which can be attributed to the weak bonding between micro-PCMs and the epoxy matrix. The activation energy and free volume concepts were used to describe the observed changes. In regards to phase transition effects, the SBS

tests at below and above the melting temperature of microcapsules were conducted. It was found that the effect of the phase transition is pronounced at higher micro-PCMs concentrations.

6.2. Recommendation

6.2.1. Thermal management capabilities

Throughout this project, the inclusion effects of micro-PCMs on the mechanical and thermal behaviour of host composites have been comprehensively characterised. However, some key aspects of thermal management capabilities are not fully investigated due to the time limitations. The design parameters such as thermal cycles (melting/freezing) can be investigated to elaborate the feasibility of the utilising the multifunctional composites in a practical application. As a consequence of the material characterisation from this thesis, the effectiveness of micro-PCMs in developing multifunctional composites can be realised. The larger scale investigation, however will enable adoption of micro-PCMs reinforced composite into engineering thermal management applications (e.g, electronic packaging).

6.2.2. Sandwiched composite structure

In this project, it was found that the thermophysical properties mainly depend on the weight fraction of embedded micro-PCMs. In regards to the structural integrity, it was also observed that the mechanical properties of multifunctional composites are significantly reduced after incorporating 12 wt.% of micro-PCMs. To achieve an optimised solution where high thermal storage capacity is accompanied with minimum deterioration of load-bearing capability, a systematic approach to design the multifunctional laminate can be adopted. One possible solution can be based on partial distribution of micro-PCMs in the cross-sectional area using a sandwich structure. For multifunctional composites, micro-PCMs can be incorporated in the

core material to provide the thermal management capacity while conventional FRP composite skins is supporting bending and protecting the core. Such multifunctional composites can be used in different engineering applications.

6.2.3. Nano-modification

Heat dissipation is one of the key elements in thermal management applications to attain optimum thermal performance. The low intrinsic thermal conductivity of polymers can cause reliability issues such as overheating of melted PCMs in multifunctional composites. Therefore, further study to improve the thermal conductivity of polymers using nano-particles is warranted to identify appropriate high thermal conductive fillers with low thermal expansion coefficients. To achieve an efficient method of incorporating nanoparticles in micro-PCMs-enhanced composites, a multiscale study is necessary. This will provides the opportunity to understand how the composite behaviours and interact in different scales from macro- to nano-scale. The combined knowledge on the multiscale nature of the composite will offer the comprehensive background information.

7. REFERENCE

[1] Gibson RF. A review of recent research on mechanics of multifunctional composite materials and structures. Composite Structures. 2010;92(12):2793-2810.

[2] Noor AK, Venneri SL, Paul DB, Hopkins MA. Structures technology for future aerospace systems. Computers & Structures. 2000;74(5):507-519.

[3] Gibson RF. Principles of composite material mechanics: CRC Press; 2011.

[4] Mouritz AP. Introduction to Aerospace Materials: American Institute of Aeronautics and Astronautics; 2012.

[5] Wang S, Qiu J. Enhancing thermal conductivity of glass fiber/polymer composites through carbon nanotubes incorporation. Composites Part B: Engineering. 2010;41(7):533-536.

[6] Sia Nemat-Nasser SN-N, Thomas Plaisted,, Anthony Starr aAVA. Multifunctional Materials. In: Bar-Cohen Y, editor. Biomimetics: biologically inspired technologies CRC Press; 2005.

[7] Salonitis K, Pandremenos J, Paralikas J, Chryssolouris G. Multifunctional Materials Used in Automotive Industry: A Critical Review. In: Pantelakis S, Rodopoulos C, editors. Engineering Against Fracture: Springer Netherlands; 2009. p. 59-70.

[8] Sen S, Schofield E, O'Dell JS, Deka L, Pillay S. The development of a multifunctional composite material for use in human space exploration beyond low-earth orbit. JOM. 2009;61(1):23-31.

[9] Moore GE. Progress in digital integrated electronics. Electron Devices Meeting, 1975 International, vol. 211975. p. 11-13.

[10] Ling Z, Zhang Z, Shi G, Fang X, Wang L, Gao X, et al. Review on thermal management systems using phase change materials for electronic components, Li-ion batteries and photovoltaic modules. Renewable and Sustainable Energy Reviews. 2014;31(0):427-438.

[11] Carlberg B, Liu J, Li-Lei Y. Polymer nanofiber based continuous metal phase composite for thermal management applications. Electronic System-Integration Technology Conference (ESTC), 2010 3rd, 2010. p. 1-6.

[12] Zhou D, Zhao CY, Tian Y. Review on thermal energy storage with phase change materials (PCMs) in building applications. Applied Energy. 2012;92(0):593-605.

[13] Torquato S, Hyun S, Donev A. Multifunctional Composites: Optimizing Microstructures for Simultaneous Transport of Heat and Electricity. Physical Review Letters. 2002;89(26):266601.

[14] Shin Y, Yoo D-I, Son K. Development of thermoregulating textile materials with microencapsulated phase change materials (PCM). II. Preparation and application of PCM microcapsules. Journal of Applied Polymer Science. 2005;96(6):2005-2010.

[15] Sarier N, Onder E. The manufacture of microencapsulated phase change materials suitable for the design of thermally enhanced fabrics. Thermochimica Acta. 2007;452(2):149-160.

[16] Mondal S. Phase change materials for smart textiles – An overview. Applied Thermal Engineering. 2008;28(11–12):1536-1550.

[17] Mulligan JC, Colvin DP, Bryant YG. Microencapsulated phase-change material suspensions for heat transfer in spacecraft thermal systems. Journal of Spacecraft and Rockets. 1996;33(2):278-284.

[18] Chen C, Guo H, Liu Y, Yue H, Wang C. A new kind of phase change material (PCM) for energy-storing wallboard. Energy and Buildings. 2008;40(5):882-890.

[19] Voelker C, Kornadt O, Ostry M. Temperature reduction due to the application of phase change materials. Energy and Buildings. 2008;40(5):937-944.

[20] Cabeza LF, Castellón C, Nogués M, Medrano M, Leppers R, Zubillaga O. Use of microencapsulated PCM in concrete walls for energy savings. Energy and Buildings. 2007;39(2):113-119.

[21] Sá AV, Azenha M, de Sousa H, Samagaio A. Thermal enhancement of plastering mortars with Phase Change Materials: Experimental and numerical approach. Energy and Buildings. 2012;49:16-27.

[22] Abhat A. Low temperature latent heat thermal energy storage: Heat storage materials. Solar Energy. 1983;30(4):313-332.

[23] Farid MM, Khudhair AM, Razack SAK, Al-Hallaj S. A review on phase change energy storage: materials and applications. Energy Conversion and Management. 2004;45(9–10):1597-1615.

[24] Hasnain SM. Review on sustainable thermal energy storage technologies, Part I: heat storage materials and techniques. Energy Conversion and Management. 1998;39(11):1127-1138.

[25] Zalba B, Marín JM, Cabeza LF, Mehling H. Review on thermal energy storage with phase change: materials, heat transfer analysis and applications. Applied Thermal Engineering. 2003;23(3):251-283.

[26] Wirtz R, Tianwen Z, Yanyao J. Thermal and Mechanical Characteristics of a Multifunctional Thermal Energy Storage Structure. Components and Packaging Technologies, IEEE Transactions on. 2009;32(1):53-62.

[27] Shaikh S, Lafdi K. C/C composite, carbon nanotube and paraffin wax hybrid systems for the thermal control of pulsed power in electronics. Carbon. 2010;48(3):813-824.

[28] Khateeb SA, Amiruddin S, Farid M, Selman JR, Al-Hallaj S. Thermal management of Li-ion battery with phase change material for electric scooters: experimental validation. Journal of Power Sources. 2005;142(1–2):345-353.

[29] Schossig P, Henning HM, Gschwander S, Haussmann T. Micro-encapsulated phase-change materials integrated into construction materials. Solar Energy Materials and Solar Cells. 2005;89(2–3):297-306.

[30] Pasupathy A, Velraj R, Seeniraj RV. Phase change material-based building architecture for thermal management in residential and commercial establishments. Renewable and Sustainable Energy Reviews. 2008;12(1):39-64.

[31] Jankowski NR, McCluskey FP. A review of phase change materials for vehicle component thermal buffering. Applied Energy. 2014;113(0):1525-1561.

[32] Sarier N, Onder E. Organic phase change materials and their textile applications: An overview. Thermochimica Acta. 2012;540(0):7-60.

[33] Li T, Lee J-H, Wang R, Kang YT. Heat transfer characteristics of phase change nanocomposite materials for thermal energy storage application. International Journal of Heat and Mass Transfer. 2014;75(0):1-11.

[34] Fang X, Fan L-W, Ding Q, Yao X-L, Wu Y-Y, Hou J-F, et al. Thermal energy storage performance of paraffin-based composite phase change materials filled with hexagonal boron nitride nanosheets. Energy Conversion and Management. 2014;80(0):103-109.

[35] Zhang Z, Zhang N, Peng J, Fang X, Gao X, Fang Y. Preparation and thermal energy storage properties of paraffin/expanded graphite composite phase change material. Applied Energy. 2012;91(1):426-431.

[36] Lane GA. Phase change materials for energy storage nucleation to prevent supercooling. Solar Energy Materials and Solar Cells. 1992;27(2):135-160.

[37] Kenisarin M, Mahkamov K. Solar energy storage using phase change materials. Renewable and Sustainable Energy Reviews. 2007;11(9):1913-1965.

[38] Baetens R, Jelle BP, Gustavsen A. Phase change materials for building applications: A state-of-the-art review. Energy and Buildings. 2010;42(9):1361-1368.

[39] Athienitis AK, Liu C, Hawes D, Banu D, Feldman D. Investigation of the thermal performance of a passive solar test-room with wall latent heat storage. Building and Environment. 1997;32(5):405-410.

[40] Hawes DW, Banu D, Feldman D. Latent heat storage in concrete. Solar Energy Materials. 1989;19(3–5):335-348.

[41] Memon SA. Phase change materials integrated in building walls: A state of the art review. Renewable and Sustainable Energy Reviews. 2014;31(0):870-906.

[42] Feldman D, Shapiro MM, Fazio P. A heat storage module with a polymer structural matrix. Polymer Engineering & Science. 1985;25(7):406-411.

[43] Inaba H, Tu P. Evaluation of thermophysical characteristics on shape-stabilized paraffin as a solid-liquid phase change material. Heat and Mass Transfer. 1997;32(4):307-312.

[44] Lazaro A, Dolado P, Marín JM, Zalba B. PCM–air heat exchangers for free-cooling applications in buildings: Experimental results of two real-scale prototypes. Energy Conversion and Management. 2009;50(3):439-443.

[45] Jamekhorshid A, Sadrameli SM, Farid M. A review of microencapsulation methods of phase change materials (PCMs) as a thermal energy storage (TES) medium. Renewable and Sustainable Energy Reviews. 2014;31(0):531-542.

[46] Salunkhe PB, Shembekar PS. A review on effect of phase change material encapsulation on the thermal performance of a system. Renewable and Sustainable Energy Reviews. 2012;16(8):5603-5616.

[47] Hawlader MNA, Uddin MS, Zhu HJ. Encapsulated phase change materials for thermal energy storage: Experiments and simulation. International Journal of Energy Research. 2002;26(2):159-171.

[48] Fu S-Y, Feng X-Q, Lauke B, Mai Y-W. Effects of particle size, particle/matrix interface adhesion and particle loading on mechanical properties of particulate–polymer composites. Composites Part B: Engineering. 2008;39(6):933-961.

[49] Bagheri R, Pearson RA. Role of particle cavitation in rubber-toughened epoxies: 1. Microvoid toughening. Polymer. 1996;37(20):4529-4538.

[50] Bagheri R, Pearson RA. Role of particle cavitation in rubber-toughened epoxies: II. Inter-particle distance. Polymer. 2000;41(1):269-276.

[51] Pearson RA, Yee AF. Toughening mechanisms in thermoplastic-modified epoxies: 1. Modification using poly(phenylene oxide). Polymer. 1993;34(17):3658-3670.

[52] Gilbert AH, Bucknall CB. Epoxy resin toughened with thermoplastic. Makromolekulare Chemie Macromolecular Symposia. 1991;45(1):289-298.

[53] Bucknall CB, Gilbert AH. Toughening tetrafunctional epoxy resins using polyetherimide. Polymer. 1989;30(2):213-217.

[54] Kawaguchi T, Pearson RA. The effect of particle–matrix adhesion on the mechanical behavior of glass filled epoxies: Part 1. A study on yield behavior and cohesive strength. Polymer. 2003;44(15):4229-4238.

[55] Kawaguchi T, Pearson RA. The effect of particle–matrix adhesion on the mechanical behavior of glass filled epoxies. Part 2. A study on fracture toughness. Polymer. 2003;44(15):4239-4247.

[56] Lee J, Yee AF. Inorganic particle toughening I: micro-mechanical deformations in the fracture of glass bead filled epoxies. Polymer. 2001;42(2):577-588.

[57] Lee J, Yee AF. Inorganic particle toughening II: toughening mechanisms of glass bead filled epoxies. Polymer. 2001;42(2):589-597.

[58] Spanoudakis J, Young RJ. Crack propagation in a glass particle-filled epoxy resin: Part 1 Effect of particle volume fraction and size. J Mater Sci. 1984;19(2):473-486.

[59] Cho J, Joshi MS, Sun CT. Effect of inclusion size on mechanical properties of polymeric composites with micro and nano particles. Composites Science and Technology. 2006;66(13):1941-1952.

[60] Wouterson EM, Boey FYC, Hu X, Wong S-C. Specific properties and fracture toughness of syntactic foam: Effect of foam microstructures. Composites Science and Technology. 2005;65(11–12):1840-1850.

[61] Dekkers MEJ, Heikens D. The effect of interfacial adhesion on the tensile behavior of polystyrene–glass-bead composites. Journal of Applied Polymer Science. 1983;28(12):3809-3815.

[62] White SR, Sottos NR, Geubelle PH, Moore JS, Kessler MR, Sriram SR, et al. Autonomic healing of polymer composites. Nature. 2001;409(6822):794-797.

[63] Tao Y, Lin Z, Min Zhi R, Ming Qiu Z. Self-healing woven glass fabric/epoxy composites with the healant consisting of micro-encapsulated epoxy and latent curing agent. Smart Materials and Structures. 2008;17(1):015019.

[64] Mochane MJ, Luyt AS. Preparation and properties of polystyrene encapsulated paraffin wax as possible phase change material in a polypropylene matrix. Thermochimica Acta. 2012;544:63-70.

[65] Tagliavia G, Porfiri M, Gupta N. Analysis of flexural properties of hollow-particle filled composites. Composites Part B: Engineering. 2010;41(1):86-93.

[66] Lee J, Yee AF. Fracture of glass bead/epoxy composites: on micro-mechanical deformations. Polymer. 2000;41(23):8363-8373.

[67] Tripathi M, Rahamtullah, Kumar D, Rajagopal C, Kumar Roy P. Influence of microcapsule shell material on the mechanical behavior of epoxy composites for self-healing applications. Journal of Applied Polymer Science. 2014;131(15):n/a-n/a.

[68] Brown EN, White SR, Sottos NR. Microcapsule induced toughening in a self-healing polymer composite. J Mater Sci.39(5):1703-1710.

[69] Tyagi VV, Kaushik SC, Tyagi SK, Akiyama T. Development of phase change materials based microencapsulated technology for buildings: A review. Renewable and Sustainable Energy Reviews. 2011;15(2):1373-1391.

[70] Sari-Bey S, Fois M, Krupa I, Ibos L, Benyoucef B, Candau Y. Thermal characterization of polymer matrix composites containing microencapsulated paraffin in solid or liquid state. Energy Conversion and Management. 2014;78:796-804.

[71] Genovese A, Amarasinghe G, Glewis M, Mainwaring D, Shanks RA. Crystallisation, melting, recrystallisation and polymorphism of n-eicosane for application as a phase change material. Thermochimica Acta. 2006;443(2):235-244.

[72] Zhang H, Xu Q, Zhao Z, Zhang J, Sun Y, Sun L, et al. Preparation and thermal performance of gypsum boards incorporated with microencapsulated phase change materials for thermal regulation. Solar Energy Materials and Solar Cells. 2012;102:93-102.

[73] Krupa I, Nógellová Z, Špitalský Z, Janigová I, Boh B, Sumiga B, et al. Phase change materials based on high-density polyethylene filled with microencapsulated paraffin wax. Energy Conversion and Management. 2014;87:400-409.

[74] Cabeza LF, Barreneche C, Martorell I, Miró L, Sari-Bey S, Fois M, et al. Unconventional experimental technologies available for phase change materials (PCM) characterization. Part 1. Thermophysical properties. Renewable and Sustainable Energy Reviews. 2015;43:1399-1414.

[75] Trigui A, Karkri M, Krupa I. Thermal conductivity and latent heat thermal energy storage properties of LDPE/wax as a shape-stabilized composite phase change material. Energy Conversion and Management. 2014;77:586-596.

[76] Joulin A, Zalewski L, Lassue S, Naji H. Experimental investigation of thermal characteristics of a mortar with or without a micro-encapsulated phase change material. Applied Thermal Engineering. 2014;66(1–2):171-180.

[77] Borreguero AM, Garrido I, Valverde JL, Rodríguez JF, Carmona M. Development of smart gypsum composites by incorporating thermoregulating microcapsules. Energy and Buildings. 2014;76:631-639.

[78] Zhang GH, Zhao CY. Thermal and rheological properties of microencapsulated phase change materials. Renewable Energy. 2011;36(11):2959-2966.

[79] Song Q, Li Y, Xing J, Hu JY, Marcus Y. Thermal stability of composite phase change material microcapsules incorporated with silver nano-particles. Polymer. 2007;48(11):3317-3323.

[80] Qiu X, Lu L, Wang J, Tang G, Song G. Fabrication, thermal properties and thermal stabilities of microencapsulated n-alkane with poly(lauryl methacrylate) as shell. Thermochimica Acta. 2015;620:10-17.

[81] Zhang X-x, Tao X-m, Yick K-l, Wang X-c. Structure and thermal stability of microencapsulated phase-change materials. Colloid Polym Sci. 2003;282(4):330-336.

[82] Qiu X, Song G, Chu X, Li X, Tang G. Preparation, thermal properties and thermal reliabilities of microencapsulated n-octadecane with acrylic-based polymer shells for thermal energy storage. Thermochimica Acta. 2013;551:136-144.

[83] Tong X-M, Zhang M, Wang M-S, Fu Y. Effects of surface modification of self-healing poly(melamine-urea-formaldehyde) microcapsules on the properties of unsaturated polyester composites. Journal of Applied Polymer Science. 2013;127(5):3954-3961.

[84] Kumlutaş D, Tavman İH, Turhan Çoban M. Thermal conductivity of particle filled polyethylene composite materials. Composites Science and Technology. 2003;63(1):113-117.

[85] Xu Y, Chung DDL, Mroz C. Thermally conducting aluminum nitride polymer-matrix composites. Composites Part A: Applied Science and Manufacturing. 2001;32(12):1749-1757.

[86] Bishay IK, Abd-El-Messieh SL, Mansour SH. Electrical, mechanical and thermal properties of polyvinyl chloride composites filled with aluminum powder. Materials & Design. 2011;32(1):62-68.

[87] Lee G-W, Park M, Kim J, Lee JI, Yoon HG. Enhanced thermal conductivity of polymer composites filled with hybrid filler. Composites Part A: Applied Science and Manufacturing. 2006;37(5):727-734.

[88] Mamunya YP, Davydenko VV, Pissis P, Lebedev EV. Electrical and thermal conductivity of polymers filled with metal powders. European Polymer Journal. 2002;38(9):1887-1897.

[89] Liang JZ, Li FH. Measurement of thermal conductivity of hollow glass-bead-filled polypropylene composites. Polymer Testing. 2006;25(4):527-531.

[90] Li B, Yuan J, An Z, Zhang J. Effect of microstructure and physical parameters of hollow glass microsphere on insulation performance. Materials Letters. 2011;65(12):1992-1994.

[91] Patankar SN, Kranov YA. Hollow glass microsphere HDPE composites for low energy sustainability. Materials Science and Engineering: A. 2010;527(6):1361-1366.

[92] Karkri M, Lachheb M, Nógellová Z, Boh B, Sumiga B, AlMaadeed MA, et al. Thermal properties of phase-change materials based on high-density polyethylene filled with micro-encapsulated paraffin wax for thermal energy storage. Energy and Buildings. 2015;88:144-152.

[93] Salaün F, Vroman I. Influence of core materials on thermal properties of melamine–formaldehyde microcapsules. European Polymer Journal. 2008;44(3):849-860.

[94] Holliday L, Robinson J. Review: The thermal expansion of composites based on polymers. J Mater Sci. 1973;8(3):301-311.

[95] Klemens PG. Theory of thermal expansion of composites. International Journal of Thermophysics. 1988;9(2):171-177.

[96] Yung KC, Zhu BL, Yue TM, Xie CS. Preparation and properties of hollow glass microsphere-filled epoxy-matrix composites. Composites Science and Technology. 2009;69(2):260-264.

[97] Shunmugasamy VC, Pinisetty D, Gupta N. Thermal expansion behavior of hollow glass particle/vinyl ester composites. J Mater Sci. 2012;47(14):5596-5604.

[98] Yusriah L, Mariatti M, Abu Bakar A. The properties of vinyl ester composites reinforced with different types of woven fabric and hollow phenolic microspheres. Journal of Reinforced Plastics and Composites. 2010;29(20):3066-3073.

[99] Ferry JD. Viscoelastic Properties of Polymers: Wiley; 1980.

[100] Menard KP. Dynamic Mechanical Analysis: A Practical Introduction, Second Edition: CRC Press; 2008.

[101] Shunmugasamy VC, Pinisetty D, Gupta N. Viscoelastic properties of hollow glass particle filled vinyl ester matrix syntactic foams: effect of temperature and loading frequency. J Mater Sci. 2012;48(4):1685-1701.

[102] Ferreira JAM, Capela C, Costa JD. Dynamic Mechanical Analysis of Hybrid Fibre/Glass Microspheres Composites. Strain. 2011;47(3):275-280.

[103] Yusriah L, Mariatti M, Abu Bakar A. Mechanical properties of particulate-filler/woven-glass-fabric-filled vinyl ester composites. Journal of Vinyl and Additive Technology. 2010;16(1):98-104.

[104] Hameed N, Sreekumar PA, Francis B, Yang W, Thomas S. Morphology, dynamic mechanical and thermal studies on poly(styrene-co-acrylonitrile) modified epoxy resin/glass fibre composites. Composites Part A: Applied Science and Manufacturing. 2007;38(12):2422-2432.

[105] Liang JZ, Li RKY, Tjong SC. Effects of glass bead size and content on the viscoelasticity of filled polypropylene composites. Polymer Testing. 2000;19(2):213-220.

[106] d'Almeida JRM. An analysis of the effect of the diameters of glass microspheres on the mechanical behavior of glass-microsphere/epoxy-matrix composites. Composites Science and Technology. 1999;59(14):2087-2091.

[107] Yuan L, Gu A, Liang G, Zhang Z. Microcapsule-modified bismaleimide (BMI) resins. Composites Science and Technology. 2008;68(9):2107-2113.

[108] Zhang H, Wang P, Yang J. Self-healing epoxy via epoxy–amine chemistry in dual hollow glass bubbles. Composites Science and Technology. 2014;94:23-29.

[109] Su J-F, Wang X-Y, Dong H. Interface Stability of Microencapsulated-Paraffin Filled Epoxy Composites: Effect of Methylation on Melamine–Formaldehyde Shell Material. Composite Interfaces. 2011;18(8):645-659.

[110] Brown EN, White SR, Sottos NR. Microcapsule induced toughening in a self-healing polymer composite. J Mater Sci. 2004;39(5):1703-1710.

[111] Bonadies I, Izzo Renzi A, Cocca M, Avella M, Carfagna C, Persico P. Heat Storage and Dimensional Stability of Poly(vinyl alcohol) Based Foams Containing Microencapsulated Phase Change Materials. Industrial & Engineering Chemistry Research. 2015;54(38):9342-9350.

[112] Delgado M, Lázaro A, Mazo J, Zalba B. Review on phase change material emulsions and microencapsulated phase change material slurries: Materials, heat transfer studies and applications. Renewable and Sustainable Energy Reviews. 2012;16(1):253-273.

[113] Shuart MJ. Failure of compression-loaded multidirectional composite laminates. AIAA Journal. 1989;27(9):1274-1279.

[114] Guild FJ, Young RJ. A predictive model for particulate-filled composite materials. Part 1 Hard particles. J Mater Sci. 1989;24(1):298-306.

[115] Guild FJ, Young RJ. A predictive model for particulate filled composite materials. Part 2 Soft particles. J Mater Sci. 1989;24(7):2454-2460.

[116] Sinien L, Lin Y, Xiaoguang Z, Zongneng Q. Microdamage and interfacial adhesion in glass bead-filled high-density polyethylene. J Mater Sci. 1992;27(17):4633-4638.

[117] Alvarado JL, Marsh C, Sohn C, Phetteplace G, Newell T. Thermal performance of microencapsulated phase change material slurry in turbulent flow under constant heat flux. International Journal of Heat and Mass Transfer. 2007;50(9–10):1938-1952.

[118] Afaghi-Khatibi A, Mai Y-W. Characterisation of fibre/matrix interfacial degradation under cyclic fatigue loading using dynamic mechanical analysis. Composites Part A: Applied Science and Manufacturing. 2002;33(11):1585-1592.

[119] Ye L, Afaghi-Khatibi A, Lawcock G, Mai Y-W. Effect of fibre/matrix adhesion on residual strength of notched composite laminates. Composites Part A: Applied Science and Manufacturing. 1998;29(12):1525-1533.

[120] Totry E, Molina-Aldareguía JM, González C, Llorca J. Effect of fiber, matrix and interface properties on the in-plane shear deformation of carbon-fiber reinforced composites. Composites Science and Technology. 2010;70(6):970-980.

[121] Cech V, Palesch E, Lukes J. The glass fiber–polymer matrix interface/interphase characterized by nanoscale imaging techniques. Composites Science and Technology. 2013;83:22-26.

[122] Drzal LT, Madhukar M. Fibre-matrix adhesion and its relationship to composite mechanical properties. J Mater Sci. 1993;28(3):569-610.

[123] Walter TR, Subhash G, Sankar BV, Yen CF. Monotonic and cyclic short beam shear response of 3D woven composites. Composites Science and Technology. 2010;70(15):2190-2197.

[124] Whitney J, Browning C. On short-beam shear tests for composite materials. Experimental Mechanics. 1985;25(3):294-300.

[125] Daniels BK, Harakas NK, Jackson RC. Short beam shear tests of graphite fiber composites. Fibre Science and Technology. 1971;3(3):187-208.

[126] Mouritz AP, Baini C, Herszberg I. Mode I interlaminar fracture toughness properties of advanced textile fibreglass composites. Composites Part A: Applied Science and Manufacturing. 1999;30(7):859-870.

[127] Compston P, Jar P-YB. The Influence of Fibre Volume Fraction on the Mode I Interlaminar Fracture Toughness of a Glass-Fibre/Vinyl Ester Composite. Applied Composite Materials.6(6):353-368.

[128] Thakre PR, Lagoudas DC, Riddick JC, Gates TS, Frankland S-JV, Ratcliffe JG, et al. Investigation of the effect of single wall carbon nanotubes on interlaminar fracture toughness of woven carbon fiber—epoxy composites. Journal of Composite Materials. 2011;45(10):1091-1107.

[129] Wu B, Zheng G, Chen X. Effect of graphene on the thermophysical properties of melamine-urea-formaldehyde/N-hexadecane microcapsules. RSC Advances. 2015;5(90):74024-74031.

[130] Chaiyasat P, Noppalit S, Okubo M, Chaiyasat A. Do encapsulated heat storage materials really retain their original thermal properties? Physical Chemistry Chemical Physics. 2015;17(2):1053-1059.

[131] Xin C, Tian Y, Wang Y, Huang Xa. Effect of curing temperature on the performance of microencapsulated low melting point paraffin using urea-formaldehyde resin as a shell. Textile Research Journal. 2014;84(8):831-839.

[132] Junfeng S, Wang L, Ren L. Fabrication and thermal properties of microPCMs: Used melamine-formaldehyde resin as shell material. Journal of Applied Polymer Science. 2006;101(3):1522-1528.

[133] Marchi S, Pagliolico S, Sassi G. Characterization of panels containing micro-encapsulated Phase Change Materials. Energy Conversion and Management. 2013;74:261-268.

[134] Su J-F, Wang X-Y, Huang Z, Zhao Y-H, Yuan X-Y. Thermal conductivity of microPCMs-filled epoxy matrix composites. Colloid Polym Sci. 2011;289(14):1535-1542.

[135] You M, Zhang XX, Li W, Wang XC. Effects of MicroPCMs on the fabrication of MicroPCMs/polyurethane composite foams. Thermochimica Acta. 2008;472(1–2):20-24.

[136] Gwinn JP, Webb RL. Performance and testing of thermal interface materials. Microelectronics Journal. 2003;34(3):215-222.

[137] Trigui A, Karkri M, Krupa I. Thermal conductivity and latent heat thermal energy storage properties of LDPE/wax as a shape-stabilized composite phase change material. Energy Conversion and Management. 2014;77(0):586-596.

[138] Bohac V, Gustavsson MK, Kubicar L, Gustafsson SE. Parameter estimations for measurements of thermal transport properties with the hot disk thermal constants analyzer. Review of Scientific Instruments. 2000;71(6):2452-2455.

[139] Gustavsson M, Karawacki E, Gustafsson SE. Thermal conductivity, thermal diffusivity, and specific heat of thin samples from transient measurements with hot disk sensors. Review of Scientific Instruments. 1994;65(12):3856-3859.

[140] Al-Ajlan SA. Measurements of thermal properties of insulation materials by using transient plane source technique. Applied Thermal Engineering. 2006;26(17–18):2184-2191.

[141] Shanks RA. Linear thermal expansion, thermal ageing, relaxations and post-cure of thermoset polymer composites using modulated temperature thermomechanometry. J Therm Anal Calorim. 2011;106(1):151-158.

[142] Zhang XX, Tao XM, Yick KL, Fan YF. Expansion space and thermal stability of microencapsulated n-octadecane. Journal of Applied Polymer Science. 2005;97(1):390-396.

[143] Han N, Gao X, Zhang R, Zhang X. Structures and properties of thermoregulated acrylonitrile–methyl acrylate sheet containing microphase change materials. Polymer Composites. 2013;34(5):641-649.

[144] Shinohara Y, Kawasaki N, Ueno S, Kobayashi I, Nakajima M, Amemiya Y. Observation of the Transient Rotator Phase of n-Hexadecane in Emulsified Droplets with Time-Resolved Two-Dimensional Small- and Wide-Angle X-Ray Scattering. Physical Review Letters. 2005;94(9):097801.

[145] Zhang XX, Fan YF, Tao XM, Yick KL. Fabrication and properties of microcapsules and nanocapsules containing n-octadecane. Materials Chemistry and Physics. 2004;88(2–3):300-307.

[146] Zhang X-x, Fan Y-f, Tao X-m, Yick K-l. Crystallization and prevention of supercooling of microencapsulated n-alkanes. Journal of Colloid and Interface Science. 2005;281(2):299-306.

[147] Anghel EM, Georgiev A, Petrescu S, Popov R, Constantinescu M. Thermo-physical characterization of some paraffins used as phase change materials for thermal energy storage. J Therm Anal Calorim. 2014;117(2):557-566.

[148] Fu D, Su Y, Gao X, Liu Y, Wang D. Confined crystallization of n-hexadecane located inside microcapsules or outside submicrometer silica nanospheres: a comparison study. The journal of physical chemistry B. 2013;117(20):6323-6329.

[149] Zhou D, Zhao CY, Tian Y. Review on thermal energy storage with phase change materials (PCMs) in building applications. Applied Energy. 2012;92:593-605.

[150] Warzoha RJ, Fleischer AS. Effect of carbon nanotube interfacial geometry on thermal transport in solid–liquid phase change materials. Applied Energy. 2015;154:271-276.

[151] Huang J-c, He C-b, Xiao Y, Mya KY, Dai J, Siow YP. Polyimide/POSS nanocomposites: interfacial interaction, thermal properties and mechanical properties. Polymer. 2003;44(16):4491-4499.

[152] Asimakopoulou EK, Kolaitis DI, Founti MA. Fire safety aspects of PCM-enhanced gypsum plasterboards: An experimental and numerical investigation. Fire Safety Journal. 2015;72:50-58.

[153] Sittisart P, Farid MM. Fire retardants for phase change materials. Applied Energy. 2011;88(9):3140-3145.

[154] M Price D. Novel methods of modulated-temperature thermal analysis. Thermochimica Acta. 1998;315(1):11-18.

[155] Wang S, Liang Z, Gonnet P, Liao YH, Wang B, Zhang C. Effect of Nanotube Functionalization on the Coefficient of Thermal Expansion of Nanocomposites. Advanced Functional Materials. 2007;17(1):87-92.

[156] Segal L. The thermal expansion of reinforced nylon-6 composites through the matrix glass transition temperature. Polymer Engineering & Science. 1979;19(5):365-372.

[157] Xie X-L, Tang C-Y, Zhou X-P, Li RK-Y, Yu Z-Z, Zhang Q-X, et al. Enhanced Interfacial Adhesion between PPO and Glass Beads in Composites by Surface Modification of Glass Beads via In Situ Polymerization and Copolymerization. Chemistry of Materials. 2004;16(1):133-138.

[158] Yao Y, Zeng X, Guo K, Sun R, Xu J-b. The effect of interfacial state on the thermal conductivity of functionalized Al2O3 filled glass fibers reinforced polymer composites. Composites Part A: Applied Science and Manufacturing. 2015;69:49-55.

[159] Pritchard G, Yang Q. Microscopy of impact damage in particulate-filled glass-epoxy laminates. J Mater Sci. 1994;29(19):5047-5053.

[160] Hale A, Macosko CW, Bair HE. Glass transition temperature as a function of conversion in thermosetting polymers. Macromolecules. 1991;24(9):2610-2621.

[161] Lin T, Gupta N, Talalayev A. Thermoanalytical characterization of epoxy matrix-glass microballoon syntactic foams. J Mater Sci. 2009;44(6):1520-1527.

[162] Shunmugasamy V, Pinisetty D, Gupta N. Viscoelastic properties of hollow glass particle filled vinyl ester matrix syntactic foams: effect of temperature and loading frequency. J Mater Sci. 2013;48(4):1685-1701.

[163] Vassileva E, Friedrich K. Epoxy/alumina nanoparticle composites. I. Dynamic mechanical behavior. Journal of Applied Polymer Science. 2003;89(14):3774-3785.

[164] Levita G, De Petris S, Marchetti A, Lazzeri A. Crosslink density and fracture toughness of epoxy resins. J Mater Sci. 1991;26(9):2348-2352.

[165] Akay M. Aspects of dynamic mechanical analysis in polymeric composites. Composites Science and Technology. 1993;47(4):419-423.

[166] Sun Y, Zhang Z, Moon K-S, Wong CP. Glass transition and relaxation behavior of epoxy nanocomposites. Journal of Polymer Science Part B: Polymer Physics. 2004;42(21):3849-3858.

[167] Ornaghi HL, Bolner AS, Fiorio R, Zattera AJ, Amico SC. Mechanical and dynamic mechanical analysis of hybrid composites molded by resin transfer molding. Journal of Applied Polymer Science. 2010;118(2):887-896.

[168] Romanzini D, Lavoratti A, Ornaghi Jr HL, Amico SC, Zattera AJ. Influence of fiber content on the mechanical and dynamic mechanical properties of glass/ramie polymer composites. Materials & Design. 2013;47:9-15.

[169] Li G, Lee-Sullivan P, Thring RW. Determination of Activation Energy for Glass Transition of an Epoxy Adhesive Using Dynamic Mechanical Analysis. J Therm Anal Calorim. 2000;60(2):377-390.

[170] Keller MW, Jellison BD, Ellison T. Moisture effects on the thermal and creep performance of carbon fiber/epoxy composites for structural pipeline repair. Composites Part B: Engineering. 2013;45(1):1173-1180.

[171] Li L, Li B, Tang F. Influence of maleic anhydride-grafted EPDM and flame retardant on interfacial interaction of glass fiber reinforced PA-66. European Polymer Journal. 2007;43(6):2604-2611.

[172] Ragosta G, Abbate M, Musto P, Scarinzi G, Mascia L. Epoxy-silica particulate nanocomposites: Chemical interactions, reinforcement and fracture toughness. Polymer. 2005;46(23):10506-10516.

[173] Montazeri A, Pourshamsian K, Riazian M. Viscoelastic properties and determination of free volume fraction of multi-walled carbon nanotube/epoxy composite using dynamic mechanical thermal analysis. Materials & Design. 2012;36:408-414.

[174] John Wiley & Sons I. Transtion and relaxation. Properties and Behavior of Polymers, 2 Volume Set, New Jersey: John Wiley & Sons, Inc; 2012. p. 1129-1269.

[175] Abiad MG, Gonzalez DC, Mert B, Campanella OH, Carvajal MT. A novel method to measure the glass and melting transitions of pharmaceutical powders. International Journal of Pharmaceutics. 2010;396(1–2):23-29.

[176] Su J-F, Wang X-Y, Dong H. Influence of temperature on the deformation behaviors of melamine–formaldehyde microcapsules containing phase change material. Materials Letters. 2012;84:158-161.